(NASA-CR-135498) DETECTION AND ESTIMATION OF AN OPTICAL IMAGE BY PHOTON-COUNTING TECHNIQUES Ph.D. Thesis (California Univ.) 218 p HC $13.00 CSCL 14B

N73-32335

Unclas
G3/14 15021

UNIVERSITY OF CALIFORNIA
SAN DIEGO

NGL 05-009-079

Detection and Estimation of an Optical Image by Photon-Counting Techniques

A dissertation submitted in partial satisfaction of the requirements
for the degree Doctor of Philosophy in
Information and Computer Science

by

Lily Lee Wang

Committee in charge:

Professor Carl W. Helstrom, Chairman
Professor Adolf W. Lohmann
Professor Elias Masry
Professor Michael J. Sharpe
Professor Harold W. Sorenson

1973

The dissertation of Lily Lee Wang is approved, and it is acceptable in quality and form for publication on microfilm:

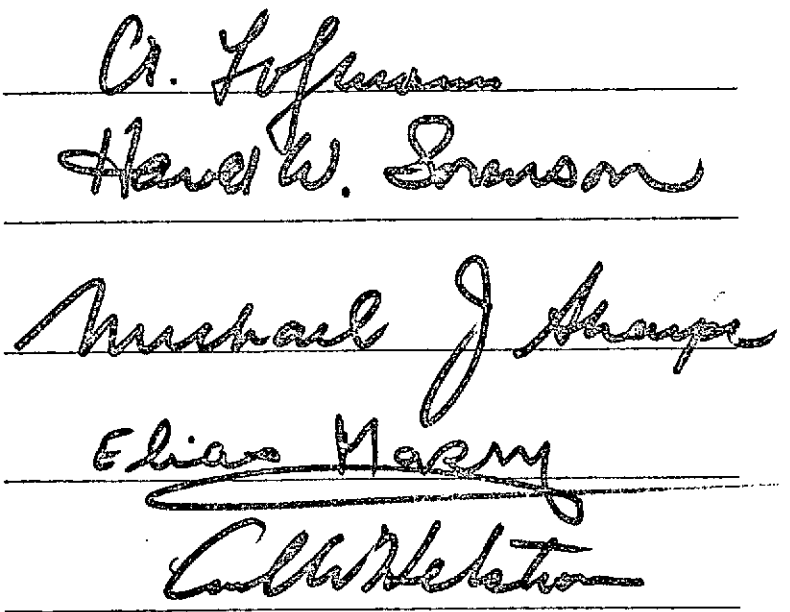

Committee Chairman

University of California, San Diego

1973

Table of Contents

List of Figures

List of Tables

Acknowledgements

The author wishes to express her appreciation to Professor Carl W. Helstrom who introduced her to this field of study and provided the direction and encouragement throughout its development. Thanks are due to her many professors who provided the insight into the theories and techniques that make this dissertation possible. Appreciation is also extended to both Dottie Bybee and Sue Pettijohn who typed the manuscript.

The author wishes to acknowledge the financial support provided by the National Aeronautics and Space Administration for the first three years and the National Science Foundation for the fourth year since 1969. This research was carried out under NASA Grant NGL 05-009-079 and NSF Grant GK-33811.

Finally, the author's deep appreciation is felt for her husband, Charles, for his encouragement and great consideration during these years of graduate study.

VITA

[redacted]

1962 -	M.S.E.E., Oklahoma State University, Stillwater
1963 - 1965	Engineer, Fairchild Control Corporation, Los Angeles, California
1965 - 1967	Project Engineer, Endevco Corporation, Pasadena, California
1967 - 1969	Technical Staff Member, Bellcomm Inc., Washington, D.C.

PUBLICATIONS

Wang, L. L. Numerical calculation of cumulative probability from the moment-generating function. Proc. IEEE, vol. 60, pp. 1452-1453, November, 1972.

Helstrom, C. W. and L. L. Wang. Optimum detection of an optical image on a photoelectric surface. IEEE Trans. on Aerospace and Electronics System (in press).

FIELDS OF STUDY

Major Field: Signal Processing
Detection and Estimation Theory
Communication Theory
Electronic Engineering

ABSTRACT OF THE DISSERTATION

Detection and Estimation of an Optical Image by Photon-Counting Techniques

by

Lily Lee Wang

Doctor of Philosophy in Information and Computer Science

University of California, San Diego, 1973

Professor Carl W. Helstrom, Chairman

The statistical description of the photoelectric detector is given. The photosensitive surface of the detector is divided into many small areas, and the moment generating function of the photo-counting statistic is derived for large time-bandwidth product. The detection of a specified optical image in the presence of the background light by using the hypothesis test is discussed. The ideal detector based on the likelihood ratio from a set of numbers $\underline{n}$ of

photoelectrons ejected from many small areas of the photosensitive surface is studied and compared with the threshold detector and a simple detector which is based on the likelihood ratio by counting the total number of photoelectrons from a finite area of the surface. The intensity of the image is assumed to be Gaussian distributed spatially against the uniformly distributed background light. The numerical approximation by the method of steepest descent is used, and the calculations of the reliabilities for the detectors are carried out by the digital computer. An almost optimum intensity estimate is proposed when the intensity of the object light is unknown, and its statistical performance is studied. The application of the photon-counting techniques is further discussed where detectors are investigated for resolving two point sources with Gaussian images.

Introduction

An optical communication system, owing to its high information-carrying capacity both in the temporal and the spatial channels, is more advantageous than electromagnetic wave systems of lower frequency. In general, the retrieval of the information will rely heavily on prior knowledge about the field and the performance of the detecting system. Usually the optical field at space point $\underline{r}$ and time t is not a measurable quantity, and only its average power at that point can be observed. A photoelectric detector, such as the photo-tube, the photomultiplier, the image tube, or the image orthicon, which carries the information about the optical field in the sense that the probability of the photoelectron emission is proportional to the intensity of the light at its photosensitive surface, plays an important role in the optical system for the detection and extraction of the information. For example, in observational astronomy it is often a practice to use an image tube or a photomultiplier to detect a star for the purpose of observation and navigation; in a binary communication system a phototube may be used to detect a bit "1" when a specified optical object is received.

In most applications, the background light, referred to as the "noise", may also pass through the optical system and thus corrupt the object light, referred to as the "signal". When the signal-to-noise ratio is low, the observer will not only be required to detect the optical signal,but also to seek the best strategy he can to make the decision whether there is only the noise or whether the object signal is also present. One way to observe the optical field by using a

photoelectric detector is to count the number of ejected photoelectrons. That is, as the photosensitive surface of the detector is divided like a mosaic into many small equal areas, the set of data can be obtained from observing the numbers of the photoelectrons ejected from each such area during the time interval (0, T). Because of the stochastic nature of the optical field, each of the observed data will be a random variable. To make decisions, detection theory and the concepts of statistical hypothesis testing can be applied when the object signal is specified. If there are also some parameters of the object signal unknown, the estimation of such parameters as well as the detection must be carried out. In this thesis we will discuss the basic binary detection and single parameter estimation of an optical image and some of their applications in optical communication systems by using photon-counting techniques.

A point source, at a known location, emits incoherent quasimonochromatic light of given spectral density and is focused on the photosensitive surface of a photoelectric detector. Its electromagnetic field[1], which is spectrally pure, is assumed to be a stationary, spatio-temporal, circular Gaussian random process. A brief description of the image formation and statistical description of the photoelectric detector will be given in Chapter I. As the observation interval T is much greater than the reciprocal of the bandwidth W^{-1}, the distribution of the number of photoelectrons ejected from a single small area of the photosensitive surface, discussed by Mandel[2] and Helstrom[3], will be derived in this chapter, following Siegert[4], and it can be approximated by a Poisson distribution

function. The derivation will be then extended to the approximation that the numbers of photoelectrons ejected from the different small areas of the surface will be Poisson distributed and statistically independent from each other. The moment-generating function (m.g.f.) of the statistic, which is the sum of the number of photoelectrons ejected from many small areas as these areas become infinitesimally small, will also be discussed.

When the optical signal is specified, the simple binary hypothesis tests can be used. Two important strategies, Bayes and Neyman-Pearson, will be briefly described in Chapter II. The optimum statistic based on the likelihood ratio and its m.g.f. for the spatially varying optical signal, discussed previously by Helstrom[5], will also be given. The performance of the ideal detector, in the absence of the background light, will be discussed,and its detection probability will be calculated for a preassigned false-alarm probability. When background light also passes through the system, only an approximate form of the distribution can be used. Because of the complexity of the m.g.f. of the statistic, a Gaussian approximation was suggested by Helstrom[5]. When the signal-to-noise ratio becomes large, the Kth order cumulant of the statistic increases as K increases, and the Gaussian approximation is not valid. Farrell[6] recommended the gamma distribution approximation. We have used the method of steepest descent to approximate the distribution with a uniform asymptotic expansion series following Rice[7], as also discussed by Daniel[8]. The performance of the optimum detector has been

investigated with a Gaussian image and uniform background light, where the detection probability at preassigned values of false-alarm probability, and the average error probability will be calculated by using the digital computer. As the signal-to-noise ratio is small, the optimum detector can be approximated by the threshold detector and will be also discussed. Besides the ideal detector, which registers the locations of the ejected photoelectrons from the surface, a simple detector, which observes the total photoelectrons ejected from the surface without dividing it into many small areas, will be also discussed. The performances of both the threshold detector and the simple detector will be investigated with the Gaussian image and uniform background light. Comparison between these three detectors will be made with the evaluation of the average error probabilities and of the detection probabilities at preassigned values of the false-alarm probabilities.

When the intensity of the point source, which is located in the field of view, is unknown, the observer must also estimate the intensity of the image simultaneously if he makes the decision that the optical signal is present. Since the observed data are a set of random variables, no two experiments will yield the same value of the intensity estimate even though the true value of the intensity is the same in both. The most one can hope for is that the estimate will be close to the true value of the intensity in the sense of "on the average". Two most important strategies, Bayes and maximum-likelihood, will be discussed in Chapter III. The intensity estimate, derived from the Bayes strategy, which has been discussed

also by Middleton and Esposito[9], will be investigated with a quadratic cost function where the prior probability density function (p.d.f.) of the intensity will be assumed to be a gamma distribution function. When the signal-to-noise ratio is not too weak, the Bayes estimate of intensity will be approximately equivalent to the maximum-likelihood estimate. An almost optimum estimate therefore will be proposed, and its statistical performance will be investigated with a truncated Gaussian or a parabolic image. The expectations of the estimate will be calculated by the digital computer at different values of parameters such as the duration of the observation interval and the radius of observation area, all at a preassigned value of the false-alarm probability.

In Chapter IV, we will further discuss some applications to optical communication of the photon-counting techniques. For example, the ideal detector derived from the likelihood ratio given in Chapter II can be applied to resolve two point sources with equal radiant power at known locations from a single point source with twice the power located between them. The m.g.f. of the ideal detector and its cumulants will be given. Since the m.g.f. of the ideal detector bears a complicated form with double integration, we will not practice the numerical calculation though it can be carried out by the digital computer. Instead, the ideal detector for detecting a bit "1" when light from a point source located at $\underline{x}$ is received or a bit "0" when a light from a point source located at $-\underline{x}$ is received will be investigated numerically in the absence of any background light. A Gaussian image will be postulated, and the calculation of the error

probability, which is dependent on the separation distance of the point sources, will be carried out. Two more detectors, the simple detector that counts the total number of photoelectrons ejected from half of the surface of the photoelectric detector and the counting comparator that compares the numbers of photoelectrons observed from the upper and lower half-surfaces of the photoelectric detector, will be also discussed, and their error probabilities will be evaluated. As the background light also passes through the aperture, the average error probabilities of both the simple detector and the counting comparator will be calculated with a finite square observation area. Since the performances of the detector for detecting binary bits will also depend on the prior knowledge about the locations of the images, the effects of mislocation on the ideal detector and counting comparator will be discussed.

Footnotes

Introduction

1. Mandel and Wolf [1].
2. Mandel [2].
3. Helstrom [3].
4. Siegert [4].
5. Helstrom]5].
6. Farrell [6].
7. Rice [7].
8. Daniel [8].
9. Middleton and Esposito [9].

Chapter I Image formation and photon-counting statistics

In this chapter, the general terms such as intensity, covariance function, and point-spread function in image forming and processing will be discussed. The optical field v will be considered as a complex circular Gaussian stochastic process which is stationary, ergodic and spectrally pure. In other words, the process can be described by the complex random functions of space $\underset{\sim}{r}$ and time t, $V_1(\underset{\sim}{r},t)$ and $V_2(\underset{\sim}{r},t)$, where $V_1(\underset{\sim}{r},t)$ and $V_2(\underset{\sim}{r},t)$ are the real and imaginary parts of the process. The statistical description of the photoelectric detector will be given. When the observation time T is much greater than the reciprocal of the bandwidth W^{-1}, the numbers of the photoelectrons ejected from different small areas of the photosensitive surface will be proved to be Poisson distributed and statistically independent of each other. The moment generating function (m.g.f.) of the photon-counting statistic will be derived in a general form and discussed.

Image formation when diffraction theory is applied

The diffraction theory of image formation has been largely used to describe imaging systems in which the process is considered both linear and spatially stationary. The basic elements for an imaging system are the luminous object o, aperture A (for example, a lens) and image I located in the planes U, A, R respectively as shown in Fig. 1, where z_1 and z_2 are the distances of the object plane U and the image plane R from the aperture A.

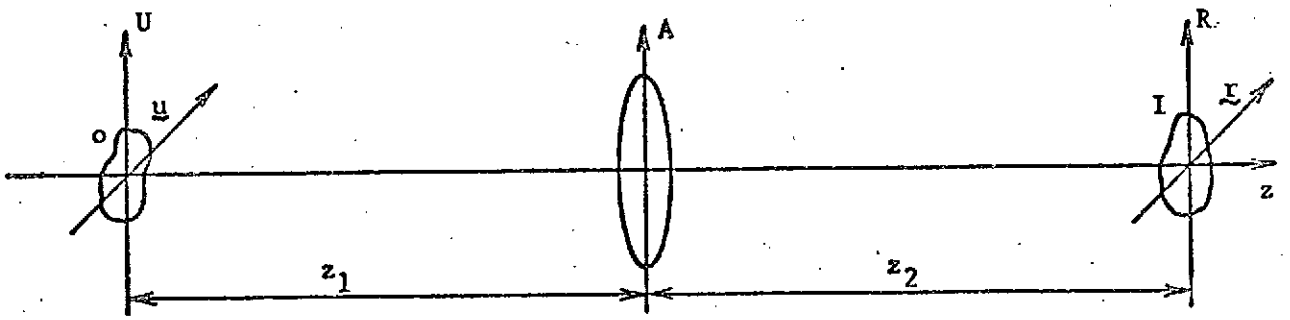

Figure 1 Image formation system

The optical field v at the point $(\underset{\sim}{u},z_1)$ of the object plane at time t is assumed to be linearly polarized and quasimonochromatic and can be characterized by

$$v(\underset{\sim}{u},z_1,t) = R\ell\, V(\underset{\sim}{u},z_1,t)\, e^{i\Omega_o t} , \qquad (1.1)$$

where

$$V(\underline{u},z_1,t) = V_1(\underline{u},z_1,t) + iV_2(\underline{u},z_1,t) \tag{1.2}$$

is the complex amplitude of the electric field and $V_1(\underline{u},z_1,t)$, $V_2(\underline{u},z_1,t)$ are its real and imaginary parts, which are Gaussian random processes[1]. Ω_o is the angular frequency at the center of the object spectrum. "Rℓ" indicates the real part of the analytic signal $V(\underline{u},z_1,t)\, e^{i\Omega_o t}$. As the distances z_1 and z_2 are much greater than the wavelength of the light, the complex amplitude $V(\underline{r},z_2,t)$ at point $(\underline{r},z_2)$ of the image plane R at time t due to the object light can be expressed[2] as

$$V(\underline{r},z_2,t) = \int_o V(\underline{u},z_1,t)\, K(\underline{u},\underline{r})\, d^2\underline{u} \quad , \tag{1.3}$$

where $K(\underline{u},\underline{r})$ is the amplitude point-spread function describing the propagation from the object plane to the image plane. o is the area of the object.

The instantaneous intensity at any point $(\underline{x},z)$ of an arbitrary plane X away from the aperture with a distance z and at time t is defined by

$$I(\underline{x},z,t) = V(\underline{x},z,t)\, V^*(\underline{x},z,t) \quad , \tag{1.4}$$

where $V^*(\underline{x},z,t)$ is the complex conjugate of the amplitude $V(\underline{x},z,t)$,

which is not directly measurable; the observable quantity is the ensemble average intensity defined[3] by

$$\langle I(\underline{x},z,t)\rangle = \langle V(\underline{x},z,t)\ V^{*}(\underline{x},z,t)\rangle . \qquad (1.5)$$

When the process is also ergodic, the ensemble average is equivalent to the time average through the interval $(-T,T)$ as $T \to \infty$.

The field is normalized so that the instantaneous power density at point $(\underline{u},z_1)$ of the object plane at time t is $\frac{1}{2}|V(\underline{u},z_1,t)|^2$, and the complex covariance function between the complex field at point $(\underline{u}_i,z_1)$ and the complex-conjugate field at point $(\underline{u}_j,z_1)$ of the object plane at times t_i and t_j respectively is defined by

$$\Gamma(\underline{u}_i,\underline{u}_j,t_i,t_j : z_1) = \frac{1}{2}\langle V(\underline{u}_i,z_1,t_i)\ V^{*}(\underline{u}_j,z_1,t_j)\rangle . \qquad (1.6)$$

(1.6) is known as the complex autocovariance function[4]; it is proportional to the mutual coherence function[5,6] with a factor $e^{i\Omega_o(t_i-t_j)}$. $\Gamma(\underline{u}_i,\underline{u}_i,t_1,t_1:z_1)$ is the average power density at point $(\underline{u}_i,z_1)$ of the object plane along the direction z. For an optical system that can be approximated by only considering the paraxial rays and has small bandwidth W such that $W \ll \Omega_o$, the property of the spectrally pure light is characterized by Mandel[7] in such a way that the superposition of light beams will not affect the spectral distribution; the covariance function from (1.6) is then reducible to the

product of two simpler functions as

$$\Gamma(\underline{u}_i,\underline{u}_j,t_i,t_j:z_1) = \phi(\underline{u}_i,\underline{u}_j,z_1)\ \chi(t_i - t_j)\ , \qquad (1.7)$$

where $\phi(\underline{u}_i,\underline{u}_j,z_1)$ and $\chi(t_i - t_j)$ are the complex spatial and temporal coherence functions[8]. In general $\chi(\tau)$ is normalized so that $\chi(0) = 1$ and $\chi(\tau) = \chi^*(-\tau)$ for real power spectrum (τ is real). The ensemble average intensity from (1.5) can also be written as

$$\langle I(\underline{x},z,t)\rangle = 2\Gamma(\underline{x},\underline{x},t,t:z)\ , \qquad (1.8)$$

which is the variance of the process $V(\underline{x},z,t)$ or the sum[9] of the variances of the two independent processes $V_1(\underline{x},z,t)$ and $V_2(\underline{x},z,t)$ at point $(\underline{x},z)$ of the plane X and at time t.

As the complex amplitude $V(\underline{u},z_1,t)$ is defined to be zero outside the object o, (1.3) can also be expressed by a convolution equation[3] for the paraxial approximation, that is

$$V(\underline{r},z_2,t) = \int_{-\infty}^{\infty}\int_{-\infty}^{\infty} d^2\underline{u}\ V(\underline{u},z_1,t)\ K(\underline{r} - \underline{u})\ . \qquad (1.9)$$

The average intensity at point $(\underline{r},z_2)$ of the image plane due to the object light according to (1.5) is

$$\langle I_{im}(\underline{r},z_2,t)\rangle = \langle V(\underline{r},z_2,t)\ V^*(\underline{r},z_2,t)\rangle$$

$$= 2 \int_{-\infty}^{\infty}\int_{-\infty}^{\infty} d^2\underset{\sim}{u}_i \int_{-\infty}^{\infty}\int_{-\infty}^{\infty} d^2\underset{\sim}{u}_j$$

$$\Gamma(\underset{\sim}{u}_i,\underset{\sim}{u}_j,t,t:z_1)\ K(\underset{\sim}{r}-\underset{\sim}{u}_i)\ K^*(\underset{\sim}{r}-\underset{\sim}{u}_j) \quad . \qquad (1.10)$$

when (1.6) and (1.9) are used. $\Gamma(\underset{\sim}{u}_i,\underset{\sim}{u}_j,t,t:z_1)$ is the covariance function between points $(\underset{\sim}{u}_i,z_1)$ and $(\underset{\sim}{u}_j,z_1)$ of the object plane at time t. As the light is assumed to be spectrally pure, the average energy received within the small area ΔA of the image plane because of the object illumination during the observation interval (0,T) is given by

$$\Delta E = \int_{\Delta A} d^2\underset{\sim}{r} \int_0^T dt\ \Gamma(\underset{\sim}{r},\underset{\sim}{r},t,t:z_2)$$

$$= T \int_{\Delta A} d^2\underset{\sim}{r} \int_{-\infty}^{\infty}\int_{-\infty}^{\infty} d^2\underset{\sim}{u}_i \int_{-\infty}^{\infty}\int_{-\infty}^{\infty} d^2\underset{\sim}{u}_j$$

$$\phi(\underset{\sim}{u}_i,\underset{\sim}{u}_j,z_1)\ K(\underset{\sim}{r}-\underset{\sim}{u}_i)\ K^*(\underset{\sim}{r}-\underset{\sim}{u}_j) \qquad (1.11)$$

as (1.6), (1.7) and (1.9) are used.

Intensity representation of light from an incoherent object

The average intensity at point $(\underset{\sim}{r},z_2)$ of the image plane and at time t due to the coherent object illumination can be expressed by (1.10) or can also be written as

$$\langle I_{im}(\underset{\sim}{r},z_2,t)\rangle = \langle \left| \int_{-\infty}^{\infty}\int_{-\infty}^{\infty} K(\underset{\sim}{r}-\underset{\sim}{u}_i)\ V(\underset{\sim}{u}_i,z_1,t)\ d^2\underset{\sim}{u}_i \right|^2 \rangle . \qquad (1.12)$$

For an incoherent object, the spatial coherence function from (1.7) can be defined[8] as

$$\phi(\underset{\sim}{u}_i,\underset{\sim}{u}_j,z_1) = \pi k_o^{-2}\ B(\underset{\sim}{u}_i)\ \ \delta(\underset{\sim}{u}_i-\underset{\sim}{u}_j) , \qquad (1.13)$$

where $B(\underset{\sim}{u}_i)$ is the radiance so defined that $B(\underset{\sim}{u}_i)/4\pi$ is the power emitted per unit area per steradian in the direction z normal to the object plane. The radiance $B(\underset{\sim}{u}_i)$ is of limited extent. Here $k_o = \Omega_o/C_o$ with C_o the velocity of the light, and $\delta(\underset{\sim}{u})$ is the two-dimensional Dirac delta function. The average intensity given by (1.10) can be expressed in terms of the radiance $B(\underset{\sim}{u}_i)$ as

$$\langle I_{im}(\underset{\sim}{r},z_2,t)\rangle = 2\pi k_o^{-2}\int_{-\infty}^{\infty}\int_{-\infty}^{\infty}\int_{-\infty}^{\infty}\int_{-\infty}^{\infty} d^2\underset{\sim}{u}_i\ d^2\underset{\sim}{u}_j\ K(\underset{\sim}{r}-\underset{\sim}{u}_i)\ K^*(\underset{\sim}{r}-\underset{\sim}{u}_j)$$

$$\cdot B(\underset{\sim}{u}_i)\ \delta(\underset{\sim}{u}_i-\underset{\sim}{u}_j)$$

$$= 2\pi k_o^{-2}\int_{-\infty}^{\infty}\int_{-\infty}^{\infty} B(\underset{\sim}{u}_i)\ S(\underset{\sim}{r}-\underset{\sim}{u}_i)\ d^2\underset{\sim}{u}_i , \qquad (1.14)$$

where $S(\underset{\sim}{r}-\underset{\sim}{u}_i) = |K(\underset{\sim}{r}-\underset{\sim}{u}_i)|^2$ is defined as the incoherent point-spread function. Thus we can see from (1.12) that for a coherent object illumination the imaging system is linear in complex amplitude. However, for an incoherent object the imaging system is linear only in intensity as given by (1.14).

The statistical description of a photoelectric detector

When the photoelectric detector is used for image detection, the photosensitive surface--for example, the surface of a photomultiplier--will be placed at the image plane. The output of the illuminated photodetector carries information about the radiation field in the sense that the instantaneous probability of the photoelectron emission is proportional to the classical instantaneous intensity $|V(\underline{r},z_2,t)|^2$ of the light as long as the intensity of the light is not so strong that the photoelectron emission cannot be described by the first-order perturbation theory. The output of the detector is a sequence $\{t_i\}$ of time-instants of absorption-emission phenomena. These instants $\{t_i\}$ are random and constitute a point process. If we observe this process for a fixed time interval $[t,t+T]$, a total number n of photoelectrons will be ejected from the area A of the photosensitive surface. The sequence $t_1,t_2, \ldots , t_i$ of instants when the photoelectrons are emitted can be written symbolically as $\{t_i\}$. When the total energy received from that area A during the interval $[t,t+T]$ is given, the probability that n photoelectrons are ejected is a Poisson function:

$$P(n \mid \lambda_T(t)) = (\lambda_T(t))^n \exp(-\lambda_T(t)) \; / \; n! \quad , \qquad (1.15)$$

where

$$\lambda_T(t) = \alpha \int_A \int_t^{t+T} |V(\underline{r},t_1)|^2 \, dt_1 \, d^2\underline{r} \qquad (1.16)$$

is the average number of photoelectrons and can be predicted if the coefficient α is given. α is proportional directly to the quantum efficiency and inversely to the energy $h\Omega/2\pi$ of each quantum of light, where h is the Planck's constant and Ω is the angular frequency of the field. $V(\underline{r},t)$ is the complex amplitude of the light field at the point $\underline{r}$ of the photosensitive surface at time t. Since $V(\underline{r},t)$ is a stochastic process, so is the number $\lambda_T(t)$. The probability for n photoelectrons in any counting interval [t,t+T] can then be expressed only by the ensemble average[10] of the conditional probability $p(n|\lambda_T(t))$. That is,

$$P_n(T,t) = \langle (\lambda_T(t))^n \exp(-\lambda_T(t)) \; / \; n! \rangle \quad . \qquad (1.17)$$

The derivation[11,12] of (1.15) is well known and will not be given here. The operation of the expectation on the probability from (1.17) makes it depart from the Poisson distribution. For a stationary process, the ensemble average is independent of the initial time t. We will use the expression $P_n(T)$ to replace $P_n(T,t)$ in (1.17) from now on.

Distribution of the photoelectrons from a single small area when the time-bandwidth product TW >> 1

When linearly polarized light impinges normally on the photosensitive surface, the probability that a number n_i photoelectrons are emitted from a small area dA_i centered at point $\underset{\sim}{r}_i$ during an interval (0,T) can be written according to (1.17) as

$$P_{n_i}(T) = \langle \lambda_i^{n_i} \exp(-\lambda_i) \; / \; n_i! \rangle \quad , \tag{1.18}$$

where

$$\lambda_i = \alpha \int_0^T \iint_{dA_i} |V(\underset{\sim}{r},t)|^2 \, dt \, d^2\underset{\sim}{r}$$

$$= \alpha \int_0^T \iint_A f_i(\underset{\sim}{r}) \; |V(\underset{\sim}{r},t)|^2 \, dt \, d^2\underset{\sim}{r} \tag{1.19}$$

with $f_i(\underset{\sim}{r})$ as the function defined by

$$\begin{aligned} f_i(\underset{\sim}{r}) &= 1 \quad , && \underset{\sim}{r} \in dA_i \\ &= 0 \quad , && \underset{\sim}{r} \notin dA_i \quad . \end{aligned} \tag{1.20}$$

A is the entire area of the surface. λ_i depends on the coefficient α, the size dA_i and the amplitude $|V(\underset{\sim}{r},t)| \in dA_i$. The distribution of the random variable n_i can also be derived from its moment generating function (m.g.f.), which is the ensemble average of the conditional m.g.f. with given λ_i. That is,

$$h_i(s) = \left\langle E[\exp(sn_i) \mid \lambda_i] \right\rangle$$

$$= \left\langle \sum_{n_i=0}^{\infty} \exp(sn_i)\ \lambda_i^{n_i}\ e^{-\lambda_i} / n_i! \right\rangle$$

$$= \left\langle \exp[\lambda_i(e^s-1)] \right\rangle \quad . \tag{1.21}$$

Now

$$\lambda_i(e^s-1) = \alpha \int_0^T \int_A f_i(\underline{x})(e^s-1)\ |V(\underline{x},t)|^2\ dt\ d^2\underline{x}$$

$$= \int_0^T \int_0^T \int_A \int_A K_i(\underline{x}_1,\underline{x}_2:t_1,t_2)\ V(\underline{x}_1,t_1)\ V^*(\underline{x}_2,t_2)\ dt_1 dt_2 d^2\underline{x}_1 d^2\underline{x}_2 \ , \tag{1.22}$$

where the kernel

$$K_i(\underline{x}_1,\underline{x}_2:t_1,t_2) = F_i(s:\underline{x}_1)\ \delta(\underline{x}_1-\underline{x}_2)\ \delta(t_1-t_2) \quad , \tag{1.23}$$

and

$$F_i(s:\underline{x}_1) = \alpha(e^s-1)\ f_i(\underline{x}_1) \quad . \tag{1.24}$$

The m.g.f. from (1.21) can be worked out as in the problem of finding the m.g.f. of a quadratic functional of a circular Gaussian random process[4,13]. One can show that $h_i(s)$ can be determined from the expression

$$h_i(s) = \exp\left[\int_0^1 du \int_0^T \int_A L(\underline{x},t,\underline{x},t:-u)\, dt\, d^2\underline{x}\right] , \qquad (1.25)$$

where $L(\underline{x}_1,t_1,\underline{x}_2,t_2:u)$ can be solved[4,14] from the following integral equation

$$L(\underline{x}_1,t_1,\underline{x}_2,t_2:u) + 2u \int_0^T \int_0^T \int_A \int_A d^2\underline{y}_1\, d^2\underline{y}_2\, dh_1\, dh_2$$

$$\cdot K_i(\underline{x}_1,\underline{y}_1:t_1,h_1)\, \Gamma(\underline{y}_1,\underline{y}_2,h_1,h_2)\, L(\underline{y}_2,h_2,\underline{x}_2,t_2:u)$$

$$= 2 \int_0^T \int_A K_i(\underline{x}_1,\underline{y}_1:t_1,h_1)\, \Gamma(\underline{y}_1,\underline{x}_2,h_1,t_2)\, d^2\underline{y}_1\, dh_1 . \qquad (1.26)$$

For spectrally pure light, the autocovariance function can be written according to (1.7) as

$$\Gamma(\underline{x}_1,\underline{x}_2,t_1,t_2) = \phi(\underline{x}_1,\underline{x}_2)\, \chi(t_1-t_2) . \qquad (1.27)$$

Thus, substituting (1.23), (1.24) and (1.27) into (1.26) and solving for $L(\underline{x}_1,t_1,\underline{x}_2,t_2:u)$ recursively we have

$$L(\underline{x}_1,t_1,\underline{x}_2,t_2:u) = 2F_i(s:\underline{x}_1)\, \phi(\underline{x}_1,\underline{x}_2)\, \chi(t_1-t_2)$$

$$-u\, 2^2 \int_0^T \int_A d^2\underline{y}_2\, dh_2\, F_i(s:\underline{x}_1)\, \phi(\underline{x}_1,\underline{y}_2)\, \chi(t_1-h_2)$$

$$F_i(s:\underline{y}_2)\, \phi(\underline{y}_2,\underline{x}_2)\, \chi(h_2-t_2)$$

$$+ u^2 2^3 \int_0^T \int_0^T \int_A \int_A d^2\underline{y}_2 d^2\underline{y}_3 \, dh_2 dh_3 \, F_i(s:\underline{x}_1) \, \phi(\underline{x}_1,\underline{y}_2)$$

$$\cdot \chi(t_1-h_2) \, F_i(s:\underline{y}_2) \, \phi(\underline{y}_2,\underline{y}_3) \, \chi(h_2-h_3) \, F_i(s:\underline{y}_3) \, \phi(\underline{y}_3,\underline{x}_2) \, \chi(h_3-t_2)$$

$$+ \ldots\ldots \qquad (1.28)$$

By substituting (1.28) into (1.25) we can write the logarithm of the m.g.f. as

$$\ell n \, h_i(s) = 2\chi(0) \, T \int_A F_i(s:\underline{x}) \, \phi(\underline{x},\underline{x}) \, d^2\underline{x}$$

$$+ \frac{1}{2} (2T)^2 \int_A \int_A F_i(s:\underline{x}) \, F_i(s:\underline{y}_1) \, \phi(\underline{x},\underline{y}_1) \, \phi(\underline{y}_1,\underline{x}) \, d^2\underline{x} \, d^2\underline{y}_1$$

$$\cdot T^{-2} \int_0^T \int_0^T \chi(t-h_1) \, \chi(h_1-t) \, dt \, dh_1$$

$$+ \frac{1}{3} (2T)^3 \int_A \int_A \int_A F_i(s:\underline{x}) \, F_i(s:\underline{y}_1) \, F_i(s:\underline{y}_2) \, \phi(\underline{x},\underline{y}_1) \, \phi(\underline{y}_1,\underline{y}_2) \, \phi(\underline{y}_2,\underline{x})$$

$$\cdot d^2\underline{x} \, d^2\underline{y}_1 \, d^2\underline{y}_2 \, T^{-3} \int_0^T \int_0^T \int_0^T \chi(t-h_1) \, \chi(h_1-h_2) \, \chi(h_2-t) \, dt dh_1 dh_2$$

$$+ \ldots \frac{1}{\ell} (2T)^\ell \int_A \ldots \int_A F_i(s:\underline{x}) \, F_i(s:\underline{y}_1) \ldots F_i(s:\underline{y}_{\ell-1}) \phi(\underline{x},\underline{y}_1) \phi(\underline{y}_1,\underline{y}_2)$$

$$\ldots \phi(\underline{y}_{\ell-1},\underline{x}) \, d^2\underline{x} d^2\underline{y}_1 \ldots d^2\underline{y}_{\ell-1} \, T^{-\ell} \int_0^T \ldots \int_0^T \chi(t-h_1) \ldots \chi(h_{\ell-1}-t) dt dh_1$$

$$\ldots d \, h_{\ell-1} + \ldots\ldots$$

$$= 2 \, \chi(0) \, T \int_A F_i(s:\underline{x}) \, \phi(\underline{x},\underline{x}) \, d^2\underline{x}$$

$$+\sum_{\ell\geq 2}\frac{1}{\ell}\,(2T)^{\ell}\int_{A}\cdots\int_{A}F_i(s:\underset{\sim}{x})F_i(s:\underset{\sim}{y}_1)\cdots F_i(s:\underset{\sim}{y}_{\ell-1})\phi(\underset{\sim}{x},\underset{\sim}{y}_1)\phi(\underset{\sim}{y}_1,\underset{\sim}{y}_2)$$

$$\cdots\phi(\underset{\sim}{y}_{\ell-1},\underset{\sim}{x})\;d^2\underset{\sim}{x}d^2\underset{\sim}{y}_1\cdots d^2\underset{\sim}{y}_{\ell-1}\cdot P_{\ell}\;, \tag{1.29}$$

where

$$P_{\ell}=T^{-\ell}\int_0^T\int_0^T\cdots\int_0^T\chi(h_1-h_2)\chi(h_2-h_3)\cdots\chi(h_{\ell}-h_1)dh_1dh_1\cdots dh_{\ell}\;,$$

$$\ell\geq 2\;. \tag{1.30}$$

Now the bandwidth W is defined[15] by

$$W=|\chi(0)|^2\left[\int_{-\infty}^{\infty}|\chi(t)|^2\,dt\right]^{-1}=\left[\int_{-\infty}^{\infty}|x(\Omega)|^2\,d\Omega/2\pi\right]^{-1}\;, \tag{1.31}$$

$$\text{as } \chi(0)=1\;,$$

where

$$x(\Omega)=\int_{-\infty}^{\infty}\chi(t)\,e^{-i\Omega t}\,dt \tag{1.32}$$

is the temporal spectral density of the complex field at the image plane and is real so that $\chi(\tau)=\chi^{*}(-\tau)$. We now let

$$h_1-h_2=t_1\;,$$

$$h_2-h_3=t_2\;,$$

$$\cdots\cdots$$

$$h_{\ell-1} - h_\ell = t_{\ell-1} ,$$

$$h_\ell - h_1 = -(t_1 + t_2 \ldots t_{\ell-1}) \quad . \tag{1.33}$$

When $T >> \frac{1}{W}$ we can extend the range of integration to $(-\infty,\infty)$ and by changing variables we can write (1.30) as

$$P_\ell = T^{-\ell+1} \int_{-\infty}^{\infty} \int_{-\infty}^{\infty} \ldots \int_{-\infty}^{\infty} \chi(t_1)\chi(t_2) \ldots \chi(-t_1-t_2 \ldots t_{\ell-1}) dt_1 dt_2 \ldots dt_{\ell-1} .$$

(1.34)

According to the convolution theorem[16] we have

$$\int_{-\infty}^{\infty} \chi(t_1)\ \chi(-t_1-t_2 \ldots -t_{\ell-1})\ dt_1$$

$$= \int_{-\infty}^{\infty} x^2(\Omega)\ \exp[-i\Omega(t_2+t_3+ \ldots t_{\ell-1})]\ d\Omega/2\pi \ . \tag{1.35}$$

By substituting (1.31), (1.32) and (1.35) into (1.34) we have

$$P_\ell = T^{-\ell+1} \int_{-\infty}^{\infty} x^2(\Omega)\ \frac{d\Omega}{2\pi} \int_{-\infty}^{\infty} \ldots \int_{-\infty}^{\infty} \chi(t_2) \ldots \chi(t_{\ell-1})$$

$$\cdot \exp[-i\Omega(t_2+t_3 \ldots t_{\ell-1})]\ dt_2 \ldots dt_{\ell-1}$$

$$= T^{-\ell+1} \int_{-\infty}^{\infty} x^\ell(\Omega)\ d\Omega/2\pi$$

$$= (TW)^{-\ell+1}\ R_I \quad . \tag{1.36}$$

where

$$R_I = \int_{-\infty}^{\infty} x^{\ell}(\Omega)\,\frac{d\Omega}{2\pi} \Big/ \left[\int_{-\infty}^{\infty} x^{2}(\Omega)\,\frac{d\Omega}{2\pi}\right]^{\ell-1}. \tag{1.37}$$

As $WT >> 1$, we can approximately write $x(\Omega) \sim \frac{1}{W}$ for $\Omega \in (-\pi W, \pi W)$ and $x(\Omega) = 0$ otherwise. Thus $R_I \sim 1$ is finite and $P_\ell \to 0$ for $\ell \geq 2$. For spatially slowly varying light and small area dA_i we define

$$\begin{aligned}\bar{n}_i &= 2\alpha T \int_{dA_i} \phi(\underset{\sim}{x},\underset{\sim}{x})\, d^2\underset{\sim}{x} \\ &\simeq 2\alpha T\, \phi(\underset{\sim}{x}_i,\underset{\sim}{x}_i)\, dA_i\,,\end{aligned} \tag{1.38}$$

as the average number of photoelectrons ejected from the small area dA_i centered as $\underset{\sim}{x}_i$. Since for the spatial coherence function

$$|\phi(\underset{\sim}{x}_i,\underset{\sim}{x}_j)| \leq \phi(\underset{\sim}{x}_i,\underset{\sim}{x}_i)\,, \quad \text{for all } i \neq j,$$

$$\begin{aligned}&\Big|\int_A\int_A \cdots F_i(s:\underset{\sim}{x})\phi(\underset{\sim}{x},\underset{\sim}{y}_1)F_i(s:\underset{\sim}{y}_1)\phi(\underset{\sim}{y}_1,\underset{\sim}{y}_2)\cdots \\ &\quad F_i(s:\underset{\sim}{y}_{\ell-1})\phi(\underset{\sim}{y}_{\ell-1},\underset{\sim}{x})\, d^2\underset{\sim}{x}d^2\underset{\sim}{y}_1 \cdots d^2\underset{\sim}{y}_{\ell-1}\Big| \\ &\leq \Big|\int_A F_i(s:\underset{\sim}{x})\phi(\underset{\sim}{x},\underset{\sim}{x})\Big|^{\ell}.\end{aligned} \tag{1.39}$$

Thus as long as $\bar{n}_i$ defined by (1.38) is not too large, all the terms

in (1.29) for $\ell \geq 2$ are negligible by comparing with the first term as WT >> 1. That is

$$\ell n\, h_i(s) \simeq \bar{n}_i(e^s - 1)\,, \tag{1.40}$$

which is the logarithm of the m.g.f. of a Poisson distribution[17] with mean $\bar{n}_i$.

Distribution of the photoelectrons from two small areas for TW >> 1

When the energy received by each of the two small areas dA_1 and dA_2 centered at $\underset{\sim}{x}_1$ and $\underset{\sim}{x}_2$ is given, the numbers of photoelectrons n_1 and n_2 ejected from these areas during the time interval $[t,t+T]$ are Poisson distributed with the given mean values λ_i for $i = 1, 2$ defined in (1.19) and are statistically independent. The joint m.g.f. of the random variables n_1 and n_2 can be derived from the expected value of the conditional m.g.f.:

$$h_{12}(s_1,s_2) = \left\langle E[e^{s_1 n_1 + s_2 n_2} \mid \lambda_i,\ i=1,2] \right\rangle$$

$$= \left\langle \exp[\lambda_1(e^{s_1}-1) + \lambda_2(e^{s_2}-1)] \right\rangle , \qquad (1.41)$$

where now

$$\lambda_1(e^{s_1}-1) + \lambda_2(e^{s_2}-1)$$

$$= \alpha \int_0^T dt \int_A d^2\underset{\sim}{x}[f_1(\underset{\sim}{x})(e^{s_1}-1)+f_2(\underset{\sim}{x})(e^{s_2}-1)]\,|V(\underset{\sim}{x},t)|^2$$

$$= \int_0^T \int_0^T \int_A \int_A dt_1 dt_2 d^2\underset{\sim}{x}_1 d^2\underset{\sim}{x}_2 K_{12}(\underset{\sim}{x}_1,\underset{\sim}{x}_2:t_1,t_2)V(\underset{\sim}{x}_1,t_1)V^*(\underset{\sim}{x}_2,t_2) ,$$

(1.42)

where $f_i(\underset{\sim}{x})$ for $i = 1$ or 2 is given by (1.20) and

$$K_{12}(\underset{\sim}{x}_1,\underset{\sim}{x}_2:t_1,t_2) = F_{12}(s_1,s_2:\underset{\sim}{x}_1)\delta(\underset{\sim}{x}_1-\underset{\sim}{x}_2)\delta(t_1-t_2), \tag{1.43}$$

with

$$F_{12}(s_1,s_2:\underset{\sim}{x}_1) = \alpha f_1(\underset{\sim}{x}_1)(e^{s_1}-1)+\alpha f_2(\underset{\sim}{x}_1)(e^{s_2}-1). \tag{1.44}$$

The m.g.f. can also be expressed in the form of (1.25) and the following integral equation must be satisfied.

$$L_{12}(\underset{\sim}{x}_1,t_1,\underset{\sim}{x}_2,t_2:u)+2u\int_0^T\int_A F_{12}(s_1,s_2:\underset{\sim}{x}_1)\phi(\underset{\sim}{x}_1,t_1,\underset{\sim}{y}_2,h_2)$$

$$\cdot L_{12}(\underset{\sim}{y}_2,h_2,\underset{\sim}{x}_2,t_2:u)d^2\underset{\sim}{y}_2dh_2$$

$$= F_{12}(s_1,s_2:\underset{\sim}{x}_1)\phi(\underset{\sim}{x}_1,t_1,\underset{\sim}{x}_2,t_2). \tag{1.45}$$

The kernel $L_{12}(\underset{\sim}{x}_1,t_1,\underset{\sim}{x}_2,t_2:u)$ is solved for recursively and substituted into the joint m.g.f. as described before where $K_i(\underset{\sim}{x}_1,\underset{\sim}{x}_2:t_1,t_2)$ and $F_i(s:\underset{\sim}{x}_1)$ in (1.23) and (1.24) are now replaced by $K_{12}(\underset{\sim}{x}_1,\underset{\sim}{x}_2:t_1,t_2)$ and $F_{12}(s_1,s_2:\underset{\sim}{x}_1)$. We have

$$\ell n\, h_{12}(s_1,s_2) = 2\chi(0)T\int_A F_{12}(s_1,s_2:\underset{\sim}{x})\phi(\underset{\sim}{x},\underset{\sim}{x})\, d^2\underset{\sim}{x}$$

$$+\frac{1}{2}(2T)^2\int_A\int_A d^2\underset{\sim}{x}d^2\underset{\sim}{y}_1\, F_{12}(s_1,s_2:\underset{\sim}{x})F_{12}(s_1,s_2:\underset{\sim}{y}_1)$$

$$\cdot\phi(\underset{\sim}{x},\underset{\sim}{y}_1)\phi(\underset{\sim}{y}_1,\underset{\sim}{x})\, P_2$$

$$+\frac{1}{3}(2T)^3\int_A\int_A\int_A d^2\underset{\sim}{x}d^2\underset{\sim}{y}_1d^2\underset{\sim}{y}_2\,F_{12}(s_1,s_2:\underset{\sim}{x})\,F_{12}(s_1,s_2:\underset{\sim}{y}_1)$$

$$\cdot F_{12}(s_1,s_2:\underset{\sim}{y}_2)\phi(\underset{\sim}{x},\underset{\sim}{y}_1)\phi(\underset{\sim}{y}_1,\underset{\sim}{y}_2)\phi(\underset{\sim}{y}_2,\underset{\sim}{x})\,P_3$$

$$+\ldots\ldots+\frac{1}{\ell}(2T)^{\ell}\int_A\cdots\int_A d^2\underset{\sim}{x}d^2\underset{\sim}{y}_1\cdots d^2\underset{\sim}{y}_{\ell-1}\,F_{12}(s_1,s_2:\underset{\sim}{x})$$

$$F_{12}(s_1,s_2:\underset{\sim}{y}_1)\cdots F_{12}(s_1,s_2:\underset{\sim}{y}_{\ell-1})\phi(\underset{\sim}{x},\underset{\sim}{y}_1)\phi(\underset{\sim}{y}_1,\underset{\sim}{y}_2)\cdots\phi(\underset{\sim}{y}_{\ell-1},\underset{\sim}{x})\,P_{\ell} \tag{1.46}$$

$$+\ldots\ldots$$

where P_{ℓ} for $\ell \geq 2$ is given by (1.30). By the same argument, that is, when the average numbers n_i defined in (1.38) for $i = 1, 2$ are not too large and $WT >> 1$, (1.46) can be approximated by the first term or

$$\ell n\, h_{12}(s_1,s_2) \simeq 2T\int_A F_{12}(s_1,s_2:\underset{\sim}{x})\phi(\underset{\sim}{x},\underset{\sim}{x})d^2\underset{\sim}{x}$$

$$\simeq 2\alpha T dA_1\,\phi(\underset{\sim}{x}_1,\underset{\sim}{x}_1)(e^{s_1}-1) + 2\alpha T dA_2\,\phi(\underset{\sim}{x}_2,\underset{\sim}{x}_2)(e^{s_2}-1)$$

$$= \bar{n}_1(e^{s_1}-1) + \bar{n}_2(e^{s_2}-1)\,. \tag{1.47}$$

Since $\ell n\, h_i(s_i) = \bar{n}_i(e^{s_i}-1)$ for $i = 1, 2$ as given by (1.40), this implies that the joint m.g.f. $h_{12}(s_1,s_2)$ is the product of the m.g.f.'s $h_1(s_1)$ and $h_2(s_2)$ as $TW >> 1$. In other words, the number of

photoelectrons ejected from areas dA_1 and dA_2 during any observation interval are Poisson distributed and statistically independent of each other when the time-bandwidth product is large.

Distribution of the sum of the photoelectrons from a large number of small areas when WT >> 1

When there are a large number N of small areas $d\underset{\sim}{A}_i$ for i = 1, 2 . . . N, the distribution of the sum of the photoelectrons from these areas can be derived in the same way just described as for N = 2. For generalization, we discuss the distribution of a statistic given by

$$Y = \sum_{i=1}^{N} n_i \beta(\underset{\sim}{x}_i) , \tag{1.48}$$

where $\underset{\sim}{x}_i$ is the center of each small area dA_i where n_i photoelectrons are ejected. $\beta(\underset{\sim}{x}_i)$ is a weighting function to characterize the location of n_i. For example, when $\beta(\underset{\sim}{x}_i) = 1$, Y is the sum of the photoelectrons ejected from the N small areas. As N is very large we will then pass to the limit as $dA_i \to 0$.

The m.g.f. of Y can be written as

$$\begin{aligned} h_Y(s) &= \left\langle E[\exp s \sum_{i=1}^{N} n_i \beta(\underset{\sim}{x}_i) \mid \underset{\sim}{\lambda}_i] \right\rangle \\ &= \left\langle \exp[\sum_{i=1}^{N} \lambda_i (e^{s\beta(\underset{\sim}{x}_i)} - 1)] \right\rangle , \end{aligned} \tag{1.49}$$

where

$$\sum_{i=1}^{N} \lambda_i (e^{s\beta(\underline{x}_1)} - 1)$$

$$= \alpha \sum_{i=1}^{N} (e^{s\beta(\underline{x}_1)} - 1) \int_0^T \int_{dA_i} |V(\underline{x},t)|^2 \, dt d^2\underline{x}$$

$$= \alpha \sum_{i=1}^{N} (e^{s\beta(\underline{x}_1)} - 1) \int_0^T \int_A f_i(\underline{x}) \, |V(\underline{x},t)|^2 \, dt \, d^2\underline{x}$$

$$= \int_0^T \int_0^T \int_A \int_A K_N(\underline{x}_1,\underline{x}_2:t_1,t_2) \, V(\underline{x}_1,t_1) \, V^*(\underline{x}_2,t_2)$$

$$\cdot dt_1 dt_2 d^2\underline{x}_1 d^2\underline{x}_2 \quad . \tag{1.50}$$

Now

$$K_N(\underline{x}_1,\underline{x}_2:t_1,t_2) = F_N(s,\underline{x}_1)\delta(\underline{x}_1-\underline{x}_2)\delta(t_1-t_2) \, , \tag{1.51}$$

with

$$F_N(s,\underline{x}_1) = \alpha \sum_{i=1}^{N} (e^{s\beta(\underline{x}_1)} - 1) \, f_i(\underline{x}_1) \, , \tag{1.52}$$

and $f_i(\underline{x}_1)$ is defined in (1.20).

We must first solve the integral equation

$$L_0(\underline{x}_1,t_1,\underline{x}_2,t_2:u) + 2u \int_0^T \int_A F_N(s,\underline{x}_1)\phi(\underline{x}_1,\underline{y}_2)\chi(t_2-h_2)$$

$$\cdot L_0(\underset{\sim}{y}_2, h_2, \underset{\sim}{x}_2, t_2 : u)\ d^2\underset{\sim}{y}_2\ dh_2$$

$$= 2\ \underset{\sim}{F}_N(s, \underset{\sim}{x}_1)\phi(\underset{\sim}{x}_1\underset{\sim}{x}_2)\chi(t_1 - t_2)\ . \tag{1.53}$$

Now

$$\int_A \underset{\sim}{F}_N(s, \underset{\sim}{x})\phi(\underset{\sim}{x}, \underset{\sim}{y})\ d^2\underset{\sim}{x}$$

$$= \alpha \sum_{i=1}^{N} (e^{s\beta(\underset{\sim}{x}_i)} - 1) \int_{dA_i} \phi(\underset{\sim}{x}, \underset{\sim}{y})\ d^2\underset{\sim}{x}$$

$$\simeq \alpha \sum_{i=1}^{N} (e^{s\beta(\underset{\sim}{x}_i)} - 1)\ \phi(\underset{\sim}{x}_i, \underset{\sim}{y})\ dA_i\ , \tag{1.54}$$

as $\phi(\underset{\sim}{x}, \underset{\sim}{y})$ is slowly varying spatially. When N is very large we can pass the limit as $dA_i \to 0$. (1.54) can be written as

$$\int_A \underset{\sim}{F}_N(s, \underset{\sim}{x})\ \phi(\underset{\sim}{x}, \underset{\sim}{y})\ d^2\underset{\sim}{x}$$

$$\simeq \alpha \int_A (e^{s\beta(\underset{\sim}{x})} - 1)\ \phi(\underset{\sim}{x}, \underset{\sim}{y})\ d^2\underset{\sim}{x}\ . \tag{1.55}$$

The logarithm of the m.g.f. can be obtained when the kernel $L_0(\underset{\sim}{x}_1, t_1, \underset{\sim}{x}_2, t_1 : u)$ is solved first recursively from (1.53) where (1.54) is substituted. We have

$$L_0(\underset{\sim}{x}_1, t_1, \underset{\sim}{x}_2, t_2 : u) \simeq 2\ \underset{\sim}{F}_N(s, \underset{\sim}{x}_1)\ \phi(\underset{\sim}{x}_1, \underset{\sim}{x}_2)\ \chi(t_1 - t_2)$$

$$- 2^2 \alpha u \, F_N(s,\underline{x}_1) \int_0^T \int_A dh_2 \, d^2\underline{y}_2$$

$$\cdot (e^{s\beta(\underline{y}_2)} - 1) \, \phi(\underline{x}_1,\underline{y}_2) \, \phi(\underline{y}_2,\underline{x}_2) \, \chi(t_1-h_2) \, \chi(h_2-t_2)$$

$$+ 2^3 (\alpha u)^2 \, F_N(s,\underline{x}_1) \int_0^T \int_0^T \int_A \int_A dh_2 \, dh_3 \, d^2\underline{y}_2 \, d^2\underline{y}_3$$

$$(e^{s\beta(\underline{y}_2)} - 1) \, (e^{s\beta(\underline{y}_3)} - 1) \, \phi(\underline{x}_1,\underline{y}_2) \, \phi(\underline{y}_2,\underline{y}_3) \, \phi(\underline{y}_3,\underline{x}_2)$$

$$\chi(t_1-h_2) \, \chi(h_2-h_3) \, \chi(h_3-t_2)$$

$$+ \ldots\ldots \qquad (1.56)$$

The logarithm of the m.g.f. can be derived as we pass to the limit $dA_i \to 0$ where (1.55) and (1.56) are used.

$$\ell n \, h_Y(s) = \int_0^1 du \int_0^T \int_A L_0(\underline{x},t,\underline{x},t;-u) \, dt \, d^2\underline{x}$$

$$\simeq 2\alpha\chi(0)T \int_A (e^{s\beta(\underline{x})} - 1) \, \phi(\underline{x},\underline{x}) \, d^2\underline{x}$$

$$+ \frac{1}{2} (2\alpha T)^2 \int_A \int_A d^2\underline{y}_1 \, d^2\underline{y}_2$$

$$\cdot (e^{s\beta(\underline{y}_1)} - 1) \, (e^{s\beta(\underline{y}_2)} - 1) \, \phi(\underline{y}_1,\underline{y}_2) \, \phi(\underline{y}_2,\underline{y}_1) \cdot P_2 + \ldots\ldots$$

$$+ \frac{1}{\ell} (2\alpha T)^\ell \int_A \int_A \ldots \int_A d^2\underline{y}_1 \, d^2\underline{y}_2 \ldots d^2\underline{y}_\ell$$

$$\cdot \left[\prod_{i=1}^{\ell} \left(e^{s\beta(\underline{x}_i)} - 1 \right) \right] \phi(\underline{x}_1, \underline{x}_2) \cdots \phi(\underline{x}_\ell, \underline{x}_1) \, P_\ell$$

$$+ \cdots \cdots \tag{1.57}$$

where P_ℓ for $\ell \geq 2$ is given by (1.30). As $WT >> 1$, $P_\ell \to 0$ for all $\ell \geq 2$, and by the same argument used in (1.39), all the terms in (1.57) except the first term become very small. Then we can approximate

$$\ell n \, h_Y(s) \simeq 2\alpha T \int_A \left(e^{s\beta(\underline{x})} - 1 \right) \phi(\underline{x}, \underline{x}) \, d^2\underline{x} \, , \tag{1.58}$$

or the m.g.f. of the statistic Y can be written approximately

$$h_Y(s) \simeq \exp \left[2\alpha T \int_A \left(e^{s\beta(\underline{x})} - 1 \right) \phi(\underline{x}, \underline{x}) \, d^2\underline{x} \right] , \tag{1.59}$$

where the mean and variance in general are

$$E[Y] = 2\alpha T \int_A \beta(\underline{x}) \, \phi(\underline{x}, \underline{x}) \, d^2\underline{x} \, ,$$

$$Var[Y] = 2\alpha T \int_A \beta^2(\underline{x}) \, \phi(\underline{x}, \underline{x}) \, d^2\underline{x} \, . \tag{1.60}$$

For $\beta(\underline{x}) = 1$, (1.59) becomes

$$h_Y(s) \simeq \exp \left[2\alpha T \int_A \phi(\underline{x}, \underline{x}) \, d^2\underline{x} \, (e^s - 1) \right] , \tag{1.61}$$

which is the m.g.f. of a Poisson distribution with equal cumulants $2\alpha T \int_A \phi(\underset{\sim}{x},\underset{\sim}{x})\, d^2\underset{\sim}{x}$ for all orders.

On the other hand, as we expand

$$(e^{s\beta(\underset{\sim}{x})}-1) = \sum_{m=1}^{\infty} (s\beta(\underset{\sim}{x}))^m / m! \quad , \tag{1.62}$$

if

$$\frac{1}{m!}\int_A \beta^m(\underset{\sim}{x})\, \phi(\underset{\sim}{x},\underset{\sim}{x})\, d^2\underset{\sim}{x} \ll \frac{1}{2}\int_A \beta^2(\underset{\sim}{x})\, \phi(\underset{\sim}{x},\underset{\sim}{x})\, d^2\underset{\sim}{x}$$

$$\text{for } m \geq 3 \quad , \tag{1.63}$$

we can further approximate (1.59) as

$$h_Y(s) \simeq \exp\left[2\alpha T \int_A s\,\beta(\underset{\sim}{x})\, \phi(\underset{\sim}{x},\underset{\sim}{x})\, d^2\underset{\sim}{x} + 2\alpha T \int_A s^2 \beta^2(\underset{\sim}{x})\, \phi(\underset{\sim}{x},\underset{\sim}{x})\, d^2\underset{\sim}{x} \right], \tag{1.64}$$

which is the m.g.f. of a Gaussian distribution.

Footnotes

Chapter 1

1. Helstrom [10], Chapter II, pp. 65-73.
2. Goodman [11], p. 58.
3. Goodman [11], p. 108.
4. Helstrom [10], Chapter XI, p. 375.
5. Wolf [12].
6. Mandel and Wolf [1].
7. Mandel [13].
8. Helstrom [14], pp. 165-166.
9. Helstrom [3], eq. (2).
10. Mandel [15], eq. (69).
11. Mandel [15], Appendix B.
12. Bar-David [16].
13. Siegert [4].
14. Helstrom [17], Appendix.
15. Helstrom [18], eq. (1.6).
16. Papoulis [19], p. 27.
17. Mandel [2].

Chapter II Binary detection of an optical signal at a photosensitive surface

Two important criteria, Bayes and Neyman-Pearson, used in the simple hypothesis test for binary detection will be briefly described. The optical signal is detected by using the photoelectric detector. The photosensitive surface of the device is divided like a mosaic into many small equal areas so that the observed data $\underset{\sim}{n}$ are the set of numbers of photoelectrons ejected from all the small areas. The optimum statistic[1] obtained from the likelihood ratio in the presence of the uniform background light will be discussed and its moment-generating function (m.g.f.) will be derived. Because of the complexity of the m.g.f., the distribution of the optimum statistic will be approximated by the method of steepest descent[2] and compared with two other approximate forms, the Gaussian and gamma distributions. The detection of the optical signal in the absence of the background light will also be discussed. Two other detectors, the threshold and the simple detector, will be studied. In order to investigate the performances of these detectors, a Gaussian image will be postulated and the false-alarm probability, the detection probability, and the average error probability will be calculated.

Binary hypothesis test

In a communication system when a set of data $\underset{\sim}{b} = \{b_1, b_2 \ldots b_N\}$ is observed, the decision between binary hypotheses[3,4] H_0 and H_1, where H_0 is the hypothesis of background noise alone and H_1 is the hypothesis that a signal is also present, can be viewed as a rule for dividing the total N-dimensional observation space Σ of the data $\underset{\sim}{b}$ into two regions, Σ_0 and Σ_1. Hypothesis H_0 will be chosen if the observed data $\underset{\sim}{b}$ fall in the region Σ_0; H_1 will be chosen otherwise. The joint conditional probability density function (p.d.f.) $P(\underset{\sim}{b}|H_k)$ under H_k for k = 0 or 1 is to be given, and the likelihood ratio defined by

$$\Lambda(\underset{\sim}{b}) = \frac{P(\underset{\sim}{b}|H_1)}{P(\underset{\sim}{b}|H_0)} \tag{2.1}$$

will be calculated. If the Bayes criterion is used, a decision level defined by

$$\Lambda_0 = \frac{\xi[C_{10} - C_{00}]}{(1-\xi)[C_{01} - C_{11}]} \tag{2.2}$$

can be evaluated, where the prior probability ξ of hypothesis H_0 and the costs C_{ij} of choosing hypothesis H_i when H_j happens to be true (i,j = 0,1), are given. The regions Σ_0 and Σ_1 are divided in such a way that Σ_0 contains all the data for $\Lambda(\underset{\sim}{b}) \leq \Lambda_0$ and Σ_1 for $\Lambda(\underset{\sim}{b}) > \Lambda_0$. The false-alarm probability and the detection probability are defined as

$$Q_0 = \Pr[\Lambda(\underline{b}) > \Lambda_0 | H_0] = \int_{\Sigma_1} P(\underline{b}|H_0)d\underline{b} ,$$

$$Q_d = \Pr[\Lambda(\underline{b}) > \Lambda_0 | H_1] = \int_{\Sigma_1} P(\underline{b}|H_1)d\underline{b} . \qquad (2.3)$$

When there is no information about the prior probability ξ and the cost functions, the appropriate way to make the decision according to the Neyman-Pearson criterion is that the false-alarm probability Q_0 will not exceed the preassigned value. The decision level Λ_0 must be solved from the expression of Q_0 by (2.3), and the hypothesis H_1 or H_0 will be selected according as $\Lambda(\underline{b}) > \Lambda_0$ or $\Lambda(\underline{b}) \leq \Lambda_0$.

If $\underline{b}$ is a set of discrete random variables, the likelihood ratio $\Lambda(\underline{b})$ defined in (2.1) will be the ratio of the probabilities $P(\underline{b}|H_1)$ and $P(\underline{b}|H_0)$. When the Neyman-Pearson criterion is used, randomization[3] must be applied. That is, a probability f of choosing H_1 must be assigned at $\Lambda(\underline{b}) = \Lambda_0$ so that the false-alarm probability

$$Q_0 = \Pr[\Lambda(\underline{b})>\Lambda_0 | H_0] + f \Pr[\Lambda(\underline{b})=\Lambda_0 | H_0]$$

$$= \sum_{\Lambda(\underline{b})>\Lambda_0} P(\underline{b}|H_0) + f P(\underline{b}:\Lambda(\underline{b})=\Lambda_0 | H_0) \qquad (2.4)$$

equals exactly the preassigned value. For given Q_0, both Λ_0 and f can be solved from (2.4) and will be discussed later for Poisson distribution. Hypothesis H_1 or H_0 will be chosen for $\Lambda(\underline{b}) > \Lambda_0$ or $\Lambda(\underline{b}) < \Lambda_0$. The detection probability for the correct decision can be evaluated in the same way after the decision level Λ_0 and probability f are obtained. That is,

$$Q_d = \sum_{\Lambda(\underset{\sim}{b})>\Lambda_0} P(\underset{\sim}{b}|H_1) + f\,P(\underset{\sim}{b}:\Lambda(\underset{\sim}{b}) = \Lambda_0|H_1). \tag{2.5}$$

The average error probability for each decision is defined by

$$P_e = \xi Q_0 + (1-\xi)(1-Q_d). \tag{2.6}$$

If the relative costs $C_{10} - C_{00}$ and $C_{01} - C_{11}$ given in (2.2) are equal, the hypothesis H_k with greater posterior probability $P(H_k|\underset{\sim}{b})$ for $k = 0$ or 1 is always selected when the Bayes criterion is used and the error probability P_e given by (2.6) is minimized[3].

The reliability and error probability are used to measure the performance of the detectors. One detector is said to be better than the other detector if for a fixed value Q_0, the former has higher detection probability and hence smaller error probability.

The operation of the hypothesis test for binary detection can best be described by the block diagram on the next page. The selection of the Bayes or the Neyman-Pearson criterion depends on the information about the system we have and its application. The block labeled "computer" implies that certain numerical calculations will be involved so that the decision level Λ_0, the reliability $\{Q_0, Q_d\}$ or the error probability P_e can be calculated.

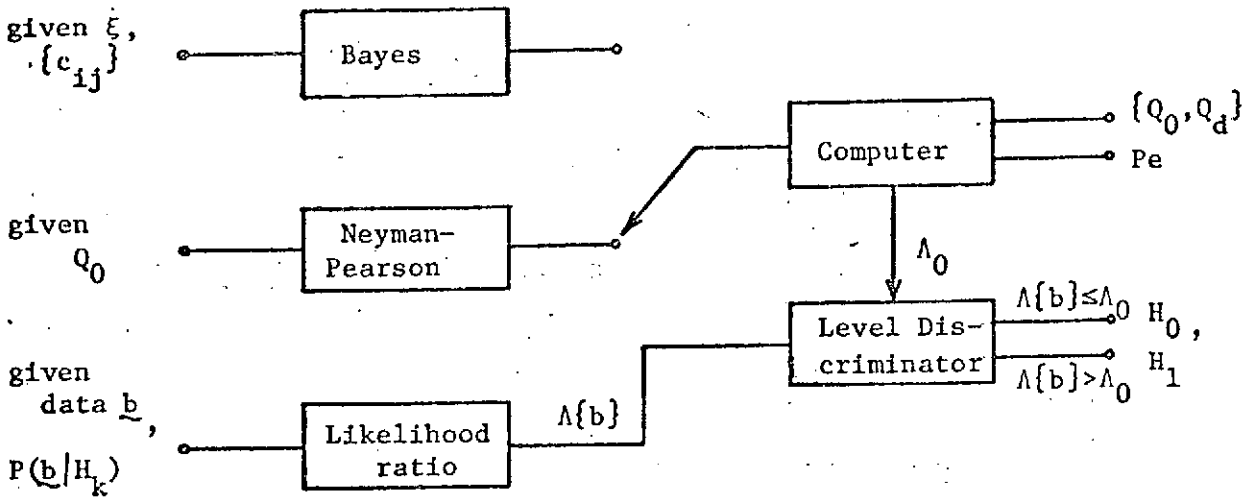

Figure 2 Block diagram of hypothesis test for binary detection.

The ideal photoelectric detector

When a luminous object is located in the field of view of an optical detector and focused on the photosensitive surface, the photoelectrons emitted from the surface will be proportional to the intensity of the object light, which is a fluctuating function of time as discussed in Chapter I. If there is also background light incident through the aperture, the information carried by the object light will be corrupted. As the intensity of the object light is not much stronger than the background light, in order to decide whether a certain luminous object is present or not, we can use strategies according to the hypothesis tests which we have just discussed. The basic elements of the optical detector have been shown in Fig. 1, where the photoelectrical emission surface of the photo-tube is placed in the image plane and is divided like a mosaic with a large number N of small equal areas dA_i as shown in Fig. 3.

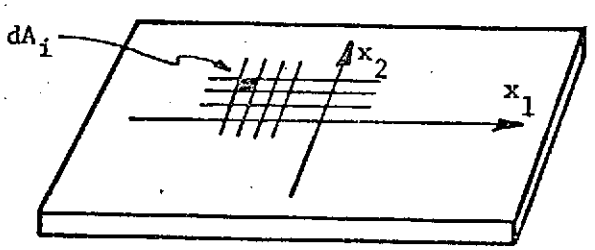

Figure 3 Photoelectrical emission surface

The received data are the values $\underset{\sim}{n} = \{n_1, n_2 \ldots n_N\}$ obtained by measuring the numbers n_i of photoelectrons ejected from each area $dA_i = dA$ for $i = 1, 2 \ldots N$ during the interval $(0,T)$. Since the background light in general also enters the aperture, the observer must choose between the two hypotheses: (H_0) only background light is present, or (H_1) object light is also incident through the aperture in addition to the background light. When the observation time T is much greater than W^{-1}, the numbers n_i of photoelectrons emitted from each area dA_i under hypothesis H_k $(k = 0, 1)$ are Poisson distributed and statistically independent of each other as discussed in Chapter I. The probability is given by

$$P_{n_i}(T|H_k) = \bar{n}_{ik}^{\,n_i} \; e^{-\bar{n}_{ik}} / n_i! \quad , \tag{2.7}$$

where $\bar{n}_{ik}$ is the average number of photoelectrons emitted during the interval $(0,T)$ for $k = 0, 1$ from the ith area dA_i and

$$\bar{n}_{ik} = \alpha T dA \; I_k(\underset{\sim}{x}_i) \quad , \quad k = 0, 1 \tag{2.8}$$

with

$$I_k(\underset{\sim}{x}_i) = 2 \, \phi_k(\underset{\sim}{x}_i, \underset{\sim}{x}_i) \quad , \quad k = 0, 1 \tag{2.9}$$

when (1.38) is used. $\phi_k(\underset{\sim}{x}_i, \underset{\sim}{x}_j)$ is the spatial coherence function under hypothesis H_k for $k = 0, 1$ at point $\underset{\sim}{x}_i$ and point $\underset{\sim}{x}_j$. $I_k(\underset{\sim}{x}_i)$ is the

mean intensity at point $\underset{\sim}{x}_i$. The joint conditional probability for observing the data $\underset{\sim}{n}$ under hypothesis H_k for k = 0 or 1 is

$$P_{\underset{\sim}{n}}(T|H_k) = \prod_{i=1}^{N} P_{n_i}(T|H_k)$$

$$= \prod_{i=1}^{N} \bar{n}_{ik}^{\,n_i} \; e^{-\bar{n}_{ik}} / n_i! \; . \qquad (2.10)$$

The likelihood ratio defined by (2.1) becomes

$$\Lambda\{\underset{\sim}{n}\} = P_{\underset{\sim}{n}}(T|H_1) \; / \; P_{\underset{\sim}{n}}(T|H_0)$$

$$= \prod_{i=1}^{N} \left(\frac{\bar{n}_{i1}}{\bar{n}_{i0}} \right)^{n_i} \; e^{-\bar{n}_{i1} + \bar{n}_{i0}} \; , \qquad (2.11)$$

and will be compared with the decision level Λ_0 according to the Bayes strategy or Neyman-Pearson strategy. Hypothesis H_1 will be chosen if $\Lambda\{\underset{\sim}{n}\} > \Lambda_0$, and H_0 will be chosen otherwise. It is also equivalent to use the optimum statistic

$$g = \sum_{i=1}^{N} n_i \; \ell n \left(\frac{\bar{n}_{i1}}{\bar{n}_{i0}} \right) . \qquad (2.12)$$

since $\Lambda\{\underset{\sim}{n}\}$ is a monotone function of g which is obtained from the logarithm of the likelihood ratio $\Lambda\{\underset{\sim}{n}\}$. The decision level of this statistic is given by

$$g_0 = \ell n\, \Lambda_0 + \Delta N \,, \tag{2.13}$$

where

$$\Delta N = \sum_{i=1}^{N} (\bar{n}_{i1} - \bar{n}_{i0}) \tag{2.14}$$

is the total average number of photoelectrons emitted over the entire area of the surface when the signal field alone is present. Thus we can compare g with g_0 instead and select H_1 if $g > g_0$ and H_0 when $g \leq g_0$. When Neyman-Pearson criterion is used, the false-alarm probability Q_0 is preassigned. The distribution of the statistic g under H_0 must be known so that the decision level g_0 can be determined from either of the expressions in (2.3) or (2.4) as discussed previously. To examine the reliability or the error probability of making each decision we must also know the distribution of the statistic g.

The mean intensity $I_k(\underset{\sim}{x}_i)$ given in (2.9) can be written as

$$I_k(\underset{\sim}{x}_i) = I_0(\underset{\sim}{x}_i) + k\, I_s(\underset{\sim}{x}_i) \,, \qquad k = 0, 1 \,. \tag{2.15}$$

where $I_0(\underset{\sim}{x}_i)$ is the mean intensity due to the background light. In most cases, such as thermal background light, $I_0(\underset{\sim}{x}_i)$ can be assumed to be spatially invariant for all areas $d\underset{\sim}{A}_i$ over the surface. $I_s(\underset{\sim}{x}_i)$ is the mean intensity due to the object light in the area dA_i. Therefore

we can write

$$I_0(\underset{\sim}{x}_i) = I_b \quad , \quad \text{for all } dA_i \quad .$$

$$I_s(\underset{\sim}{x}_i) = I_S \, \gamma(\underset{\sim}{x}_i) \quad , \quad i = 1, 2 \ldots N . \tag{2.16}$$

where $I_S = \int_A I_s(\underset{\sim}{x}) \, d^2\underset{\sim}{x}$ is the total power transmitted to the surface from the object and $\gamma(\underset{\sim}{x}_i)$ is the weighting function to characterize the distribution of the power at point $\underset{\sim}{x}_i$. A is the entire area which is divided into N equal areas dA.

We also define a function

$$\begin{aligned} H(\underset{\sim}{x}_i) &= \bar{n}_{i1} \, / \, \bar{n}_{i0} \\ &= [I_0(\underset{\sim}{x}_i) + I_s(\underset{\sim}{x}_i)] \, / \, I_0(\underset{\sim}{x}_i) \\ &= 1 + I_S \, \gamma(\underset{\sim}{x}_i) \, / \, I_b \\ &= 1 + D^2 \, u(\underset{\sim}{x}_i) \quad , \end{aligned} \tag{2.17}$$

where D^2 is called the signal-to-noise and is the ratio of the total average number $\alpha T I_S$ of photoelectrons ejected from the surface by the object light illumination to the average number $\alpha T I_b A_o$ of photoelectrons ejected from a finite area A_o of the surface by the background light illumination. The function $u(\underset{\sim}{x}_i)$ is only different from $\gamma(\underset{\sim}{x}_i)$ by the

factor A_o, that is $u(\underset{\sim}{x}_i) = A_o \gamma(\underset{\sim}{x}_i)$. A_o is arbitrarily defined. The statistic g from (2.12) can be written as

$$g = \sum_{i=1}^{N} n_i \ln H(\underset{\sim}{x}_i) , \tag{2.18}$$

which is similar to the statistic Y of (1.48) with $\beta(\underset{\sim}{x}_i) = \ln H(\underset{\sim}{x}_i)$ as discussed in Chapter I. As N is very large, by passing to the limit as $dA \to 0$, the m.g.f. of the statistic g under hypothesis H_k as $TW >> 1$ can be written according to (1.59) as

$$\begin{aligned} h_k(s) &= E\left[e^{-sg} \mid H_k \right] \\ &\simeq \exp\left[\alpha T \int_A \left(e^{-s \ln H(\underset{\sim}{x})} - 1 \right) I_k(\underset{\sim}{x}) \, d^2\underset{\sim}{x} \right] \\ &= \exp\left[\alpha T I_b \int_A H^k(\underset{\sim}{x}) \left[H^{-s}(\underset{\sim}{x}) - 1 \right] d^2\underset{\sim}{x} \right] , \end{aligned}$$

$$k = 0, 1 . \tag{2.19}$$

The logarithm of $h_k(s)$ is

$$\ln h_k(s) = \alpha T I_b \int_A H^k(\underset{\sim}{x}) \left[H^{-s}(\underset{\sim}{x}) - 1 \right] d^2\underset{\sim}{x} ,$$

$$\text{for } k = 0, 1 . \tag{2.20}$$

The distribution of the statistic g cannot in general be obtained in

exact form. Only an approximation can be used and will be discussed later.

The logarithm of $h_k(s)$ from (2.20) is differentiable for any order with respect to the variable s, and the nth cumulant under hypothesis H_k for k = 0, 1 can be expressed as

$$G_k^n = (-1)^n \frac{d^n}{ds^n} \ln h_k(s) \Big|_{s=0}$$

$$= \alpha T I_b \int_A H^k(\underline{x}) \ln^n H(\underline{x}) \, d^2\underline{x} \quad . \tag{2.21}$$

In particular, the mean and variance of the statistic g can be calculated by

$$E[g|H_k] = \alpha T I_b \int_A H^k(\underline{x}) \ln H(\underline{x}) \, d^2\underline{x}$$

$$\mathrm{Var}[g|H_k] = \alpha T I_b \int_A H^k(\underline{x}) \ln^2 H(\underline{x}) \, d^2\underline{x} \quad ,$$

$$k = 0, 1 \quad . \tag{2.22}$$

If the average intensity $I_s(\underline{x}_j)$ given in (2.16) is zero outside a finite area A_1 of the photosensitive surface, that is, if $I_1(\underline{x}_i) = I_s(\underline{x}_i) + I_0(\underline{x}_i)$ for $\underline{x}_i \in A_1$ and $I_1(\underline{x}_i) = I_0(\underline{x}_i)$ otherwise, then $H(\underline{x}_i) = 1$ when $\underline{x}_i \notin A_1$ and the optimum statistic g involves only the emission within the area A_1, so that there will be a finite probability of getting no electrons under hypothesis H_k,

$$\Pr\left[g=0|H_k\right] = \exp\left[-\alpha T \int_{A_1} I_k(\underset{\sim}{x})\, d^2\underset{\sim}{x}\right] ,$$

$$k = 0, 1 \qquad (2.23)$$

which is the result of (2.19) as $s \to \infty$.

When $I_s(\underset{\sim}{x}_i)$ is also spatially invariant, so is the function $H(\underset{\sim}{x}_i)$. The optimum statistic is therefore equivalent to $g/\ell n\ C$, where $C = H(\underset{\sim}{x}_i)$ is constant for all i, and the statistic can be written as

$$g' = \sum_{i=1}^{N} n_i \qquad , \qquad (2.24)$$

which is the sum of the photoelectrons from the total number N of small areas dA. As TW >> 1, the m.g.f. of the statistic g' is given by (1.59) with $\beta(\underset{\sim}{x}) = 1$ as discussed in Chapter I. g' is therefore a random variable with a Poisson distribution.

The detector just described represents a particular way of processing the light field behind the aperture of the optical system in order to choose between the hypotheses. It has been compared with the optimum means of processing the field from the point of view of quantum detection theory[5]. When diffraction is negligible and the surface has unit quantum efficiency, this detector is equivalent to the optimum detector of the image-forming light[6].

Threshold detector

The structure of the optimum statistic is based on the function $H(\underline{x})$ which is a function of $D^2 u(\underline{x}_i)$ as given by (2.17). When the signal-to-noise ratio D^2 is not known, the detector must be designed for some reasonable standard value. If D^2 is very small, the appropriate thing to do in detection theory is to expand the logarithm of the conditional likelihood ratio $\Lambda[\underline{n}|D^2]$ from (2.11) into a power series in D^2, and the optimum statistic is equivalent to the threshold statistic, which is based on the lowest order of D^2 in that expansion[7]. For detecting the image on the photoelectric surface we have just discussed, the optimum statistic g from (2.18) can be expanded into a power series in D^2 or

$$g = \sum_{i=1}^{N} n_i \sum_{m=1}^{\infty} (-1)^{m-1} [D^2 u(\underline{x}_i)]^m / m! \quad . \tag{2.25}$$

Since D^2 is very small and is independent of the location, we can base the decision on the threshold statistic, which is the coefficient of the lowest order of D^2 in (2.25). We have

$$g_\theta = \sum_{i=1}^{N} n_i u(\underline{x}_i) \quad . \tag{2.26}$$

The m.g.f. of this statistic can be derived for TW >> 1 and is given by (1.59) where $\beta(\underline{x}_i) = u(\underline{x}_i)$. That is when N is very large. By passing to the limit as $dA \to 0$ we have

$$h_{\theta k}(s) = E\left[e^{-sg_\theta} \mid H_k\right]$$

$$= \exp\left\{\alpha T\, I_b \int_A H^k(\underline{x}) \left[e^{-su(\underline{x})}-1\right] d^2\underline{x}\right\},$$

$$k = 0, 1 \quad , \tag{2.27}$$

where $H(\underline{x})$ and $u(\underline{x})$ are given in (2.17), and the logarithm of (2.27) is

$$\ell n\, h_{\theta k}(s) = \alpha T\, I_b \int_A H^k(\underline{x}) \left[e^{-su(\underline{x})}-1\right] d^2\underline{x} \quad ,$$

$$\text{for } k = 0, 1 \quad . \tag{2.28}$$

The nth cumulant of the threshold statistic g_θ under H_k can be written as

$$G_{\theta k}{}^n = (-1)^n \frac{d^n}{ds^n} \ell n\, h_{\theta k}(s) \Big|_{s=0}$$

$$= \alpha T\, I_b \int_A H^k(\underline{x})\, u^n(\underline{x})\, d^2\underline{x} \quad ,$$

$$\text{for } k = 0, 1 \quad , \tag{2.29}$$

and the mean and variance are

$$E[g_\theta \mid H_k] = \alpha T\, I_b \int_A H^k(\underline{x})\, u(\underline{x})\, d^2\underline{x} \quad ,$$

$$\mathrm{Var}[g_\theta | H_k] = \alpha T I_b \int_A H^k(\underline{x})\, u^2(\underline{x})\, d^2\underline{x} \quad . \tag{2.30}$$

Since the m.g.f. from (2.27) is dependent on the signal-to-noise ratio D^2 only through the function $H(\underline{x})$, the distribution of the threshold statistic g_θ will not depend on D^2 when H_0 is true.

Simple detector

Instead of weighting the number n_i of photoelectrons from each area dA_i with a factor $\ell n\, H(\underset{\sim}{x}_i)$, a simple way is to collect all the photoelectrons ejected from a certain area A_1' of the surface without any weighting factor about the location. As TW >> 1, the probability of n photoelectrons ejected from the area A_1' under hypothesis H_k has been proved in Chapter I to be Poisson distributed and

$$P_n(T|H_k) = \bar{n}_{Tk}^{\,n} \; e^{-\bar{n}_{Tk}} / n! \;, \tag{2.31}$$

where

$$\bar{n}_{Tk} = \alpha T \int_{A_1'} I_k(\underset{\sim}{x})\, d^2\underset{\sim}{x} \;, \qquad k = 0 \text{ or } 1, \tag{2.32}$$

is the average number of photoelectrons ejected from the area A_1' under H_k, and $I_k(\underset{\sim}{x})$ is given by (2.9). The likelihood ratio of the simple detector according to (2.1) is

$$\begin{aligned} \Lambda_s(n) &= P_n(T|H_1) \,/\, P_n(T|H_0) \\ &= \left(\frac{\bar{n}_{T1}}{\bar{n}_{T0}}\right)^n e^{-\bar{n}_{T1} + \bar{n}_{T0}} \;. \end{aligned} \tag{2.33}$$

Hypothesis H_0 will be chosen if $\Lambda_s(n) \le \Lambda_{s0}$ and H_1 will be chosen otherwise, where Λ_{s0} is the decision level, which can be obtained according to the criterion we use. Because the likelihood ratio $\Lambda_s(n)$

of the simple detector is a monotone function of n, it is therefore equivalent to use the optimum statistic from the logarithm of $\Lambda_s(n)$

$$g_s = n \quad , \tag{2.34}$$

and hypothesis H_1 will be chosen if $g_s > g_{s0}$ and H_0 otherwise except that at $g_s = g_{s0}$ a probability f will be assigned for choosing H_1. When the Bayes criterion is used the decision level g_{s0} of the statistic can be determined from the likelihood-ratio decision level Λ_{s0} and

$$g_{s0} = (\ell n\, \Lambda_{s0} + \Delta n_T)\, [\ell n(1 + \Delta n_T/\bar{n}_{T0})]^{-1} , \tag{2.35}$$

where $\Delta n_T = \bar{n}_{T1} - \bar{n}_{T0}$ is the average number of photoelectrons ejected from the area A_1' by the object light illumination alone and can be calculated from the expression

$$\Delta n_T = \alpha T\, I_S \int_{A_1'} \gamma(\underset{\sim}{x})\, d^2\underset{\sim}{x} \quad . \tag{2.36}$$

The optimum area A_1' for the observer to adopt is the area where the detection probability is maximum for a fixed false-alarm probability or the error probability is minimum.

Reliability and error probability of the ideal detector in the absence of the background light

The performance of a detector can be characterized by the reliability, Q_0 and Q_d, and the error probability P_e as defined by (2.3) and (2.6). When there is no background light, there will be no photoelectrons ejected from the photosensitive surface under the hypothesis H_0. For both Bayes and Neyman-Pearson criteria the strategy is to choose H_1 whenever one or more than one photoelectron have been observed. As TW >> 1, the joint probability for observing the data $\underline{n} = (n_1, n_2 \ldots n_N)$ from the N small areas under hypothesis H_1 is given by (2.10). Since the probability of zero photoelectron emission under H_0 is 1, the likelihood ratio at $\underline{n} = 0$ is

$$\Lambda(\underline{n}=0) = e^{-N_s} , \tag{2.37}$$

where

$$N_s = \alpha T I_S \tag{2.38}$$

is the total average number of photoelectrons ejected from the photosensitive surface due to the object light. For the detection of the image when Bayes criterion is used, hypothesis H_1 will be chosen at $\underline{n} = 0$ if $e^{-N_s} > \Lambda_0$ and H_0 otherwise, with Λ_0 given by (2.2). If the relative costs $C_{10} - C_{00}$ and $C_{01} - C_{11}$ are equal, the hypothesis with greater posterior probability $P(H_k|\underline{n}=0)$ for k = 0, 1 is always

selected where

$$P(H_k \mid \underset{\sim}{n}=0) = P(H_k)\, P(\underset{\sim}{n}=0 \mid H_k) \,/\, P(\underset{\sim}{n}=0) ,$$

$$k = 0 \text{ or } 1 . \tag{2.39}$$

The minimum average error probability will be

$$P_e = \min(\xi,\ (1-\xi)\, e^{-N_s}) . \tag{2.40}$$

In particular, when the hypotheses are equally likely

$$P_e = \frac{1}{2} e^{-N_s} , \qquad \xi = \frac{1}{2} . \tag{2.41}$$

For the Neyman-Pearson criterion, the randomized strategy must be used. As the false-alarm probability Q_0 is preassigned, hypothesis H_1 will be chosen with a probability Q_0 when no photoelectron is emitted from the surface during the interval (0,T). The detection probability at this case becomes

$$Q_d = 1 - (1-Q_0)\, e^{-N_s} . \tag{2.42}$$

Thus the error probability P_e can be calculated again according to (2.6).

Reliability and error probability of the ideal detector in the presence of the background light

When the background light is present and $I_0(\underline{x}) = I_b$, the optimum statistic g is expressed by (2.18), where its m.g.f. is given by (2.19). It is not in general possible to evaluate the distribution, which is known as an infinitely divisible distribution[8,9]. Helstrom[10] treated the distribution by a Gaussian approximation, where the p.d.f. of the statistic g is approximated by

$$N_k(g) = \frac{1}{\sqrt{2\pi}\,\sigma_k} \exp[-(g-\bar{g}_k)^2 / 2\sigma_k^2] \qquad (2.43)$$

with

$$\bar{g}_k = E[g|H_k] ,$$

$$\sigma_k^2 = \mathrm{Var}[g|H_k] ,$$

for k = 0, 1 ,

given in (2.22).

The reliability of the detector can then be expressed by the error-function integral,

$$Q_0 = \Pr[g>g_0|H_0] = \mathrm{erfc}\,(y_0) ,$$

$$Q_d = \Pr[g>g_0|H_1] = \mathrm{erfc}\,(y_1) , \qquad (2.44)$$

with

$$\text{erfc}\ (y_k) = \frac{1}{\sqrt{2\pi}} \int_{y_k}^{\infty} e^{-y^2/2}\, dy \ ,$$

$$y_k = (g_0 - \bar{g}_k) / \sigma_k \qquad , \quad k = 0, 1$$

As we have discussed in Chapter I, with the m.g.f. given by (2.19) the distribution of the statistic g can be approximated by the Gaussian function if only the condition from (1.63) is true. In other words, with $\beta(x) = \ln H(x_i)$ the condition from (1.63) will be satisfied if $D^2 << 1$. For large values of the signal-to-noise ratio D^2, the Gaussian approximation will not be accurate because the mth order cumulant of the statistic increases as m increases. Farrell[11] recommended approximating the distribution of the statistic g by a gamma distribution function. The p.d.f. of the statistic is approximated by

$$G_k(g) = [a_k / \Gamma(b_k)]\ (a_k g)^{b_k - 1}\ e^{-a_k g} \tag{2.45}$$

with

$$a_k = E[g|H_k] / \text{Var}[g|H_k]$$

$$b_k = (E[g|H_k])^2 / \text{Var}[g|H_k] \qquad , \quad k = 1, 0$$

so that the mean and variance of the gamma random variable are matched with the mean and variance given by (2.22). Here $\Gamma(b_k)$ is the gamma function.

The reliability of the optimum detector is then approximated by

$$Q_0 = P[g>g_0|H_0] = \int_{z_0}^{\infty} \beta_0(z)\, dz \ ,$$

$$Q_d = P[g>g_0|H_1] = \int_{z_1}^{\infty} \beta_1(z)\, dz \ , \qquad (2.46)$$

where

$$\beta_k(z) = \frac{1}{\Gamma(b_k)} \ z^{b_k-1} \ e^{-z} \ ,$$

$$z_k = a_k g_0 \ , \qquad k = 1, 0 \ .$$

On the other hand, it is reasonable to use the method of steepest descent as illustrated in Appendix A,where well-known distributions, such as Gaussian, gamma and Poisson, have been used as examples and good numerical agreement has been obtained, as listed in Table 3 and Table 4.

The optimum statistic g given by (2.18) is a non-negative random variable since the function $H(\underline{x})$ exceeds 1 for all $\underline{x}$. The m.g.f. is given by (2.19). The probability that g exceeds the decision level under H_k can be written as

$$\Pr[g>g_0|H_k] = \int_{g_0}^{\infty} dF_k(g) \quad ,$$

$$k = 0, 1 \qquad (2.47)$$

and can be approximated by the asymptotic expansion series given by (A12) in Appendix A, where $F_k(g)$ is the distribution function of the random variable g. The complex phase of the integral defined by (A7) under hypothesis H_k for k = 0 or 1 is

$$\phi_k(s) = g_0^{-1} \ln h_k(s) + s$$

$$= g_0^{-1} \alpha T I_b \int_A H^k(\underset{\sim}{x}) [(H(\underset{\sim}{x}))^{-s}-1] d^2\underset{\sim}{x} + s \quad ,$$

$$\text{for } k = 0, 1 \qquad (2.48)$$

when (2.20) is used.

There is only one saddle point for this complex phase as discussed in Appendix B, and it can be determined from the equation $\frac{d}{ds} \phi_k(s) = 0$ or

$$g_0 = \alpha T I_b \int_A (H(\underset{\sim}{x}))^{k-s} \ln H(\underset{\sim}{x}) d^2\underset{\sim}{x} \quad . \qquad (2.49)$$

If we use the statistic

$$g' = \sum_{i=1}^{N} n_i \ln \frac{\bar{n}_{i1}}{\bar{n}_{i0}} + N_s$$

instead of the statistic from (2.12) we can derive the m.g.f. of g' under hypothesis H_k for k = 0, 1 as

$$h_k'(s) = \exp\left\{\alpha T\, I_b \iint_A \left[(H(\underset{\sim}{x}))^{k-s}-1\right] d^2\underset{\sim}{x} + (s-k)\, N_s\right\},$$

which gives us the fundamental relation for all likelihood-ratio detectors as

$$h_1'(s) = h_0'(s-1) . \tag{2.50}$$

The saddle point s_1 under H_1 can be directly obtained through the saddle point s_0 under H_0 for real values by

$$s_1 = s_0 + 1 . \tag{2.51}$$

The relation from (2.51) also satisfies (2.49) for a fixed value of g_0 for both H_1 and H_0. Whether the saddle point s_k for k = 0 or 1 is positive or negative will depend on the following conditions

$$\begin{aligned} s_k < 0 \quad &\text{if} \quad g_0 > E[g|H_k] , \\ > 0 \quad &\text{if} \quad g_0 < E[g|H_k] , \\ = 0 \quad &\text{if} \quad g_0 = E[g|H_k] , \end{aligned}$$

$$k = 0, 1 . \tag{2.52}$$

The nth derivative of the complex phase $\phi_k(s)$ for $n \geq 2$ under hypothesis H_k is

$$\phi_k^{\,n}(s) = \frac{d^n}{ds^n}\phi_k(s)$$

$$= (-1)^n\, g_0^{-1}\, \alpha T\, I_b \int_A (H(\underline{x}))^{k-s}\, \ell n^n H(\underline{x})\, d^2x \quad ,$$

$$\text{for } k = 0,\ 1 \quad . \tag{2.53}$$

From the relation (2.51) we can have

$$\phi_0^{\,n}(s_0) = \phi_1^{\,n}(s_1) \quad , \qquad \text{for } n \geq 1 \ . \tag{2.54}$$

The false-alarm probability and the detection probability can be approximated[12,13] by using (A12) from Appendix A

$$Q_0 = 1 - E_0(g_0) - I_0(g_0) \quad ,$$

$$Q_d = 1 - E_1(g_0) - I_1(g_0) \quad , \tag{2.55}$$

where

$$E_k(g_0) = \begin{cases} 1 - \text{erfc}[(-2\, g_0\, \phi_k(s_k))^{\frac{1}{2}}] \ , & \text{for} \quad s_k < 0 \\ \text{erfc}[(-2\, g_0\, \phi_k(s_k))^{\frac{1}{2}}] \ , & \text{for} \quad s_k > 0 \end{cases}$$

and

$$I_k(g_0) = \frac{\exp[g_0\ \phi_k(s_k)]}{[2\pi\ g_0\ \phi_k^{(2)}(s_k)]^{\frac{1}{2}}} \sum_{j=0}^{\infty} \left\{ \left(\frac{-2}{g_0\ \phi_k^{(2)}(s_k)} \right)^j s_k^{-1} \right.$$

$$\cdot \sum_{n=0}^{2j} (-s_k)^{-2j+n} \sum_{\ell=0}^{n} A_{\ell,n} \left(\frac{1}{2}\right)_{\ell+j}$$

$$\left. - \operatorname{sign}(s_k) \left(\frac{1}{2}\right)_k \left(\frac{-\phi_k^{(2)}(s_k)}{2\phi_k(s_k)} \right)^{\frac{1}{2}} (g_0\ \phi_k(s_k))^{-j} \right\},$$

where $A_{\ell,n}$, $\left(\frac{1}{2}\right)_{\ell+j}$, $\operatorname{sign}(x)$ are defined in (A12) and (A10) for integers ℓ, n, j. If the Bayes criterion is used, the decision level g_0 is calculated by (2.13). The saddle point can be obtained by solving (2.49), and $\phi_k(s_k)$ and $\phi_k^{n}(s_k)$ for $k = 0, 1$ can be evaluated from (2.48), (2.53) and (2.54) where numerical integration will be required. The probability Q_0 or Q_d will then be approximated by summing the series given in (2.55) up to the term after which the absolute values of the terms either begin to increase or become insignificantly small. If the Neyman-Pearson criterion is used, the value of Q_0 is preassigned and the decision level g_0 must be hunted by iteration. Since g_0 is a monotone function of the real value s_0, both g_0 and s_0 can be found simultaneously by iteration until the false-alarm probability calculated by the asymptotic expansion approaches the preassigned value Q_0 within a tolerable error such that (2.49) is satisfied. The saddle point s_1 under H_1 will be obtained according to (2.51), and the detection probability Q_d will

be approximated by the expansion (2.55). The numerical iteration procedure for searching for the saddle points s_0, s_1, and the decision level g_0 is described in Appendix B.

When the relative costs $C_{10} - C_{00}$ and $C_{01} - C_{11}$ are equal, the decision level g_0 for Bayes criterion is given by (2.13) with $\Lambda_0 = \xi/(1-\xi)$. The saddle points s_0 and s_1 are calculated from (2.49) and (2.51). The average error probability is minimized and can be obtained after the probabilities Q_0 and Q_d are approximated by the asymptotic expansion (2.55). The performance of the ideal detector will be studied with a Gaussian image and compared with the threshold detector and simple detector in the following paragraphs.

Performance of the ideal detector for a Gaussian image

In order to investigate the performance of the ideal detector and compare it with the other two detectors, the threshold and the simple detector, a Gaussian image will be postulated. The average intensity function on the photosensitive surface due to the object light given in (2.16) is described by the weighting function

$$\gamma(\underline{x}) = \frac{1}{2\pi\sigma^2} \exp\left[-\frac{x_1^2 + x_2^2}{2\sigma^2}\right], \tag{2.56}$$

where σ is the width of the image, this might be the image of a circular nebula or, more important, of a point source whose light has passed through a turbulent medium[14]. If we define

$$N_0 = 2\pi\,\sigma^2\, I_b\, \alpha T \tag{2.57}$$

as the average number of photoelectrons emitted from an area $A_o = 2\pi\,\sigma^2$ of the photosensitive surface due to the background light and with N_s given by (2.38), the signal-to-noise ratio D^2 and and function $u(\underline{x})$ from (2.17) can be written as

$$D^2 = N_s/N_0 , \qquad \text{for } N_0 \neq 0$$

$$u(\underline{x}) = \exp\left[-\frac{x_1^2 + x_2^2}{2\sigma^2}\right] . \tag{2.58}$$

In the absence of the background light, that is $N_0 = 0$, and for a false-alarm probability Q_0 preassigned at 0.2, 0.1 or 0.01, the detection probability Q_d is plotted as a function of N_s in Fig. 4; (2.42) is used to calculate Q_d.

If the background light is present, the m.g.f. of the ideal statistic g at WT >> 1 for the Gaussian image is given by

$$h_k(s) = \exp\left\{\frac{N_0}{2\pi\sigma^2}\int_{-\infty}^{\infty}\int_{-\infty}^{\infty}(1+D^2u(\underset{\sim}{x}))^k\,[(1+D^2u(\underset{\sim}{x}))^{-s}-1]\,d^2\underset{\sim}{x}\right\},$$

$$k = 0,\ 1 \qquad (2.59)$$

when (2.19), (2.56), (2.57), and (2.58) are used.

Now we can change variables by letting

$$x_1 = R\sigma\cos\theta \quad , \quad x_2 = R\sigma\sin\theta$$

so that

$$u(\underset{\sim}{x}) = \exp\left[-\frac{R^2}{2}\right] .$$

The m.g.f. from (2.59) becomes

$$h_k(s) = \exp\left\{\frac{N_0}{2\pi\sigma^2}\int_0^{2\pi}\int_0^{\infty}(1+D^2\exp(-R^2/2))^k\right.$$

$$\left.[(1+D^2\exp(-R^2/2))^{-s}-1]\;\sigma^2 R\,dR\,d\theta\right\}$$

$$= \exp\left\{ N_0 \int_0^1 (1+D^2 y)^k \left[(1+D^2 y)^{-s} - 1\right] y^{-1}\, dy \right\},$$

$$k = 0 \text{ or } 1 , \qquad (2.60)$$

where (2.60) is obtained by changing the variable $y = e^{-R^2/2}$. The complex phase required in the asymptotic expansion series under H_k for k = 0, 1 as given by (2.48) can be written as

$$\phi_k(s) = g_0^{-1} N_0 \int_0^1 (1+D^2 y)^k \left[(1+D^2 y)^{-s} - 1\right] y^{-1} dy + s ,$$

$$k = 0, 1 , \qquad (2.61)$$

where the saddle point is obtained by solving the equation

$$g_0 = N_0 \int_0^1 (1+D^2 y)^{k-s} \ln(1+D^2 y)\, y^{-1} dy ,$$

$$k = 0, 1 \qquad (2.62)$$

and s_1 and s_0 satisfy (2.51).

The nth derivative of the complex phase $\phi_k(s)$ for $n \geq 2$ under hypothesis H_k is

$$\phi_k^{n}(s) = (-1)^n g_0^{-1} N_0 \int_0^1 (1+D^2 y)^{k-s} \ln^n(1+D^2 y)\, y^{-1} dy ,$$

$$k = 0 \text{ or } 1 . \qquad (2.63)$$

Figure 4 Detection probability Q_d as a function of N_s defined in (2.38) for the ideal detector in the absence of background light; false-alarm probability $Q_0 = 0.01$, 0.1, 0.2.

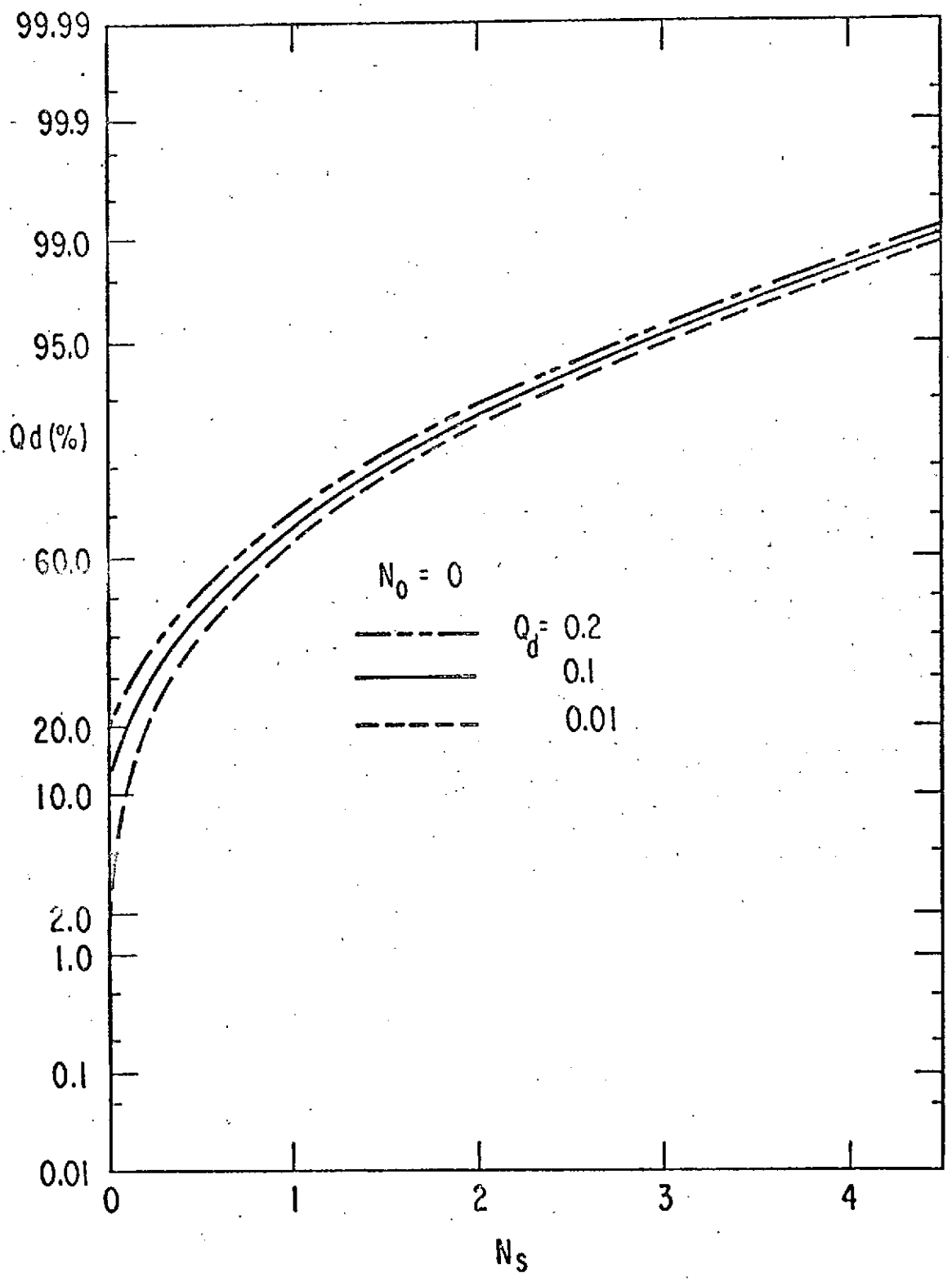
99.99
99.9
99.0
95.0
Qd (%)
60.0
20.0
10.0
2.0
1.0
0.1
0.01
0
1
2
3
4
Ns
N0 = 0
Qd = 0.2
0.1
0.01

The mean and variance of the optimum statistic g from (2.22) for the Gaussian image under H_k for k = 0, 1 becomes

$$E[g|H_k] = N_0 \int_0^1 (1+D^2y)^k \ln(1+D^2y)y^{-1}dy ,$$

$$\text{Var}[g|H_k] = N_0 \int_0^1 (1+D^2y)^k \ln^2(1+D^2y)y^{-1}dy . \qquad (2.64)$$

In order to compare the three approximation methods, steepest descent, Guassian, and gamma, the reliability of the ideal detector has been calculated by the three approximate forms as given in (2.55), (2.44), and (2.46) respectively. At typical values of $N_0 = N_s = 5$ ($D^2 = 1$), the false-alarm and detection probabilities of the statistic are plotted as functions of the decision level g_0 in Fig. 5. It can be noticed that both Gaussian and gamma approximations with the mean and variance matched by (2.64) are least accurate in the tails of the distributions. For small false-alarm probability Q_0, there may be a serious error in the decision level g_0 if either one of the approximate forms is used under the Neyman-Pearson criterion where Q_0 is preassigned. To apply the asymptotic expansion series given in (2.55), an iterative search method was used to determine the decision level g_0 and the associated saddle point s_0. Detailed description of the iteration is given in Appendix B.

To investigate the performance of the optimum detector and later the threshold detector, the detection probability Q_d of the optimum detector is calculated by using the asympotic expansion series

from (2.55) and is plotted as a function of the signal-to-noise ratio D^2 for typical values of N_0 at 0.5 and 5 in Fig. 6 where the false-alarm probability Q_0 is preassigned at 10^{-3} and 10^{-5}. The detection probability is also plotted as a function of the mean number N_s by the solid curves in Fig. 7 at $Q_0 = 10^{-3}$ and in Fig. 8 at $Q_0 = 10^{-5}$. The detection probability Q_d at $N_0 = 0$, given by (2.42), is also plotted in Fig. 7 and Fig. 8 for the purpose of comparison. When the relative costs $C_{10} - C_{00}$ and $C_{01} - C_{11}$ are equal, the minimum error probability of the optimum detector at $\xi = \frac{1}{2}$ can be calculated by using (2.6) and the asymptotic expansion series (2.55) and is plotted as a function of the mean number N_s by the solid curves in Fig. 9 where the decision level $g_0 = N_s$ is obtained according to (2.13) and the saddle point s_0 is searched for by iteration to satisfy (2.62).

Figure 5 Probability Q_0 and probability Q_d as a function of decision level g_0 for the ideal detector calculated by the saddle point, Gaussian and gamma approximations; $N_0 = N_s = 5$, where N_0 is defined in (2.57).

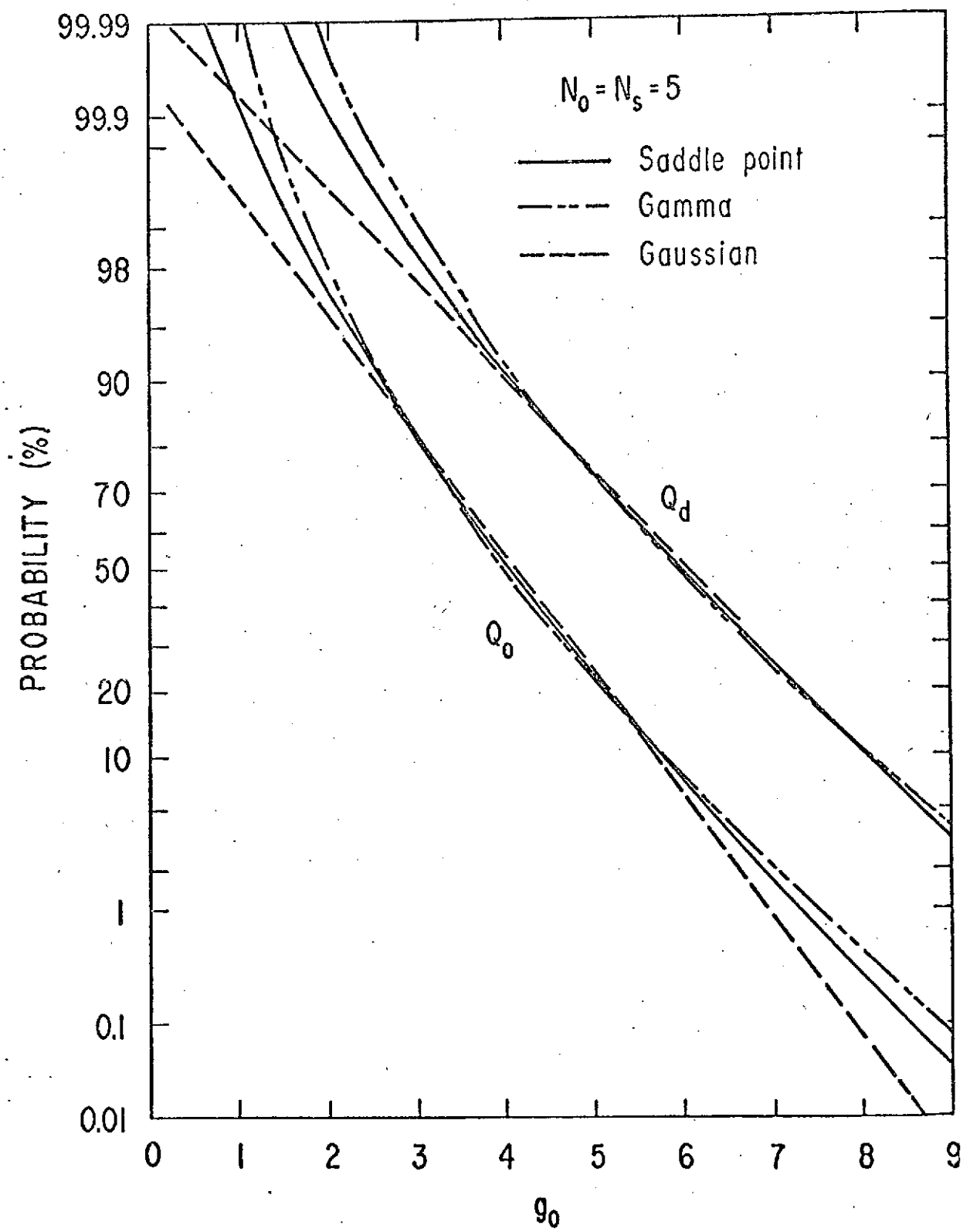
99.99
99.9
98
90
70
50
20
10
1
0.1
0.01
PROBABILITY (%)
$N_0 = N_s = 5$
Saddle point
Gamma
Gaussian
Q_d
Q_0
0
1
2
3
4
5
6
7
8
9
g_0

Figure 6 Probability Q_d as a function of the signal-to-noise ratio D^2 defined in (2.58) for the ideal detector; $N_0 = 0.5, 5$, $Q_0 = 10^{-3}, 10^{-5}$.

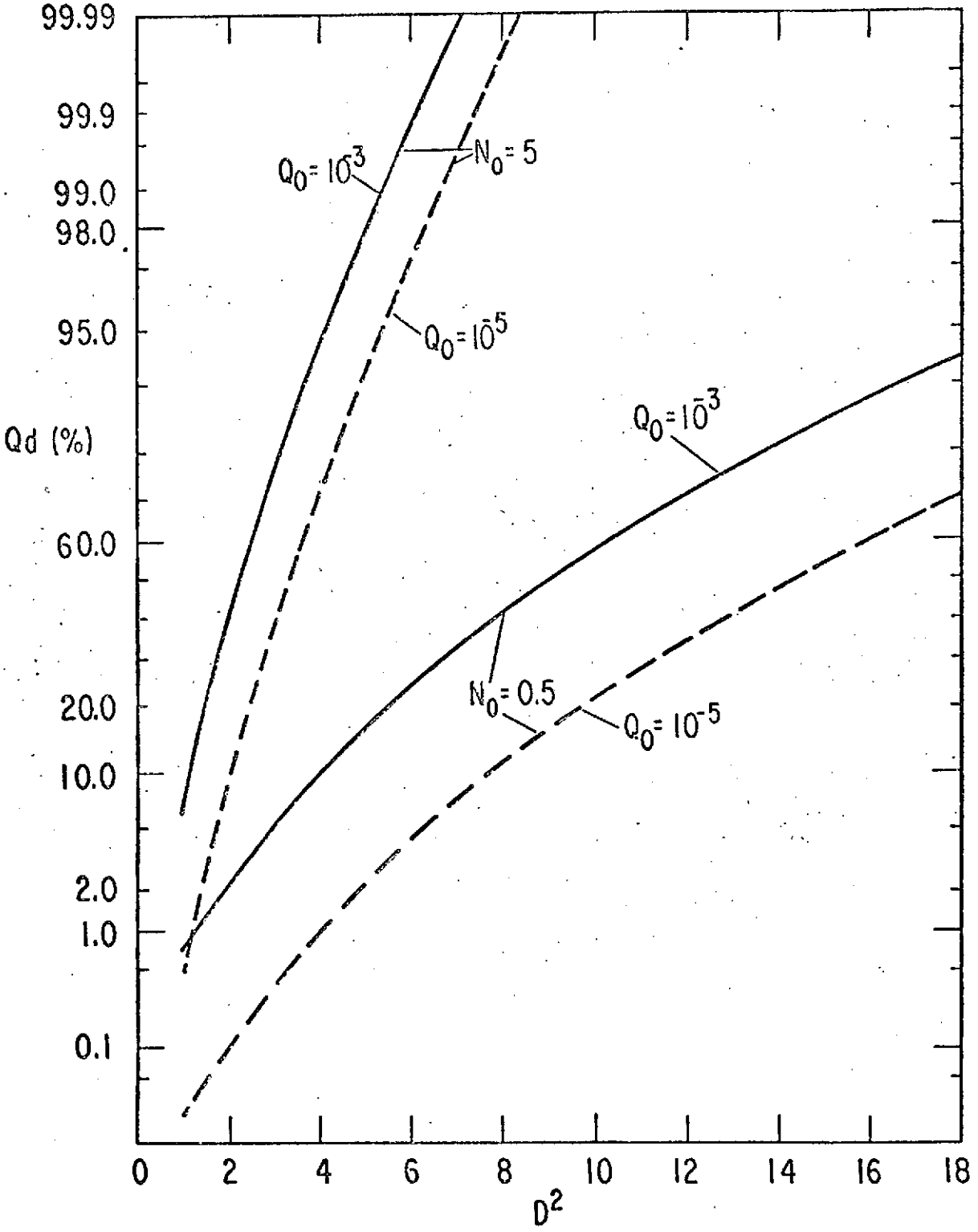
99.99
99.9
99.0
98.0
95.0
60.0
20.0
10.0
2.0
1.0
0.1
Qd (%)
$Q_0 = 10^{-3}$
$N_0 = 5$
$Q_0 = 10^{-5}$
$Q_0 = 10^{-3}$
$N_0 = 0.5$
$Q_0 = 10^{-5}$
0
2
4
6
8
10
12
14
16
18
D^2

Figure 7 Probability Q_d as a function of N_s for ideal, threshold and simple detectors; $Q_0 = 10^{-3}$ at $N_0 = 0, 0.5, 5$.

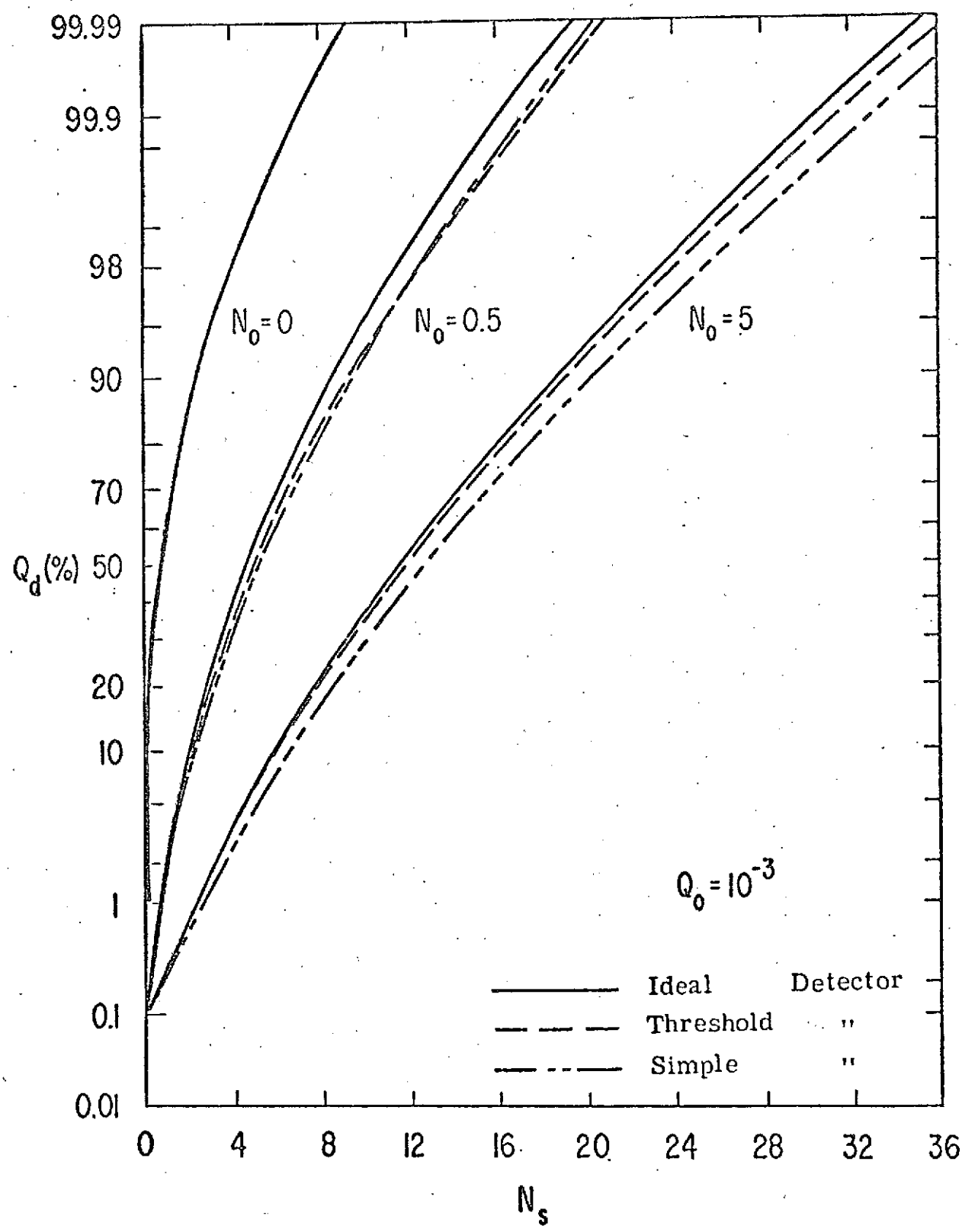
99.99
99.9
98
90
70
50
20
10
1
0.1
0.01
Q_d(%)
N_0=0
N_0=0.5
N_0=5
$Q_0 = 10^{-3}$
Ideal Detector
Threshold "
Simple "
0
4
8
12
16
20
24
28
32
36
N_s

Figure 8 Probability Q_d as a function of N_s for ideal, threshold and simple detectors, $Q_0 = 10^{-5}$ at $N_0 = 0, 0.5, 5$.

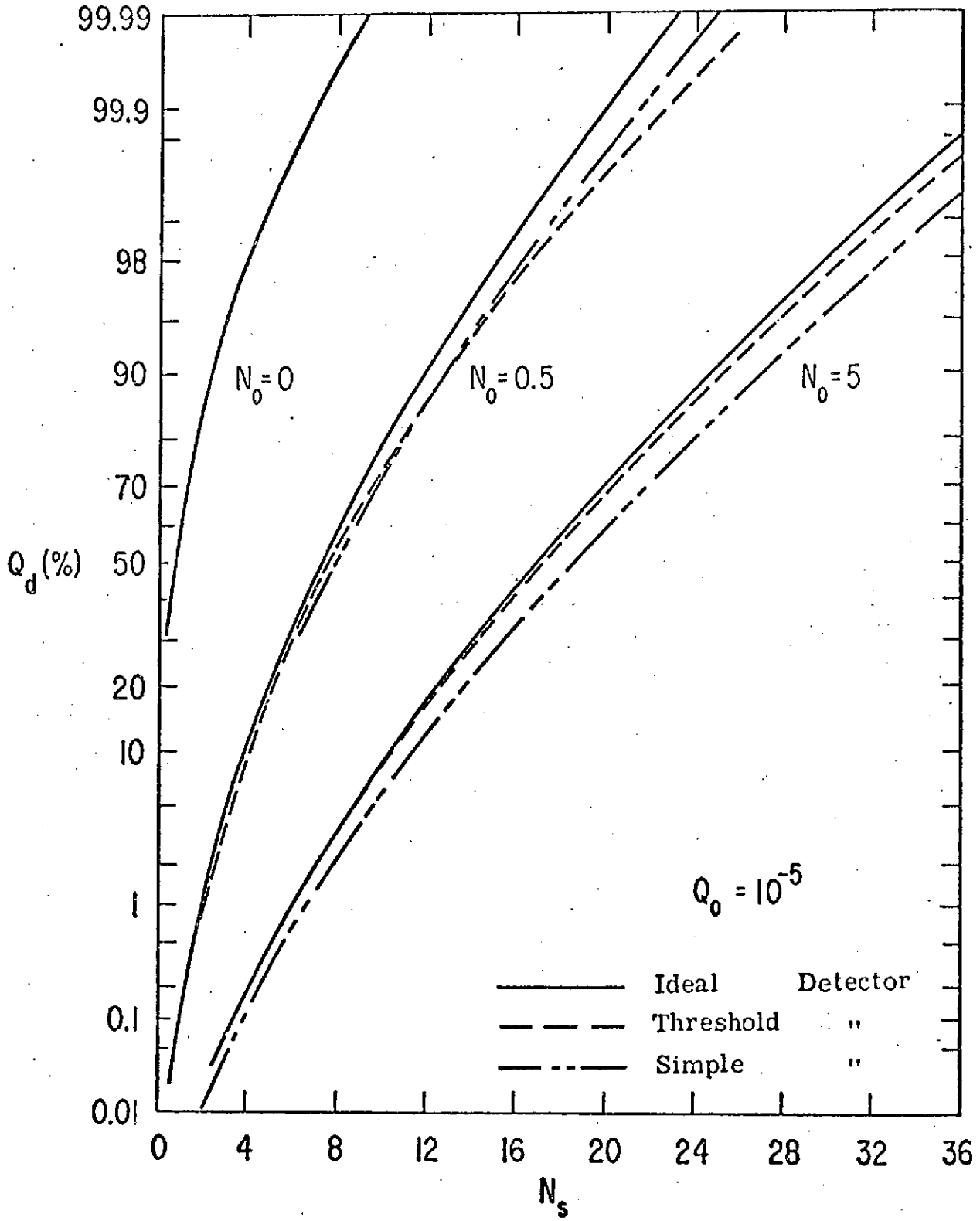
99.99
99.9
98
90
70
50
20
10
1
0.1
0.01
Q_d (%)
$N_0 = 0$
$N_0 = 0.5$
$N_0 = 5$
$Q_0 = 10^{-5}$
Ideal Detector
Threshold "
Simple "
0
4
8
12
16
20
24
28
32
36
N_s

Figure 9 Average error probability P_e in detecting the Gaussian image against the uniform background light vs. the mean number N_s for ideal and simple detectors; N_0 = 0, 0.01, 0.5, 5.

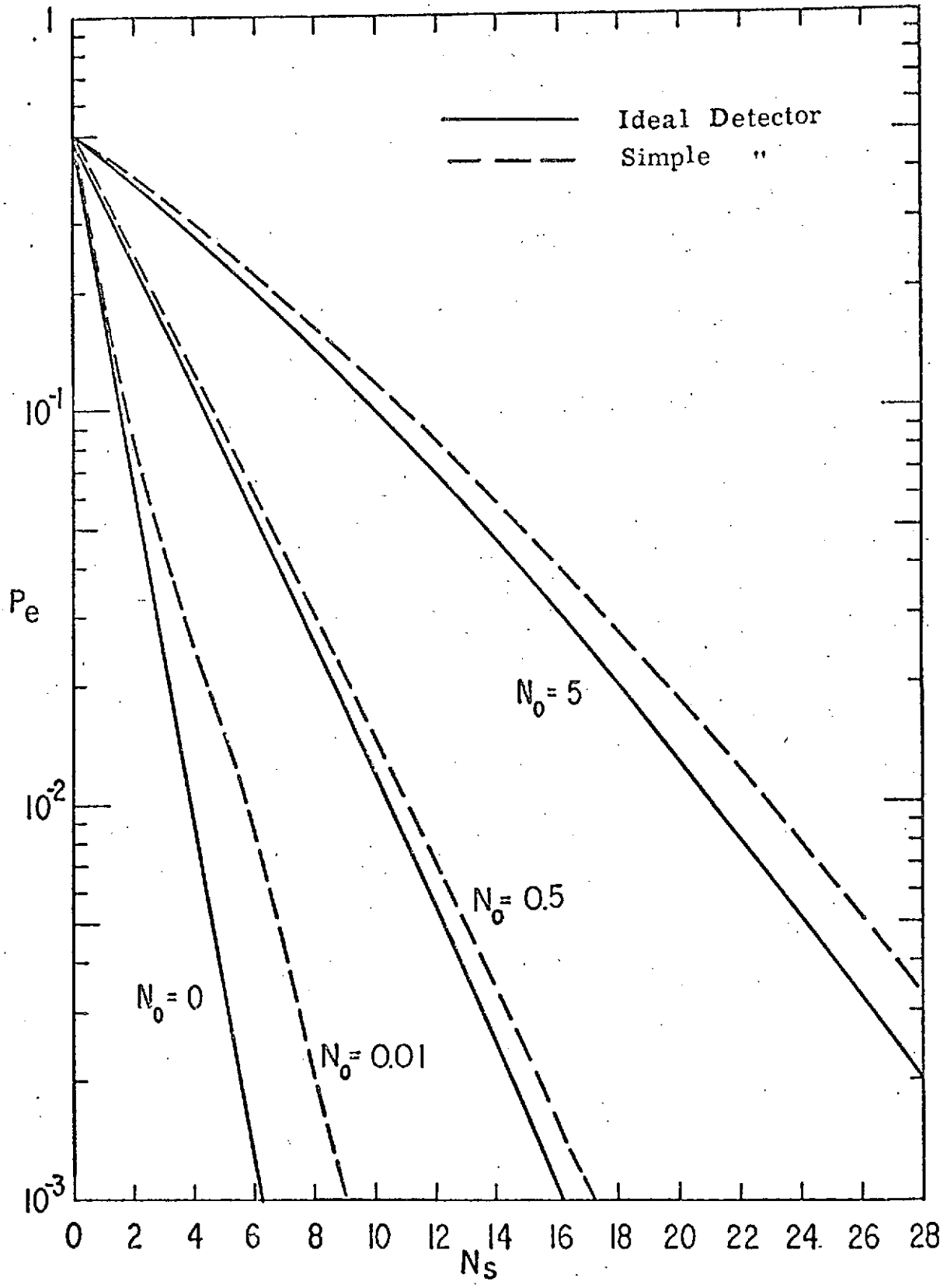
1
10^{-1}
10^{-2}
10^{-3}
P_e
Ideal Detector
Simple "
$N_0 = 5$
$N_0 = 0.5$
$N_0 = 0.01$
$N_0 = 0$
0 2 4 6 8 10 12 14 16 18 20 22 24 26 28
N_s

Performance of the threshold detector for a Gaussian image in the presence of the background light

When the signal-to-noise ratio D^2 is small and the threshold statistic g_θ from (2.26) is used, the m.g.f. given by (2.27) for a Gaussian image becomes

$$h_{\theta k}(s) = \exp\left\{\alpha T\, L_b \int_{-\infty}^{\infty}\int_{-\infty}^{\infty} (1+D^2 u(\underset{\sim}{x}))^k \right.$$

$$\left. [\exp(-su(\underset{\sim}{x}))-1]\, d^2\underset{\sim}{x}\right\},$$

$$k = 0 \text{ or } 1 \quad . \tag{2.65}$$

Again by changing variables, we have

$$h_{\theta k}(s) = \exp\left\{\frac{N_0}{2\pi\sigma^2}\int_0^{2\pi}\int_0^{\infty} (1+D^2\exp(-R^2/2))^k \right.$$

$$\left. (\exp(-s\exp(-R^2/2))-1)\ \sigma^2 R dR d\theta\right\}$$

$$= \exp\left\{N_0 \int_0^1 (1+D^2 y)^k\, (\exp(-sy)-1)\, y^{-1} dy\right\},$$

$$k = 0 \text{ or } 1 \quad . \tag{2.66}$$

The mean and variance of the threshold statistic g_θ under H_k for $k = 0, 1$ are

$$E[g_\theta|H_k] = N_0 \int_0^1 (1+D^2y)^k dy = N_0(1+kD^2/2) ,$$

$$Var[g_\theta|H_k] = N_0 \int_0^1 (1+D^2y)^k y dy = N_0(\tfrac{1}{2}+kD^2/3) ,$$

$$k = 0, 1 . \qquad (2.67)$$

The complex phase defined by (A7) under H_k for k = 0, 1 is

$$\phi_{\theta k}(s) = g_{\theta 0}^{-1} \ln h_{\theta k}(s) + s$$

$$= g_{\theta 0}^{-1} N_0 \int_0^1 (1+D^2y)^k [\exp(-sy)-1] y^{-1} dy + s$$

(2.68)

from which the saddle point s is determined by the equation

$$\frac{d}{ds} \phi_{\theta k}(s) = 0 \qquad \text{or}$$

$$g_{\theta 0} = N_0 \int_0^1 (1+D^2y)^k \exp(-sy)\, dy$$

$$= s^{-1} N_0 \left\{ 1-\exp(-s)+kD^2[s^{-1}-(1+s^{-1})\exp(-s)] \right\} ,$$

$$k = 0, 1 . \qquad (2.69)$$

Since the relation of the m.g.f.'s by (2.51) does not hold for the

statistic g_θ, the saddle point s under hypothesis H_k for both k = 0, 1 must be calculated from (2.69), which has only one root of real value as discussed in Appendix B. The nth derivatives of $\phi_k(s)$ for $n \geq 2$ are given by

$$\phi_k^{\,n}(s) = (-1)^n \, g_{\theta 0}^{\,-1} \, N_0 \int_0^1 (1+D^2 y)^k \, y^{n-1} \exp(-sy) \, dy$$

$$= (-1)^n \, g_{\theta 0}^{\,-1} \, N_0 \left\{ f_{n-1}(s) + kD^2 \, f_n(s) \right\},$$

$$k = 0, 1 \qquad (2.70)$$

where

$$f_n(s) = \int_0^1 y^n \exp(-sy) \, dy$$

$$= n! \, s^{-n-1} - s^{-1} \exp(-s) \sum_{j=0}^{n} [n! \,/ (n-j)!] \, s^{-j} .$$

(2.71)

Again, with the mean number N_0 and the signal-to-noise ratio D^2 given, the reliability of the statistic can be approximated by the asymptotic expansion as given in (2.55). For each decision level $g_{\theta 0}$ the saddle points s_0, s_1 can be solved for from (2.69). The false-alarm probability and the detector probability are plotted as a function of $g_{\theta 0}$ in Fig. 10 at $N_0 = 5$ and $D^2 = 0.1$, 1, 2, 3, 4, and 6. Since the

distribution of the threshold statistic g_θ is independent of the signal strength under hypothesis H_0, the advantage of the threshold detector is that for each preassigned Q_0 the decision level $g_{\theta 0}$ is fixed for all values of D^2 as shown by Fig. 10. The detection probability Q_d is also plotted as a function of the mean number N_s by the dashed curves in Fig. 7 and Fig. 8 for typical values of N_0 at $Q_0 = 10^{-3}$ and $Q_0 = 10^{-5}$. The detection probability Q_d of the threshold detector approaches the curves of the optimum detector when D^2 is very small; however, the optimum detector always has higher detection probability. To calculate the minimum error probability P_e one has to solve the decision level $g_{\theta 0}$ such that the ratio of the probabilities for $g_\theta = g_{\theta 0}$ under H_1 and H_0 is equal to $\xi/(1-\xi)$. We have not carried out the calculation.

Figure 10 Probability Q_0 and probability Q_d vs. decision level g_0 for threshold detector; $N_0 = 0.5$, $D^2 = 0.1, 1, 2, 3, 4, 6$.

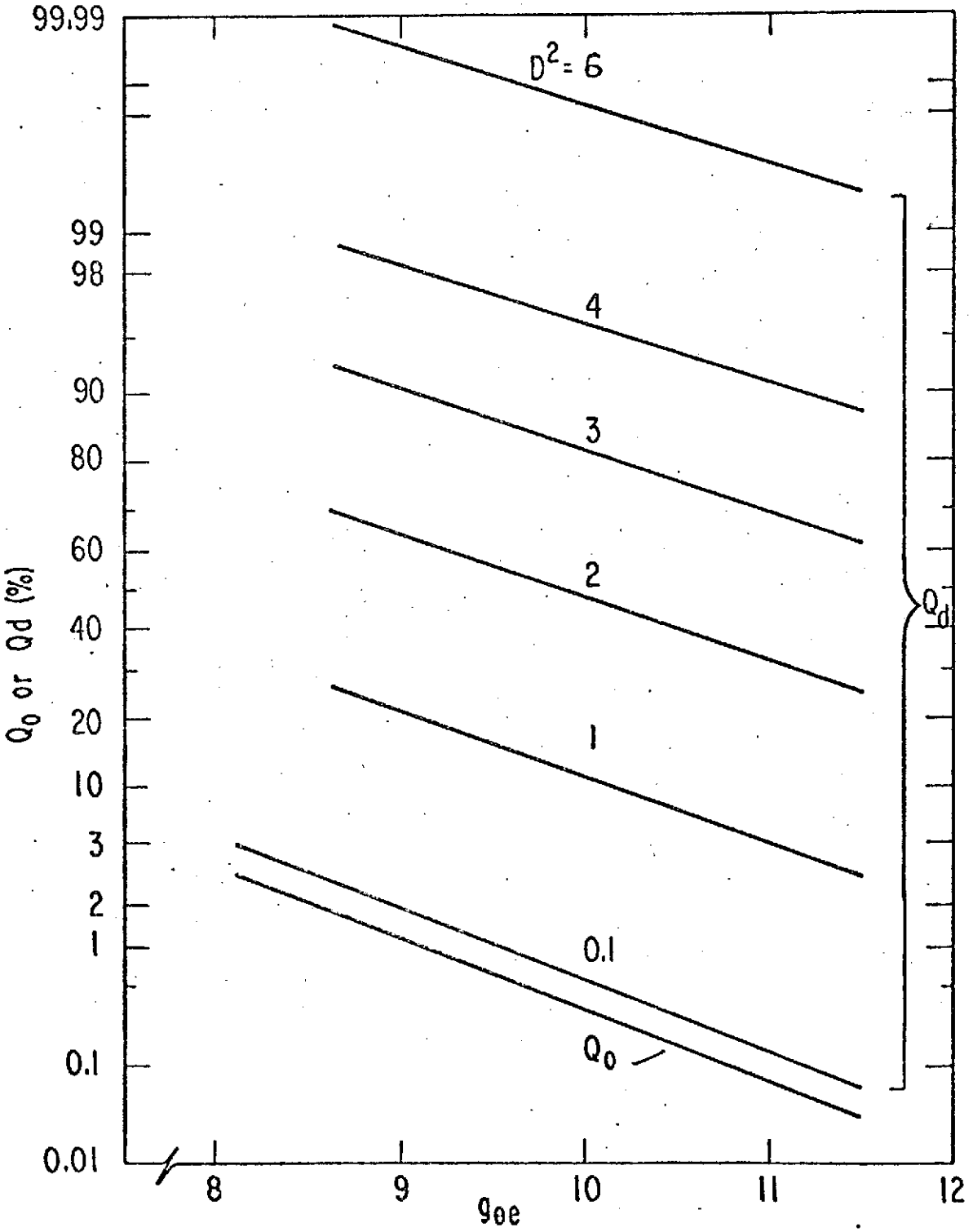
99.99
99
98
90
80
60
40
20
10
3
2
1
0.1
0.01
Q_0 or Qd (%)
$D^2 = 6$
4
3
2
1
0.1
Q_0
Q_d
8
9
10
11
12
g_{oe}

Performance of the simple detector for a Gaussian image in the presence of the background light

For the simple detector, the optimum statistic from the likelihood ratio is the total number n of the photoelectrons emitted from the optimum area A_1' as given by (2.34). If the radius of the area A_1' is given by σR_o, the average number $\bar{n}_{Tk}$ of the photoelectrons emitted from A_1' under hypothesis H_k for the Gaussian image according to (2.32) becomes

$$\begin{aligned}
\bar{n}_{Tk} &= \alpha T \int_{A_1'} [I_b + kI_S \gamma(\underset{\sim}{x})] \, d^2\underset{\sim}{x} \\
&= \alpha T \int_0^{2\pi} \int_0^{\sigma R_o} \left(I_b + kI_S \frac{1}{2\pi\sigma^2} \exp(-R^2/2\sigma^2) \right) \\
&\quad \cdot R dR d\theta \\
&= \alpha\pi \sigma^2 R_o^2 I_b T + k\alpha I_S T (1 - \exp(-R_o^2/2)) \\
&= N_0 [\rho + kD^2(1 - e^{-\rho})] \quad , \\
&\qquad k = 0, 1 \, , \qquad (2.72)
\end{aligned}$$

where $\rho = \frac{1}{2} R_o^2$ and $A_1' = \pi \sigma^2 R_o^2$.

Since the statistic g_s is a discrete random variable, when the Neyman-Pearson criterion is used, randomization must be applied.

That is, the reliability of the simple detector according to (2.4) and (2.5) can be written as

$$Q_0 = \sum_{n>g_{s0}}^{\infty} \bar{n}_{T0}^{\,n} \; e^{-\bar{n}_{T0}} / n! + f\, \bar{n}_{T0}^{\,g_{s0}} \; e^{-\bar{n}_{T0}} / g_{s0}\,! \;,$$

$$Q_d = \sum_{n>g_{s0}}^{\infty} \bar{n}_{T1}^{\,n} \; e^{-\bar{n}_{T1}} / n! + f\, \bar{n}_{T1}^{\,g_{s0}} \; e^{-\bar{n}_{T1}} / g_{s0}\,! \;, \tag{2.73}$$

where for preassigned Q_0 the decision level g_{s0} is the smallest integer such that

$$\sum_{n=0}^{g_{s0}} e^{-\bar{n}_{T0}} \, (\bar{n}_{T0})^{n} / n! \; > 1 - Q_0 \; . \tag{2.74}$$

f is the probability to choose H_1 when $n = g_{s0}$ and can be determined from

$$f = \left[\left(\sum_{n=0}^{g_{s0}} e^{-\bar{n}_{T0}} \, (\bar{n}_{T0})^{n} / n! \right) + Q_0 - 1 \right] \cdot (\bar{n}_{T0})^{-g_{s0}} \; e^{\bar{n}_{T0}} \; g_{s0}\,! \;, \tag{2.75}$$

where $\bar{n}_{T0}$, $\bar{n}_{T1}$ are given by (2.72) for k = 0, 1. Hypothesis H_1 will be then chosen if $n > g_{s0}$ and H_0 will be chosen if $n < g_{s0}$. As the

false-alarm probabilities Q_0 are preassigned at 10^{-3} and 10^{-5}, the detection probabilities Q_d of the simple detector are calculated from (2.73) at $N_0 = 0.5$ and 5 and are plotted as a function of the mean value N_s in Fig. 7 and Fig. 8. For each point on the curves, the radius R_o was varied to yield maximum detection probability.

When the Bayes criterion is used, with Λ_{s0} given by (2.2), the decision level from (2.35) becomes

$$g_{s0} = [\ell n \Lambda_{s0} + N_0 D^2 (1-e^{-\rho})] \, [\ell n (1+D^2 \rho^{-1} (1-e^{-\rho}))]^{-1} . \tag{2.76}$$

Hypothesis H_1 will be chosen if the number $n > g_{s0}$ or H_0 will be chosen otherwise. The reliability of the detector can be evaluated according to (2.73), except that we let $f = 0$ because the probability for g_{s0} to be an integer is negligible. When the relative costs are equal, the average error probability given by (2.6) is minimum and can be written as

$$P_e = \xi \sum_{n>g_{s0}}^{\infty} \bar{n}_{T0}^{\,n} \, e^{-\bar{n}_{T0}} / n! + (1-\xi) \sum_{n=0}^{<g_{s0}} \bar{n}_{T1}^{\,n} \, e^{-\bar{n}_{T1}} / n! \, . \tag{2.77}$$

At $\xi = \frac{1}{2}$, g_{s0} is calculated from (2.76) with $\Lambda_{s0} = 1$, and the error probabilities P_e are calculated and plotted as a function of mean

number difference $\Delta N = N_s$ at $N_0 = 0, 0.01, 0.5$ and 5 by the dashed curves in Fig. 9. For each point on these curves the value R_o was varied to yield maximum P_e.

When the false-alarm probability Q_0 is preassigned, the decision level g_{s0} determined from (2.74) is a monotonically increasing function of R_o. The optimum radius R_o at which the detection probability Q_d yields a maximum can easily be searched by the digital computer. The values of the optimum radius R_o at different values of N_s are listed in Table 1 at typical values of $N_0 = 0.5, 5$. The maxima are quite flat and the radius R_ρ of the observation area is not critical. For the calculation of the average error probability when the decision level g_{s0} is determined from (2.76), g_{s0} is also a monotonically increasing function of R_ρ. However, both Q_0 and Q_d are varied by changing g_{s0}, and their sensitivities toward the change are different. We found that there are several minima in a certain small region as we vary the radius R_o, and we have picked the smallest one for the plots in Fig. 9.

Discussion

It is important in detection theory to calculate the distribution of the statistic as accurately as possible so that the statistical performances of the detectors can be investigated. The statistic given by (2.18) or (2.26) is the sum of N independent random variables and is very common in detection and estimation theory. Since the exact distribution of the statistic cannot be obtained, the Gaussian approximation has been largely used for the statistical evaluations in the past. On the other hand, the method of steepest descent has been proved mathematically to provide approximations of an accuracy that is often high; usually the error of the approximation is of the order of the first term neglected in the asymptotic expansion series. Furthermore, the asymptotic expansion series expressed by (2.55) gives the exact expression of a Gaussian distribution and a fairly good numerical agreement with the other two well-known distributions, the exponential and Poisson distributions, as discussed in Appendix A. It is therefore appropriate for us to use the method of steepest descent to approximate the tail distribution of the ideal and threshold detectors in order to investigate their performances, although more numerical calculations may be required such as searching for saddle point. With the availability of the digital computer at the present time, the asymptotic-expansion approximation should be very useful for solving many problems in detection and estimation theory.

Each of the detection statistics we have discussed is the sum of every ejected number n_i of photoelectrons weighted by a factor as given by (2.18), (2.26), and (2.34). In order to design a better detector, we must make the false-alarm probability of the detector small and its detection probability as large as possible, or, equivalently, make the magnitude of the statistic as small under hypothesis H_0 and as large under hypothesis H_1 as we can. From Figs. 7, 8 and 9 we can see that the ideal and threshold detectors, which utilize the information about the shape of image, are not much better than the simple detector when the optimum observation area of the simple detector is used to yield maximum detection probability or minimum error probability. In other words, to register the locations of photoelectrons does not help much to improve the detection of the image. This is because when the background light is assumed to be uniform, the effectiveness of reducing the magnitude of the statistic on the average under H_0 or increasing the magnitude of the statistic on the average under H_1 is limited, especially when the signal-to-noise ratio D^2 is low. On the other hand, by varying the observation area, we can optimize the mean numbers of photoelectrons under H_0 and H_1 effectively and reduce the error probability or improve the reliability of the simple detector.

TABLE 1

Optimum Radius for Simple Counter

$N_0 = 0.5$

N_s	$R_o (Q_0 = 10^{-3})$	$R_o (Q_0 = 10^{-5})$
1	1.31	1.37
2	1.72	1.68
4	1.72	1.68
8	2.10	1.68
12	2.10	1.98
20	2.10	1.98
24	2.46	2.28

$N_0 = 5$

N_s	$R_o (Q_0 = 10^{-3})$	$R_o (Q_0 = 10^{-5})$
1	1.36	1.37
2	1.44	1.44
4	1.60	1.58
8	1.60	1.58
12	1.75	1.65
20	1.82	1.78
24	1.82	1.78

Footnotes

Chapter II

1. Helstrom [5].

2. Papoulis [19]. Appendix II-4 gives a brief description of the saddle point method of integration. For a more thorough explanation, see Erdélyi [33] and Jeffreys [34].

3. Helstrom [10], Chapter III.

4. Van Trees [20], Chapter II.

5. Helstrom [21].

6. Helstrom and Wang [22].

7. Helstrom [10], Chapter V, §1d.

8. Gnedenko and Kolmogorov [23], Chapter 3, §17.

9. Feller [24], Chapter VI, §3.

10. Helstrom [5].

11. Farrell [6].

12. Rice [7].

13. Wang [25].

14. Helstrom [14].

Chapter III Simultaneous detection and estimation of the mean intensity of an optical image

The detection of the image on a photosensitive surface described in Chapter II is based on the knowledge about the intensity and location of the light source. In practice, however, the estimation of the parameters such as the intensity I_s and the center location $\underset{\sim}{x}_0$ of the image may be needed as well as the detection. The observer must estimate these parameters as best he can on the basis of the observed set of data $\underset{\sim}{n}$. In this chapter we will assume that if the object image is detected, the location of the image is known, but its intensity must be simultaneously estimated. One seeks a strategy to estimate the intensity, $\hat{I}_s = I_s(\underset{\sim}{n})$, which is a function of the data $\underset{\sim}{n} = (n_1, n_2 \ldots n_N)$. Two most important strategies, Bayes and maximum likelihood[1,2], will be discussed. A quadratic cost function will be used to derive the Bayes estimate. When the signal is not too weak, the Bayes estimate is approximately equivalent to the maximum likelihood estimate. An almost optimum estimate is therefore proposed and its statistical properties will be studied. The expectation of the biased estimate will be evaluated and plotted as a function of relative intensity at different observation times or total numbers N of small areas with a truncated Gaussian or parabolic image.

Simultaneous detection and estimation for a single parameter

As we have discussed in connection with the binary hypotheses tests in Chapter II, when a set of data $\underset{\sim}{b} = \{b_1, b_2 \ldots b_N\}$ is obtained, the observer will choose the hypothesis between the binary hypotheses H_0 and H_1. Since the signal received under hypothesis H_1 now depends on a certain unknown parameter θ, the observer must seek a strategy based on the N measurements of $\underset{\sim}{b}$ so that when hypothesis H_1 is chosen, the parameter θ will also be estimated[3]. If, however, H_0 is chosen, it implies that there is only background noise; therefore the parameter θ does not exist or is equal to zero. The conditional p.d.f. $P(\underset{\sim}{b}|\theta)$ is assumed to be given in general. If the cost functions $C(\hat{\theta},\theta)$, which are the costs for choosing hypothesis H_0 or H_1 and making estimate $\hat{\theta} = 0$ or $\hat{\theta}(\underset{\sim}{b})$ for given true parameter θ, are given, and if the prior p.d.f. $z(\theta)$ of the parameter θ and the conditional p.d.f. $\gamma_o(\hat{\theta}|\underset{\sim}{b})$ of the estimate $\hat{\theta}$ for given data $\underset{\sim}{b}$ are known, then the Bayes strategy can be used. The average risk[4] per experiment for simultaneous detection and estimation of the parameter is given by

$$\overline{C} = \int_{\Omega} d\theta \int_{\Delta} d\hat{\theta} \int_{\Sigma} d^N\underset{\sim}{b}\ \sigma(\theta)\ \gamma_o(\hat{\theta}|\underset{\sim}{b})\ P(\underset{\sim}{b}|\theta)\ C[\hat{\theta},\theta] \quad , \tag{3.1}$$

where Ω, Δ and Σ are the spaces for parameters θ, $\hat{\theta}$ and $\underset{\sim}{b}$ respectively.

The Bayes strategy is to properly choose the function $\gamma_o(\hat{\theta}|\underset{\sim}{b})$

so that the average risk $\overline{C}$ can be minimized. Let us define

$$\gamma_o(\hat{\theta}|\underset{\sim}{b}) = \psi(H_0|\underset{\sim}{b})\ \delta(\hat{\theta}) + \Pi(\hat{\theta}|\underset{\sim}{b}) , \tag{3.2}$$

where $\delta(\hat{\theta})$ is the Dirac delta function. $\psi(H_0|\underset{\sim}{b})$ is the conditional probability for the system to choose H_0. $\Pi(\hat{\theta}|\underset{\sim}{b})$ is the conditional p.d.f. for estimate $\hat{\theta}$ when H_1 is chosen with observed data $\underset{\sim}{b}$. Furthermore, we have

$$\int_\Delta \Pi(\hat{\theta}|\underset{\sim}{b})\ d\hat{\theta} = \psi(H_1|\underset{\sim}{b}) , \tag{3.3}$$

where $\psi(H_1|\underset{\sim}{b})$ is the conditional probability for the system to choose H_1 with given data $\underset{\sim}{b}$ and $\psi(H_1|\underset{\sim}{b}) + \psi(H_0|\underset{\sim}{b}) = 1$. We also let

$$\sigma(\theta) = \xi\ \delta(\theta) + (1-\xi)\ z(\theta) , \tag{3.4}$$

where ξ, $1-\xi$ are the prior probabilities for hypotheses H_0 and H_1 as discussed in Chapter II. $z(\theta)$ is the prior p.d.f. of parameter θ under H_1.

By substituting (3.2), (3.3) and (3.4) into (3.1) we can write the average risk as

$$\overline{C} = \int_\Sigma d^N\underset{\sim}{b} \left\{ \xi \left[\psi(H_0|\underset{\sim}{b}) C_{00} + \int_\Delta d\hat{\theta}\ \Pi(\hat{\theta}|\underset{\sim}{b})\ C_{10}(\hat{\theta}) \right] P_0(\underset{\sim}{b})
$$

$$+ (1-\xi) \int_{\Omega} d\theta \; z(\theta) \left[\psi(H_0|(\underline{b})) \; C_{01}(\theta) + \int_{\Delta} d\hat{\theta} \; \Pi(\hat{\theta}|\underline{b}) \right.$$

$$\left. C_{11}(\hat{\theta},\theta) \right] P(\underline{b}|\theta) \Bigg\} \qquad (3.5)$$

where $P_0(\underline{b}) = P(\underline{b}|H_0)$,

C_{00} is the cost of choosing H_0 when H_0 is true,

$C_{01}(\theta)$ is the cost of choosing H_0 when H_1 is true with parameter θ,

$C_{10}(\hat{\theta})$ is the cost of choosing H_1 with estimate $\hat{\theta}$ when H_0 is true,

$C_{11}(\hat{\theta},\theta)$ is the cost of choosing H_1 with estimate $\hat{\theta}$ when H_1 is true with parameter θ.

Now since

$$P(\underline{b}|\theta) \; z(\theta) = P(\theta|\underline{b}) \; P(\underline{b}) \quad , \qquad (3.6)$$

where $P(\theta|\underline{b})$ is the posterior p.d.f. and

$$P(\underline{b}) = \int_{\Omega} P(\underline{b}|\theta) \; z(\theta) \; d\theta \quad , \qquad (3.7)$$

we can also write the average risk $\overline{C}$ in terms of the conditional risks as

$$\overline{C} = \int_{\Sigma} d^{N}\underline{b}\, P(\underline{b}) \left[C_{H_0|\underline{b}} + \int_{\Delta} d\hat{\theta}\, \Pi(\hat{\theta}|\underline{b})\, C(\hat{\theta}\,|\underline{b}) \right] , \tag{3.8}$$

where

$$C_{H_0|\underline{b}} = \psi(H_0|\underline{b}) \left[\xi C_{00}\, P_0(\underline{b}) / P(\underline{b}) + (1-\xi) \int_{\Omega} d\theta\, C_{01}(\theta)\, P(\theta|\underline{b}) \right] \tag{3.9}$$

is the conditional risk when H_0 is chosen for given $\underline{b}$ and

$$C(\hat{\theta}\,|\underline{b}) = \xi\, C_{10}(\hat{\theta})\, P_0(\underline{b}) / P(\underline{b}) + (1-\xi) \int_{\Omega} d\theta\, C_{11}(\hat{\theta},\theta)\, P(\theta|\underline{b}) \tag{3.10}$$

is the conditional risk when H_1 is chosen with $\hat{\theta}$ for given $\underline{b}$. Now the p.d.f. $P(\underline{b})$ and conditional p.d.f. $\Pi(\hat{\theta}|\underline{b})$ are both positive over the space Σ of the outcome $\underline{b}$, and the conditional risk $C_{H_0|\underline{b}}$ is not a function of estimate $\hat{\theta}$, the average risk $\overline{C}$ is minimized with respect to $\hat{\theta}$ by making the conditional risk $C(\hat{\theta}\,|\underline{b})$ as small as possible for every set of data $\underline{b}$. Now we choose the p.d.f. $\Pi(\hat{\theta}|\underline{b})$ as

$$\Pi(\hat{\theta}|\underline{b}) = \psi(H_1|\underline{b})\, \delta(\hat{\theta} - \hat{\theta}(\underline{b})) , \tag{3.11}$$

where $\hat{\theta}(\underline{b})$ is the optimum estimate $\hat{\theta}$ obtained from minimizing the conditional risk $C(\hat{\theta}|\underline{b})$ and can be determined from the following

equation

$$\frac{\partial}{\partial\hat{\theta}} C(\hat{\theta}|\underline{b}) = 0 \quad \text{or}$$

$$\xi\, P_0(\underline{b})\, \frac{\partial}{\partial\hat{\theta}} C_{10}(\hat{\theta}) + (1-\xi)\, P(\underline{b}) \int_\Omega d\theta\, P(\theta|\underline{b}) \cdot \frac{\partial}{\partial\hat{\theta}} C_{11}(\hat{\theta},\theta) = 0 \,. \tag{3.12}$$

Thus the minimum average risk from (3.8) at $\hat{\theta} = \hat{\theta}(\underline{b})$ becomes

$$\begin{aligned} \overline{C}_{min} = \int_\Sigma d^N\underline{b} \Big\{ &\Big[1-\psi(H_1|\underline{b})\Big] \Big[\xi C_{00} P_0(\underline{b}) \\ &+ (1-\xi)\, P(\underline{b}) \int_\Omega d\theta\, C_{01}(\theta)\, P(\theta|\underline{b})\Big] \\ &+ \psi(H_1|\underline{b}) \Big[\xi\, C_{10}(\hat{\theta}(\underline{b}))\, P_0(\underline{b}) \\ &+ (1-\xi)\, P(\underline{b}) \int_\Omega d\theta\, C_{11}(\hat{\theta}(\underline{b}),\theta)\, P(\theta|\underline{b})\Big]\Big\}. \end{aligned} \tag{3.13}$$

If we now define

$$A(\underline{b}) = \xi\, C_{00}\, P_0(\underline{b}) + (1-\xi)\, P(\underline{b}) \int_\Omega d\theta\, C_{01}(\theta)\, P(\theta|\underline{b})$$

$$B(\underline{b},\hat{\theta}(\underline{b})) = \xi\, C_{10}(\hat{\theta}(\underline{b}))\, P_0(\underline{b}) + (1-\xi)\, P(\underline{b}) \cdot \int_\Omega d\theta\, C_{11}(\hat{\theta}(\underline{b}),\theta)\, P(\theta|\underline{b}) \,, \tag{3.14}$$

then (3.13) can be written as

$$\bar{C}_{min} = \int_{\Sigma} d^{N}\underline{b} \left\{ A(\underline{b}) + \psi(H_1|\underline{b}) \left[B(\underline{b},\hat{\theta}(\underline{b})) - A(\underline{b}) \right] \right\} . \tag{3.15}$$

As the cost functions can be chosen so that both functions $A(\underline{b})$ and $B(\underline{b},\hat{\theta}(\underline{b}))$ are positive. Then we can further minimize the average risk from (3.15) so that

$$\psi(H_1|\underline{b}) = 1 \qquad \text{if } B(\underline{b},\hat{\theta}(\underline{b})) < A(\underline{b}) ,$$

$$\left.\begin{aligned} &\psi(H_1|\underline{b}) = 0 \\ \text{or} \quad &\psi(H_0|\underline{b}) = 1 \end{aligned}\right\} \qquad \text{otherwise} . \tag{3.16}$$

This is equivalent to defining a cost likelihood ratio Λ_c where

$$\Lambda_c = \frac{(1-\xi)\, P(\underline{b}) \int_{\Omega} d\theta [C_{01}(\theta) - C_{11}(\hat{\theta}(\underline{b}),\theta)]\, P(\theta|\underline{b})}{\xi\, P_0(\underline{b})\, [C_{10}(\hat{\theta}(\underline{b})) - C_{00}]} , \tag{3.17}$$

and a decision level $\Lambda_{c0} = 1$ so that hypothesis H_1 will be chosen if $\Lambda_c > \Lambda_{c0}$ and estimate $\hat{\theta}(b)$ will be issued; otherwise, H_0 will be

chosen.

When there is no information about the cost functions, the prior probabilities of the hypotheses, or the prior p.d.f. $z(\theta)$ of the parameter, the maximum-likelihood strategy can be used. The estimate $\hat{\theta}$ will be determined from maximizing the posterior p.d.f. $P(\theta|\underset{\sim}{b})$, which is expressed in (3.6). Since $P(\underset{\sim}{b})$ is independent of θ, it is equivalent to maximizing the product of $P(\underset{\sim}{b}|\theta)$ and $z(\theta)$. With very little knowledge about $z(\theta)$, we must assume that the prior p.d.f. $z(\theta)$ is very broad, so that $z(\theta)$ will not affect the decision and estimate we have made. This implies that the estimate $\hat{\theta}$ is simply obtained by maximizing the joint conditional p.d.f. $P(\underset{\sim}{b}|\theta)$ or determined from the following equation

$$\frac{\partial}{\partial\theta} P(\underset{\sim}{b}|\theta) = 0 . \tag{3.18}$$

The estimate $\hat{\theta}$ determined from (3.18) will be a function of the data $\underset{\sim}{b}$.

When the data $\underset{\sim}{b}$ are a set of discrete random variables, the function $P(\underset{\sim}{b}|\theta)$ will be the conditional probability function instead of conditional p.d.f. All the equations we have discussed in this chapter are still valid except that we have to change the integrals $\int_{\Sigma} d^{N}\underset{\sim}{b}$ into summations $\sum_{\underset{\sim}{b}}$. For the detection of the image and estimation of its intensity of a light source, both Bayes strategy and maximum likelihood strategy will be discussed in the following paragraphs.

The operation of simultaneous detection and estimation of the signal and its parameter θ can be described by the following block diagram.

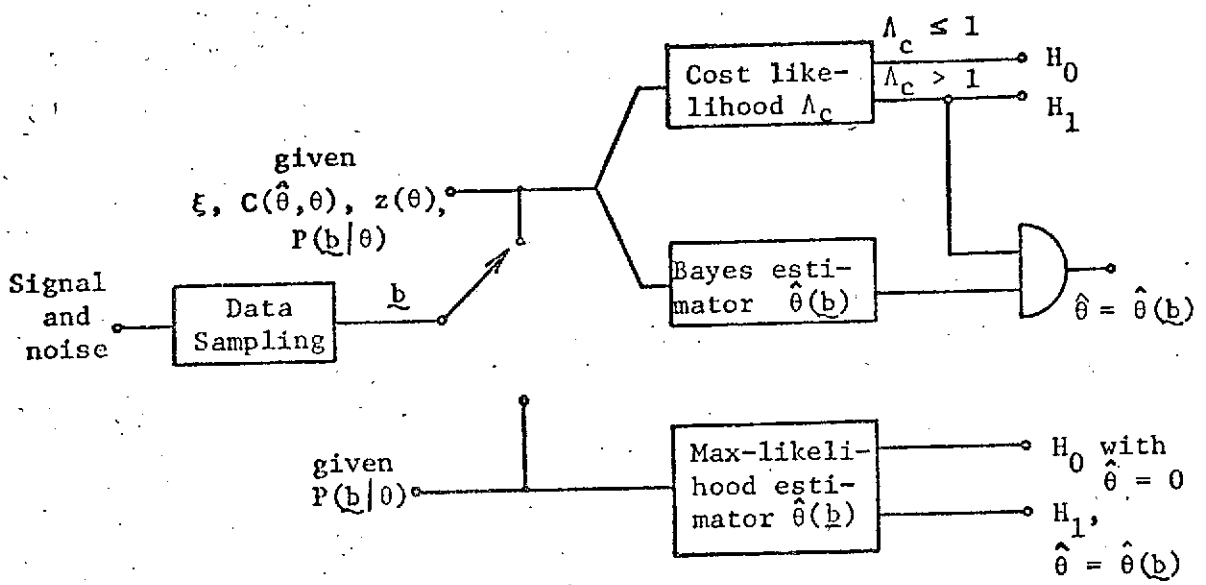

Figure 11 Block diagram for simultaneous detection and estimation of a single parameter θ from the signal.

Bayes strategy for detecting the image and estimating its intensity of a point source with a quadratic cost function

When the photosensitive surface is divided into N small areas dA, the data $\underset{\sim}{n}$ are the numbers of photoelectrons ejected from the N small areas $dA_i = dA$, $i = 1, 2 \ldots N$; $\underset{\sim}{n}$ is a set of N discrete random variables. As $TW \gg 1$, they are Poisson distributed and statistically independent. The joint conditional probability under hypothesis H_0 can be written as

$$P(\underset{\sim}{n}|I_s=0) = P_0(\underset{\sim}{n}) = \prod_{i=1}^{N} \mu^{n_i} e^{-\mu} / n_i! , \qquad (3.19)$$

where

$$\mu = \alpha T I_b \, dA \qquad (3.20)$$

is the average number of photoelectrons ejected from each area dA due to the background light illumination. The joint conditional probability under hypothesis H_1 can be written as

$$P(\underset{\sim}{n}|I_S) = \prod_{i=1}^{N} (\mu+I_S q_i)^{n_i} e^{-(\mu+I_S q_i)} / n_i! , \qquad (3.21)$$

where

$$q_i = \alpha T \gamma_i \, dA , \quad \gamma_i = \gamma(\underset{\sim}{x}_i) \qquad (3.22)$$

with $\gamma(\underset{\sim}{x}_i)$ as the weighting function given by (2.16). We let the cost functions described in (3.5) be

$$C_{10}(\hat{I}_S) = C_{10} ,$$

$$C_{11}(\hat{I}_S, I_S) = C_0(\hat{I}_S - I_S)^2 , \tag{3.23}$$

where C_{00}, C_{01}, C_{10}, C_0 are all given constants.

The Bayes estimate $\hat{I}_S(\underset{\sim}{n})$ can be determined from (3.12)

$$\hat{I}_S(\underset{\sim}{n}) = \int_0^\infty I_S \, P(I_S|\underset{\sim}{n}) \, dI_S , \tag{3.24}$$

which is the conditional expectation[5] of the intensity I_S. The posterior p.d.f. $P(I_S|\underset{\sim}{n})$ can be expressed by using (3.6) and (3.7) as

$$P(I_S|\underset{\sim}{n}) = \frac{z(I_S) \, P(\underset{\sim}{n}|I_S)}{\int_0^\infty z(I_S) \, P(\underset{\sim}{n}|I_S) \, dI_S} \tag{3.25}$$

for positive values I_S. The denominator of (3.25) can be written as

$$\int_0^\infty z(I_S) \, P(\underset{\sim}{n}|I_S) \, dI_S$$

$$= \int_0^\infty dI_S \, z(I_S) \prod_{i=1}^{N} (\mu + I_S q_i)^{n_i} \, e^{-(\mu + I_S q_i)} / n_i! \tag{3.26}$$

When the p.d.f. $z(I_S)$ is given, the Bayes estimate from (3.24) can be evaluated.

We now assume that the p.d.f. $z(I_S)$ is a gamma distributed probability function

$$z(I_S) = \frac{C^B}{\Gamma(B)} I_S^{B-1} e^{-CI_S} U(I_S) \tag{3.27}$$

with B, C real and positive constants. U(x) is the step function. If the object light is very much weaker than the background light, $I_S << I_b$, (3.26) can be calculated approximately as

$$\begin{aligned} &\int_0^\infty z(I_S)\, P(\underline{n}|I_S)\, dI_S \\ &\simeq \int_0^\infty dI_S \frac{C^B}{\Gamma(B)} I_S^{B-1} e^{-CI_S} \\ &\quad \cdot \prod_{i=1}^{N} \mu^{n_i} \left(1 + n_i \frac{I_S}{I_b} \gamma_i\right) e^{-\mu} / n_i! \\ &= \prod_{i=1}^{N} e^{-\mu} \mu^{n_i} \left(1 + n_i \gamma_i \frac{B}{CI_b}\right) / n_i! \,. \end{aligned} \tag{3.28}$$

The Bayes estimate from (3.24) becomes

$$\hat{I}_S(\underline{n}) \simeq \prod_{i=1}^{N} \frac{e^{-\mu} \mu^{n_i} \frac{B}{C} [1 + n_i \gamma_i (B+1)/CI_b] / n_i!}{e^{-\mu} \mu^{n_i} (1 + n_i \gamma_i B/CI_b) / n_i!}$$

$$= \frac{B}{C} \prod_{i=1}^{N} \left[1 + \frac{1}{B\left(1 + \frac{C}{B}\frac{I_b}{n_i \gamma_i}\right)} \right] , \qquad (3.29)$$

where all the values n_i, γ_i, I_b, B, C are known. If the object light is so strong that we can assume that there are m_1 areas dA which are so close to the image center and such that $\gamma_i I_S >> I_b$, and m_0 areas which are far away from the image center and $\gamma_i I_S << I_b$ ($m_0 + m_1 = N$ is the total number of areas into which we have divided the image), then (3.26) can be calculated approximately

$$\int_0^\infty z(I_S)\, P(\underline{n}|I_S)\, dI_S$$

$$\simeq \frac{C^B}{\Gamma(B)}\, \mu^{M_0}\, e^{-m_0\mu} \left(\prod_{i=1}^{m_1} q_i^{n_i} \right) F_N^{-1}$$

$$\int_0^\infty I_S^{B-1 + M_1}\, e^{-(C+M_q)I_S}\, dI_S \quad , \qquad (3.30)$$

where

$$F_N = \prod_{i=1}^{N} n_i! \quad , \quad M_q = \sum_{i=1}^{m_1} q_i \quad .$$

$$M_0 = \sum_{i=1}^{m_0} n_i$$

is the total number of photoelectrons ejected from the m_0 areas far from the image center.

$$M_1 = \sum_{i=1}^{m_1} n_i$$

is the total number of photoelectrons ejected from the m_1 areas close to the image center, where

$$\int_0^\infty I_S^{B-1+M_1} e^{-(C+M_q)I_S} dI_S = \frac{\Gamma(B+M_1)}{(C+M_q)^{B+M_1}} . \tag{3.31}$$

The Bayes estimate $\hat{I}_S(\underset{\sim}{n})$ according to (3.24) can be approximated as

$$\hat{I}_S(\underset{\sim}{n}) \simeq \frac{\Gamma(B+1+M_1)}{(C+M_q)\,\Gamma(B+M_1)} = \frac{B+M_1}{C+M_q} . \tag{3.32}$$

When $M_1 >> B$ we have

$$\hat{I}_S(\underset{\sim}{n}) \simeq K_b \sum_{i=1}^{m_1} n_i \tag{3.33}$$

with $K_b^{-1} = C + M_q$.

Maximum-likelihood strategy and the almost optimum intensity estimate

When there is no information about the cost function, the prior probabilities of the hypotheses, or the prior p.d.f. $z(I_S)$ of the intensity, the maximum-likelihood strategy will be used and the estimate $\hat{I}_S(\underline{n})$ will be determined from (3.18); it satisfies the following equation

$$\sum_{i=1}^{N} \frac{n_i q_i}{q_i \hat{I}_S(\underline{n}) + \mu} = \sum_{i=1}^{N} q_i \,. \tag{3.34}$$

When the object light is so much weaker than the background light that $I_S << I_b$, the estimate $\hat{I}_S(\underline{n})$ can be determined approximately from

$$\sum_{i=1}^{N} q_i \simeq \sum_{i=1}^{N} n_i q_i \mu^{-1} [1 - q_i \hat{I}_S(\underline{n}) \mu^{-1}]$$

$$\text{or} \qquad \hat{I}_S(\underline{n}) = \sum_{i=1}^{N} \mu^2 (n_i \mu^{-1} - 1) q_i \Big/ \sum_{i=1}^{N} n_i q_i^2 \,. \tag{3.35}$$

If the object light is so strong that there are m_1 areas close to the image center and $q_i \hat{I}_S(\underline{n}) >> \mu$, and m_0 areas away from the image center and $q_i \hat{I}_S(\underline{n}) << \mu$ so that they contribute little to the sum, then we approximate the estimate $\hat{I}_S(\underline{n})$ from (3.34) by

$$\hat{I}_S(\underline{n}) \simeq K \sum_{i=1}^{m_1} n_i \,, \tag{3.36}$$

where

$$K^{-1} = \sum_{i=1}^{N} q_i \quad .$$

The estimate $\hat{I}_S(\underline{n})$ we have just obtained resembles the approximate form of the Bayes estimate given by (3.33) when the object light is not too weak. In general we may not have any information about the cost functions and the prior p.d.f. $z(I_S)$. We therefore propose an almost optimum estimate $\hat{I}_{Sa}(\underline{n})$ as

$$\hat{I}_{Sa}(\underline{n}) = K \sum_{i}^{N} (n_i - \theta)\, U(n_i - \theta) \,, \tag{3.37}$$

where $U(x) = 1$ for $x > 0$ and 0 for $x \leq 0$, K is defined in (3.36). θ is the threshold level which can be determined from a preassigned false-alarm probability Q_0 such that θ is the smallest integer that satisfies the following equation

$$N \sum_{n=0}^{\theta} \mu^n \, e^{-\mu} / n! \; > N - Q_0 \,. \tag{3.38}$$

In other words, the number n_i of photoelectrons ejected from each area dA_i, $i = 1, 2 \ldots N$, will be compared with the decision level θ; if $n_i > \theta$, we will consider that some of the photoelectrons ejected from the ith area of the surface are due to the object illumination. We therefore will keep the term. If $n_i < \theta$ we

assume that the number n_i of photoelectrons ejected from the surface are due only to the background illumination; thus we will discard the term. When all the numbers n_i, $i = 1, 2 \ldots N$ are less than θ, the hypothesis H_0 will be chosen. Otherwise, the hypothesis H_1 will be chosen, and the intensity estimate $\hat{I}_S(\underline{n})$ is calculated according to (3.37).

Performance of the almost optimum intensity estimate for a truncated Gaussian or a parabolic image

The estimate $\hat{I}_S(\underline{n})$ we have discussed is a function of the N measurements $\underline{n}$. Since the data $\underline{n}$ are a set of random variables, no two experiments will yield the same value of the estimate $\hat{I}_S(\underline{n})$ even though the true value of the parameter I_S is the same in both. The most one can hope for is that the estimate $\hat{I}_S(\underline{n})$ will be close to the true value I_S in the sense of "on the average".

The mean and variance of the estimate $\hat{I}_{Sa}$ we have just discussed can be derived as follows

$$E[\hat{I}_{Sa}] = E\left[K \sum_{i=1}^{N} (n_i-\theta)\, U(n_i-\theta) \right]$$

$$= K \sum_{i=1}^{N} E[(n_i-\theta)\, U(n_i-\theta)]$$

$$= K \sum_{i=1}^{N} \left[\bar{n}_i - \theta - \sum_{n_i=0}^{\theta} (n_i-\theta)\, P(n_i|I_S) \right],$$

$$\mathrm{Var}[\hat{I}_{Sa}] = \mathrm{Var}\left[K \sum_{i=1}^{N} (n_i-\theta)\, U(n_i-\theta) \right]$$

$$= K^2 \sum_{i=1}^{N} \mathrm{Var}[(n_i-\theta)\, U(n_i-\theta)]$$

$$= K^2 \sum_{i=1}^{N} \left\{ \bar{n}_i + \bar{n}_i^2 - 2\bar{n}_i\theta + \theta^2 \right.$$

$$- \sum_{n_i=0}^{\theta} (n_i-\theta)^2 \, P(n_i|I_S) - \left[\bar{n}_i - \theta - \sum_{n_i=0}^{\theta} (n_i-\theta) \, P(n_i|I_S) \right]^2 \Bigg\} , \tag{3.39}$$

where

$$P(n_i|I_S) = \bar{n}_i^{\,n_i} \, e^{-\bar{n}_i} / n_i! ,$$

$$\bar{n}_i = \mu + q_i I_S .$$

To investigate the statistical performance of the estimate $\hat{I}_{Sa}$ as discussed in (3.37), a truncated Gaussian image will be postulated. The image surface with radius R_o is divided into M small rings as shown in Fig. 12.

The average number of photoelectrons ejected from each ring by the background light illumination is assumed to be evenly distributed and symmetrical with respect to the image center. The area dR_i of the ith ring can be calculated as

$$dR_i = \int_{(i-1)\Delta\rho}^{i\Delta\rho} \int_0^{2\pi} \rho d\rho \, d\phi$$

$$= \pi(2i - 1)\Delta\rho^2 = (2i - 1) A_o , \tag{3.40}$$

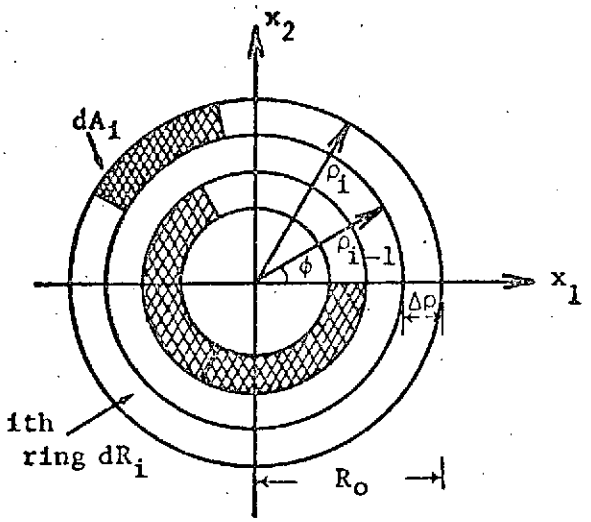

Figure 12 Image surface divided into rings

where $A_o = \pi\Delta\rho^2$, $\Delta\rho = \rho_i - \rho_{i-1}$ for $i = 1, 2 \ldots M$. Here $\rho^2 = x_1^2 + x_2^2$ with $x_1 = \rho \cos \phi$, $x_2 = \rho \sin \phi$ as the rectangular coordinates used in Fig. 3.

The total number of rings is

$$M = R_o / \Delta\rho \quad . \tag{3.41}$$

If we further divide each ith ring into a number (2i-1) of small equal areas dA_i such that $dA_i = A_o$, the total number of small equal areas dA_i from the whole image is

$$N = \sum_{i=1}^{M} (2i-1) = M^2 \quad . \tag{3.42}$$

The distribution of the mean number of photoelectrons ejected from the image surface by the object light is described by the weighting function $\gamma(\underline{x}_i)$ as given in (2.16) and (2.56) for a Gaussian image, or in polar coordinates we can write

$$r(\rho) = B_0 e^{-\rho^2/2\sigma^2} , \tag{3.43}$$

where B_0 is a constant and σ is the width of the Gaussian function. The average number of photoelectrons emitted from each small area dA_i $(= A_o)$ is assumed to be evenly distributed and is proportional to the intensity I_S. We calculate the coefficient

$$q_i' = \alpha T \int_0^{2\pi} \int_{(i-1)\Delta\rho}^{i\Delta\rho} \gamma(\rho)\, \rho d\rho\, d\phi$$

$$= \alpha T B_0 2\pi\sigma^2 \left\{ e^{-(i-1)^2 R_A^2/2N} - e^{-i^2 R_A^2/2N} \right\} , \tag{3.44}$$

where

$$q_i' = q_i(2i-1) \tag{3.45}$$

with q_i defined in (3.22). $R_A = R_o/\sigma$. R_o is the radius of the truncated image under observation. i is the index (i = 1, 2 . . . M).

Because of the presence of the background light, one would

like to investigate the estimate $\hat{I}_{Sa}$ with respect to the true intensity I_S in terms of the signal-to-noise ratio. In other words one could assume that the energy of the background light falling on the image surface within the radius R_o of the truncated image is equivalent to that from the object light with intensity

$$I_{SO} = \frac{\mu M^2}{\sum_{i=1}^{M} q'_i} \quad . \tag{3.46}$$

Since the total average number of photoelectrons ejected from the surface of the image is proportional to the incident energy , the intensity of the point source can be described by

$$I_S = d^2 I_{SO} \quad , \tag{3.47}$$

where d^2 is called the signal-to-noise ratio for the truncated Gaussian image.

The mean and variance of the estimate $\hat{I}_{Sa}$ according to (3.37) can be written as

$$E[\hat{I}_{Sa}] = K \sum_{i=1}^{M} \left\{ (2i-1) \left[\bar{n}_i - \theta - \sum_{n_i=0}^{\theta} (n_i-\theta)\, P_1(n_i) \right] \right\},$$

$$Var[\hat{I}_{Sa}] = K^2 \sum_{i=1}^{M} (2i-1) \left\{ \bar{n}_i + \bar{n}_i^2 - 2\bar{n}_i\theta + \theta^2 \right.$$

$$- \sum_{n_i=0}^{\theta} (n_i-\theta)^2 \, P_1(n_i) \; - \left[\bar{n}_i - \theta - \sum_{n_i=0}^{\theta} (n_i-\theta) \, P_1(n_i) \right]^2 \Bigg\}, \tag{3.48}$$

where $P_1(n_i) = \bar{n}_i^{\,n_i} \; e^{-\bar{n}_i} / n_i!$ with $\bar{n}_i = \mu + q_i' I_S/(2i-1)$ and μ and q_i' are given in (3.20) and (3.45).

We also define the error of the estimate $\hat{I}_{Sa}$ by

$$\text{Err} = (\text{Var } \hat{I}_{Sa})^{\frac{1}{2}} / E[\hat{I}_{Sa}] \tag{3.49}$$

as the ratio of the standard deviation to the mean value of the estimate $\hat{I}_{Sa}$ given by (3.48).

To investigate the estimate $\hat{I}_{Sa}$ in terms of various parameters we assume the background light intensity corresponding to an object light with unit intensity $I_{S0} = 1$. The average number of photo-electrons ejected from each area dA due to the background light is assumed to be 0.1 for an observation time T and coefficient α (i.e., $\mu = \alpha T \, I_b A_o = 0.1$). The false-alarm probability is preassigned at 0.01. Where the parameters B_0 and σ are set at 1, the expected value of the estimate $\hat{I}_{Sa}$ is calculated at various ratios $R_A = 0.5$, 1, 2 and 3 and is plotted as a function of the relative intensity I_S defined in (3.47) in Fig. 13. As the size of the observation area changes, the estimate $\hat{I}_{Sa}$ will also be affected. In Fig. 14, the estimate $\hat{I}_{Sa}$ is plotted as a function of the relative intensity I_S

Figure 13 Mean intensity estimate $\hat{I}_{Sa}$ vs. relative intensity I_S for truncated Gaussian image; $Q_0 = 10^{-2}$, the number of rings is 100. Mean background counts $\mu = 0.1$ at $R_A = \sigma = 1$ for time T. Curves are indexed by parameter R_A defined in (3.44).

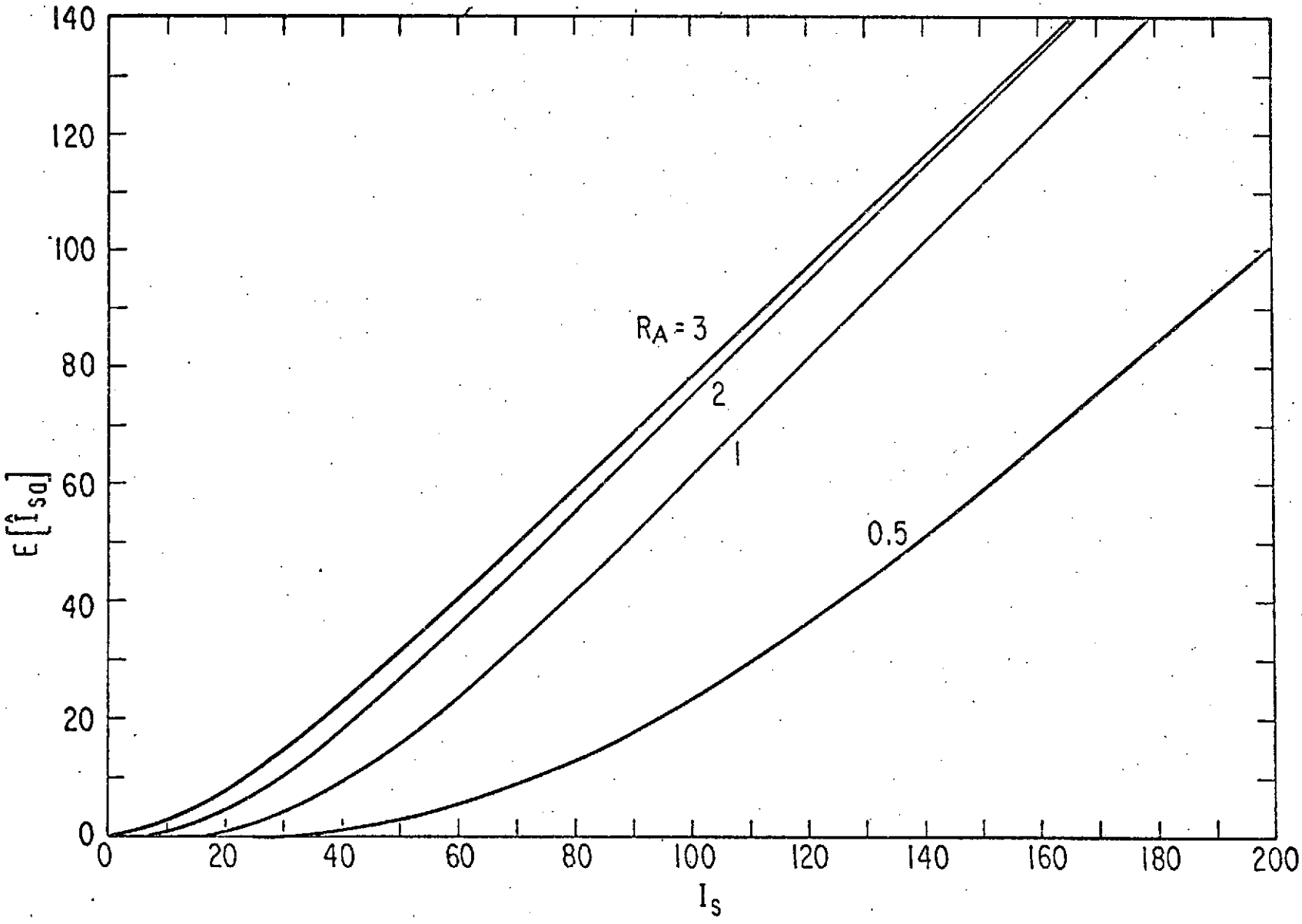
140
120
100
80
60
40
20
0
E[$\hat{I}_{sq}$]
$R_A = 3$
2
1
0.5
0
20
40
60
80
100
120
140
160
180
200
I_s

Figure 14 Mean estimate $\hat{I}_{Sa}$ vs. relative intensity I_S for truncated Gaussian image; $Q_0 = 10^{-2}$, $\mu = 0.1$ at $R_A = 1$ for 100 rings for time T. Curves are indexed by the parameter M defined in (3.41).

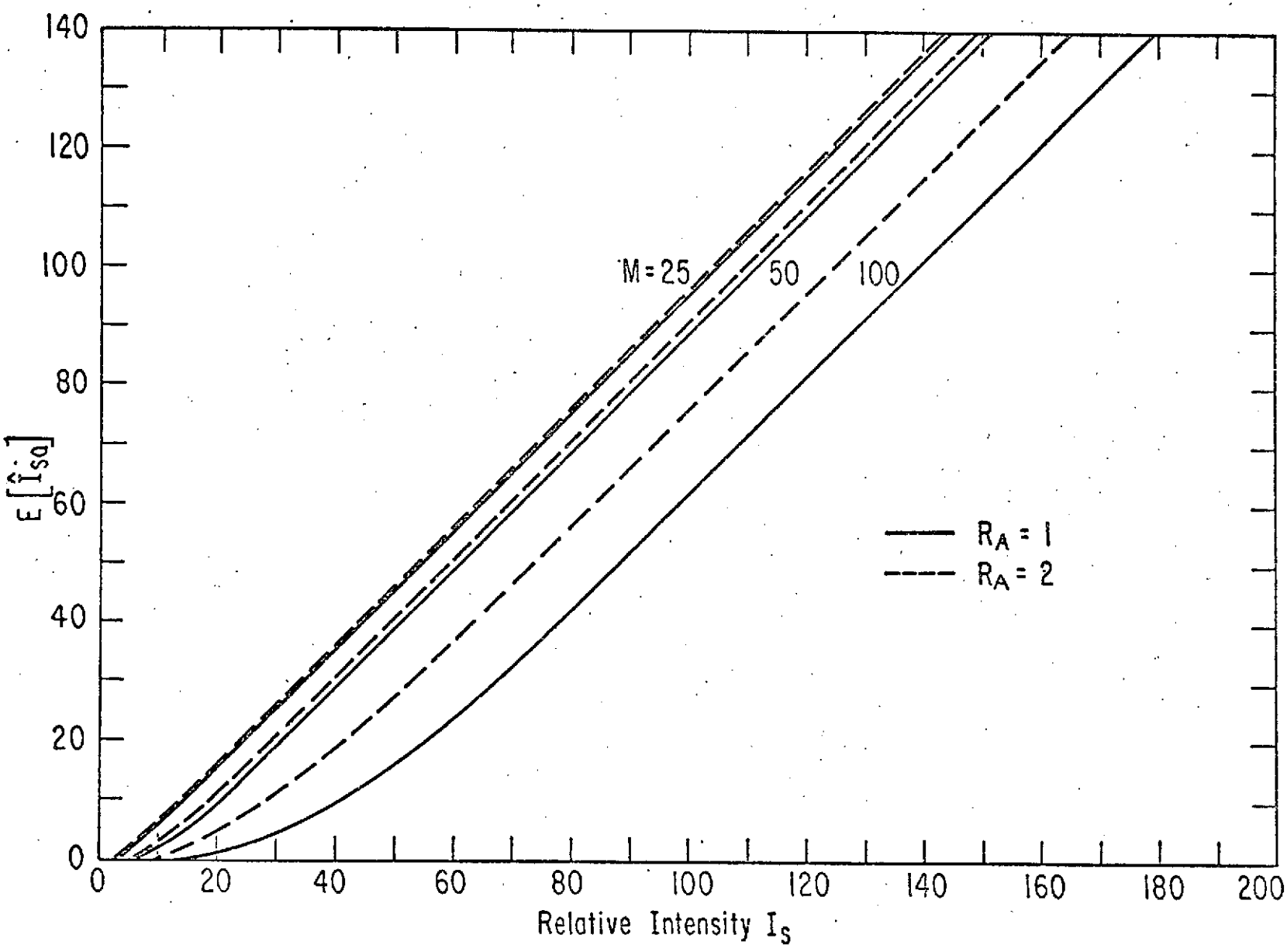
140
120
100
80
60
40
20
0
E[Î²sq]
M = 25
50
100
R_A = 1
R_A = 2
0
20
40
60
80
100
120
140
160
180
200
Relative Intensity I_S

Figure 15 Mean estimate $\hat{I}_{Sa}$ vs. relative intensity I_S for truncated Gaussian image; $Q_0 = 10^{-2}$, $M = 100$, $\mu = 0.1$ at $R_A = 1$ for time T. Curves are indexed by observation intervals T.

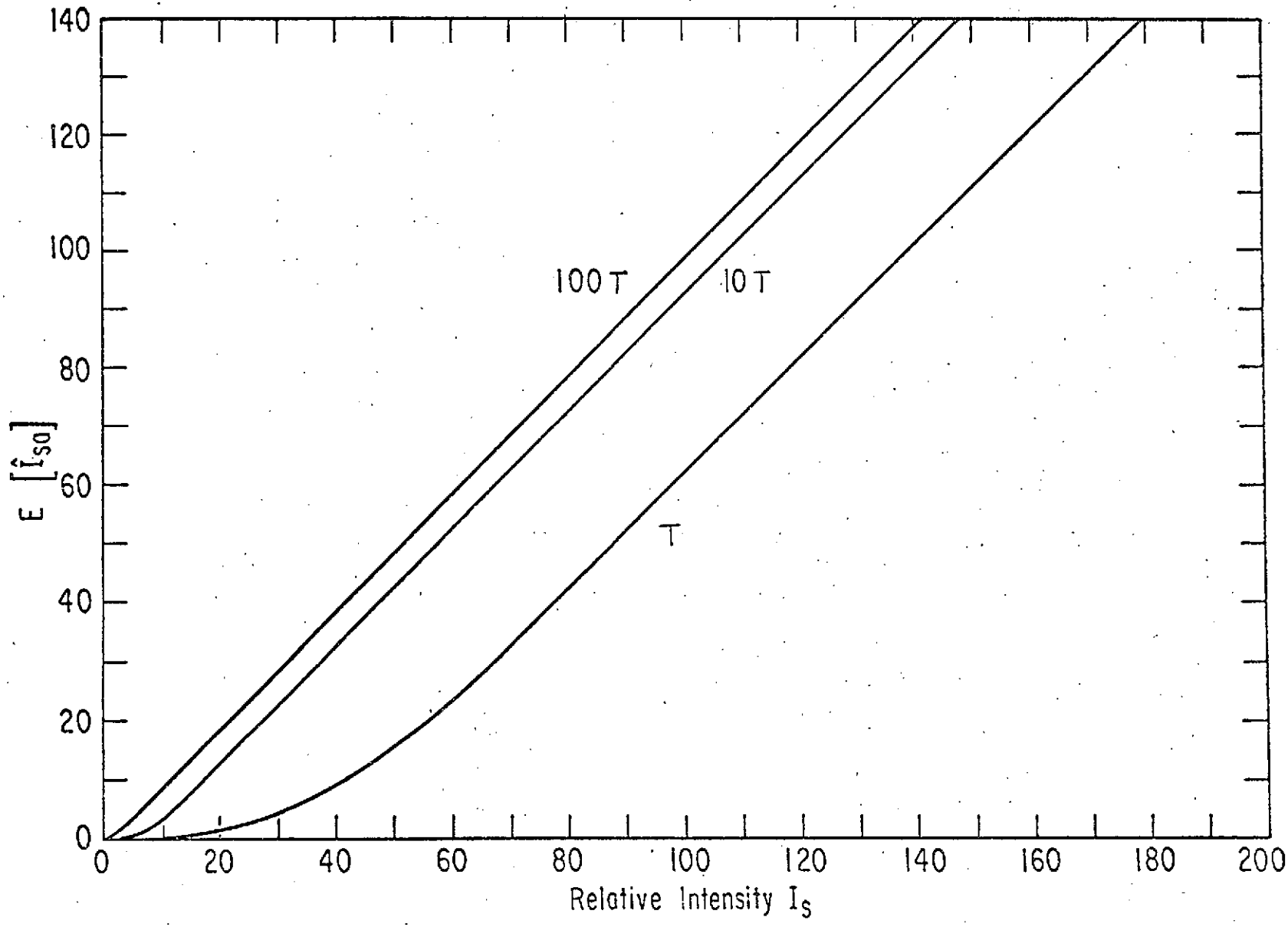
140
120
100
80
60
40
20
0
E [$\hat{I}_{SO}$]
100 T
10 T
T
0
20
40
60
80
100
120
140
160
180
200
Relative Intensity I_S

when the observation area is fixed but divided into three different numbers of rings, 25, 50 and 100. In Fig. 15 the estimate $\hat{I}_{Sa}$ is also plotted as a function of I_S with three different observation times T, 10T and 100T.

Observations also have been made by assuming the image as a parabolic function. That is (3.43) replaced by

$$\begin{aligned} \gamma'(y) &= B'(R_o^2 - \rho^2) && |\rho| < R_o , \\ &= 0 && |\rho| > R_o , \end{aligned} \tag{3.50}$$

where R_o is the radius of the image; B' is a constant. The coefficient q_i'' can be calculated from

$$\begin{aligned} q_i'' &= \alpha T \int_0^{2\pi} d\phi \int_{(i-1)\Delta\rho}^{i\Delta\rho} \gamma'(\rho)\, \rho d\rho \\ &= \alpha T\, B' \pi\, R_o^4\, M^{-2} \left[(2i-1)M^2 - (2i^3-3i^2+2i-\tfrac{1}{2})\right]^{-1} . \end{aligned} \tag{3.51}$$

The mean, variance, and error can be calculated by using (3.48) and (3.49). At B' = 1, R_o = 1 we have plotted the expected value of the estimate $\hat{I}_{Sa}$ as a function of I_S at three different values of parameters M and T in Fig. 16 and Fig. 17 with Q_0 = 0.01. The error of the estimate $\hat{I}_{Sa}$ for the parabolic image is also plotted as a

function of the average background photoelectrons μ at fixed $I_S = 10$ and 20 in Fig. 18, where the error for $\mu = 0.1$ is 9.24% at $I_S = 10$ or 3.15% at $I_S = 20$ with the image surface divided into 100 rings. The average number μ is then varied either by changing the size of each dA or the observation time T.

Figure 16 Mean estimate $\hat{I}_{Sa}$ vs. relative intensity I_S for parabolic image; $Q_0 = 10^{-2}$, $\mu = 0.1$ at $R_o = 1$ for time T. Curves are indexed by parameter M.

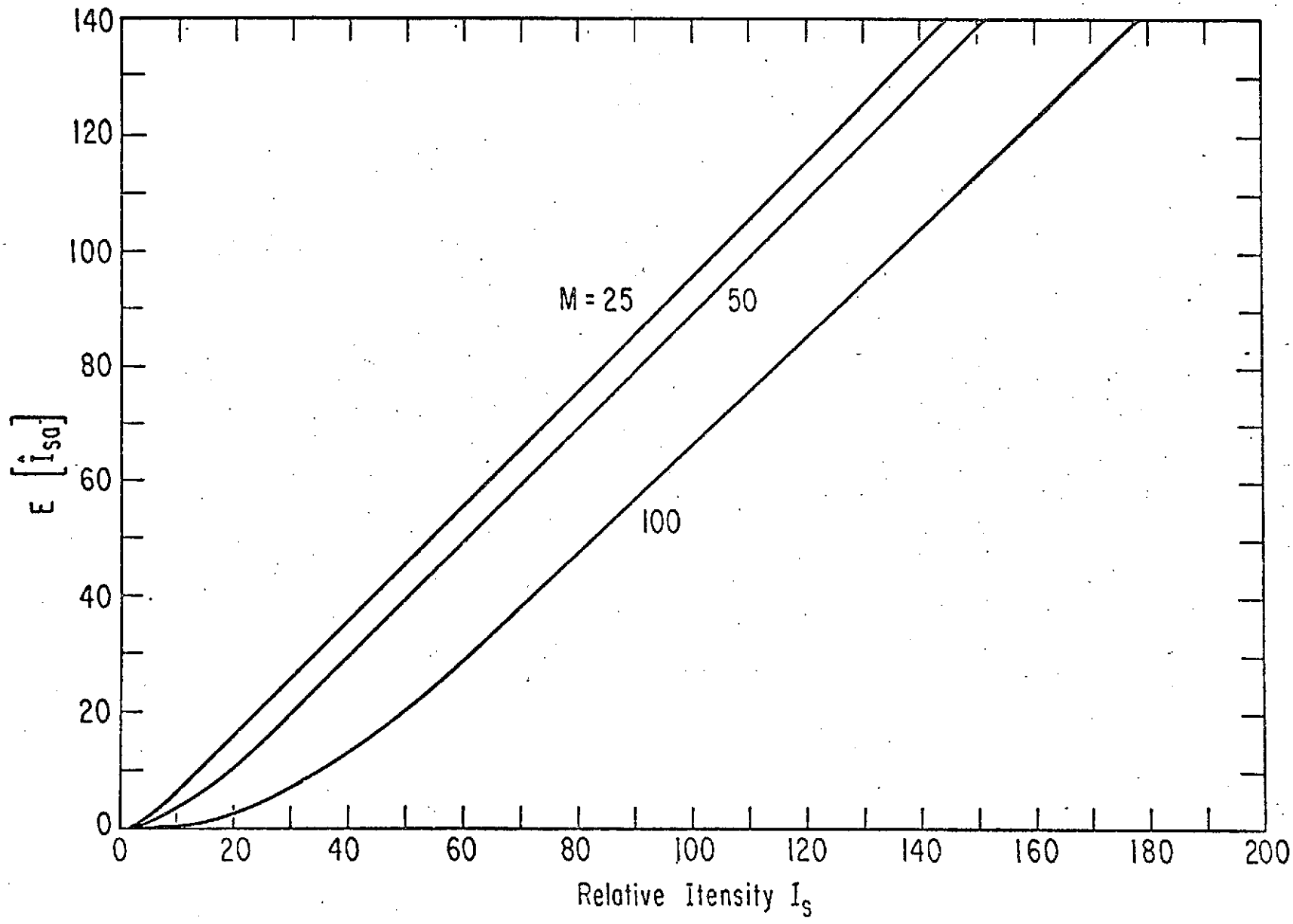
140
120
100
80
60
40
20
0
E [$\hat{i}_{sq}$]
M = 25
50
100
0
20
40
60
80
100
120
140
160
180
200
Relative Itensity I_s

Figure 17 Mean estimate $\hat{I}_{Sa}$ vs. relative intensity I_S for parabolic image: $Q_0 = 10^{-2}$, $\mu = 0.1$ at $R_o = 1$ for time T. Curves are indexed by observation intervals T.

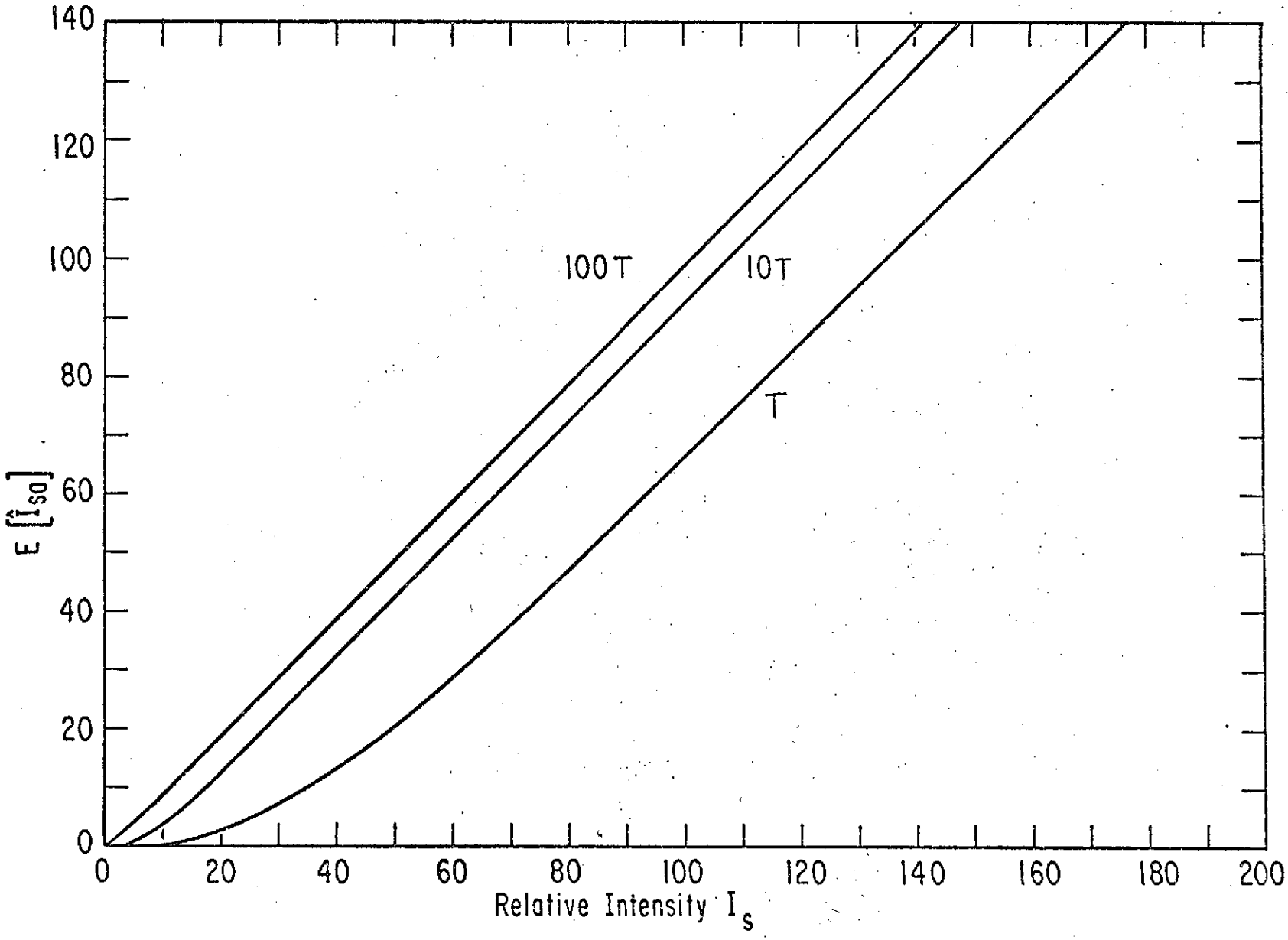
140
120
100
80
60
40
20
0
E [$\hat{i}_{sq}$]
100T
10T
T
0
20
40
60
80
100
120
140
160
180
200
Relative Intensity I_s

Figure 18 Error vs. mean counts μ for parabolic image; $Q_0 = 10^{-2}$. Curves are indexed by parameters I_S defined in (3.47) and M.

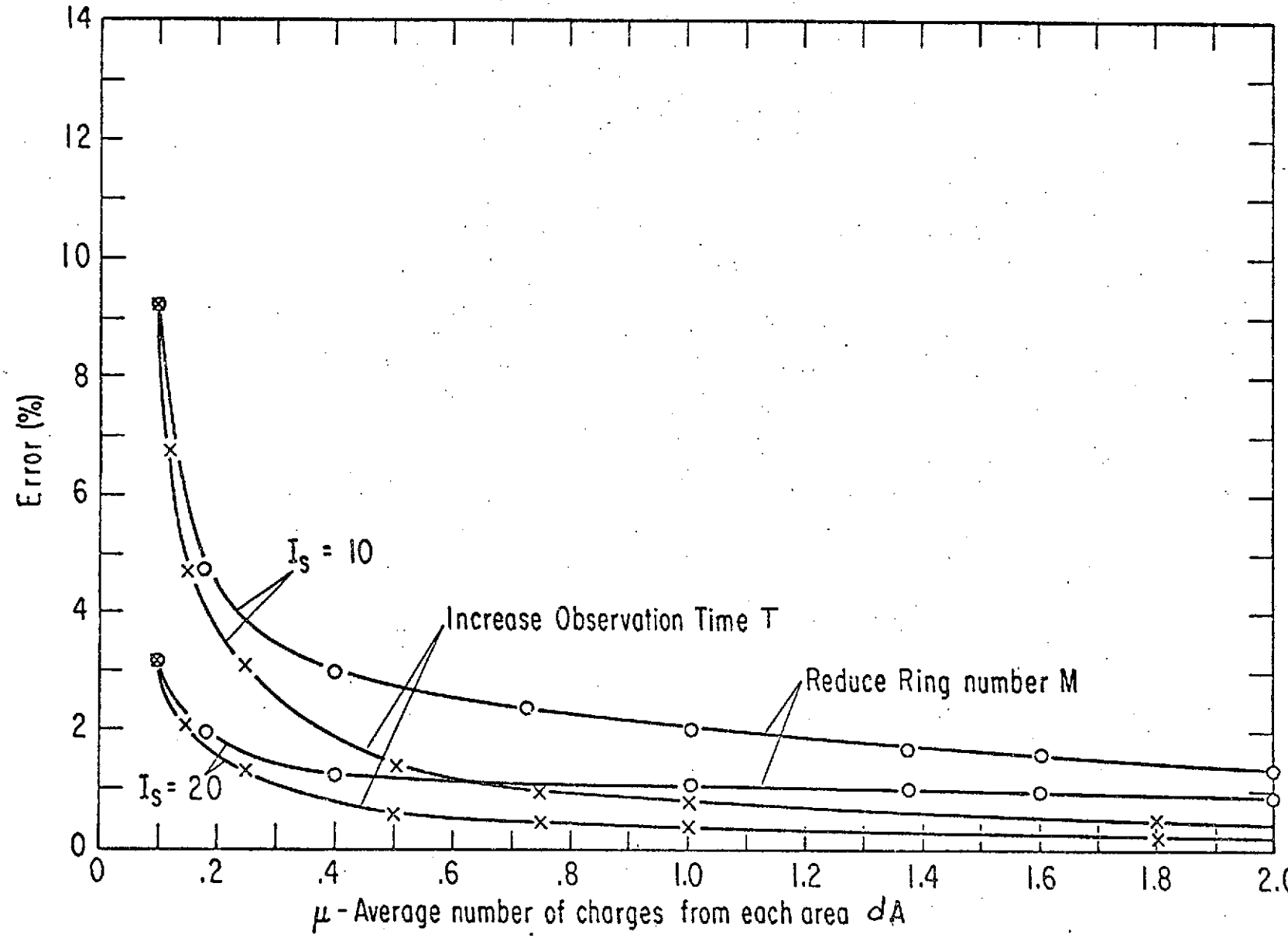
14
12
10
8
6
4
2
0
Error (%)
I_S = 10
I_S = 20
Increase Observation Time T
Reduce Ring number M
0
.2
.4
.6
.8
1.0
1.2
1.4
1.6
1.8
2.0
μ - Average number of charges from each area dA

Discussion

A statistical model for simultaneous detection and estimation of a stochastic image is proposed. When the prior p.d.f. of the source intensity and the prior probability ξ are known and the cost functions are available, the Bayes strategy leads to the optimum operation. If there is no information about the prior probability and the cost functions, the maximum-likelihood strategy can be used. Upon examining the estimate $\hat{I}_S$ for both strategies, it is interesting to note that the Bayes estimate $\hat{I}_S$ from (3.33) for a quadratic cost function is approximately the same as the maximum-likelihood estimate from (3.36) when the signal is not very weak.

For a Gaussian image, the bias and linearity will be improved when R_A is increased; however, after R_A is larger than 2, very little improvement will be gained by increasing R_A farther. In order to reduce the bias of the estimate, it is always wise to use longer observation time, to divide the observed image into a smaller number M of rings, or to use larger observation image area. In addition, a suitable constant should be added into the estimate $\hat{I}_{Sa}$ to compensate for the bias. The observed image has an effective range of R_A between 1 and 2 for the Gaussian truncated image. For the image of parabolic shape, one should always use the whole image area. As long as the observation area on the image surface is properly defined, the shape of the function $\gamma(\rho)$ has no significant effect on the quality of the estimate. To reduce the estimation error, increasing

the observation time is more effective than decreasing the total number M of rings as we can see from Fig. 18.

When the false-alarm probability Q_0 is preassigned, randomization can be used and the probability f for choosing H_1 when $n_i = \theta$ can be calculated from the difference in (3.38) or

$$f = \left(1 + Q_0/N - \sum_{n=0}^{\theta} \mu^n \ e^{-\mu} / n!\right) e^{\mu} \mu^{-\theta} \theta! .$$

The estimate $\hat{I}_{Sa}$ from (3.37) can be modified as

$$\hat{I}'_{Sa} = K \left[\sum_{i=1}^{N} n_i \, U(n_i - \theta - 0.5) + f\theta m_0 - C\right] . \quad (3.52)$$

m_0 is the total number of the areas where $n_i = \theta$. C is some constant. Since the bias of the estimate approaches a constant as the intensity becomes larger, as we can see from Fig. 15 or Fig. 17, a proper constant C can be found to compensate for the bias.

Footnotes

Chapter III

1. Helstrom [10], Chapter VIII.
2. Van Trees [20], Chapter II.
3. Middleton [9].
4. Middleton [26], Chapter I.
5. Helstrom [10], Chapter VIII, eq. (1.11).

Chapter IV Detectors for resolving two point sources in optical communication by photon-counting techniques

The techniques we have discussed of counting the photoelectrons from the photosensitive surface for the detection and estimation of the object light intensity have great usefulness in binary optical communication. Since those devices, such as photomultipliers, image tubes, and image orthicons are well developed in commercial industry, photon-counting techniques, combined with adequate digital computer facilities can be used for many purposes. In this chapter we will further discuss some detectors used for resolving the point sources in optical communication by photon-counting techniques. The ideal detector described in Chapter II can be used for distinguishing two light sources of equal radiant power from a single source with twice the radiant power or for deciding which one of the two light sources is present. In the absence of background light, the performance of the ideal detector for deciding which one of the two light sources is present will be compared with two other receivers, the simple detector and the counting comparator. The intensities of the optical images due to the point sources will be postulated to be Gaussian distributed spatially. As uniform background light also passes through the aperture, the error probabilities of the simple detector and the counting comparator will be calculated with a finite observation area. When the point sources are mislocated, the effects on the ideal detector and the counting comparator will be discussed, and their average error probabilities will be calculated.

Ideal detector for resolving two light sources from the one light source

When two point sources with equal radiant power are very close to each other, they may often appear to the observer as one source with twice the radiant power, located midway between them. The criterion given by Rayleigh for two point sources to be resolved is that the peak illuminance of the diffraction pattern of one source will not fall closer than the first minimum of the diffraction pattern of the other. In this section, we will construct the optimum statistic for the resolution of the two point sources from the standpoint of a classical hypothesis test[1]. The observer will choose between two hypotheses, (H_1) two point sources whose images have equal intensities are present at $\underset{\sim}{x}$ and $-\underset{\sim}{x}$ in the image plane, and (H_0) one source with twice the power is located at the origin. The optimum statistic g described by (2.18) in Chapter II, based on observing the set of $\underset{\sim}{n}$ photoelectrons, can still be applied here. The intensity $I_k(\underset{\sim}{x})$ given by (2.15) can now be written as

$$I_k(\underset{\sim}{x}_i) = I_b + I_S \gamma_k(\underset{\sim}{x}_i), \quad \text{for } k = 0, 1 , \tag{4.1}$$

where the weighting functions are given by

$$\gamma_k(x_{1i},x_{2i}) = \frac{1}{2}\left[\gamma(x_{1i} - kx_0,x_{2i}) + \gamma(x_{1i} + kx_0,x_{2i})\right], \tag{4.2}$$

and $\gamma(x_{1i},x_{2i}) = \gamma(\underset{\sim}{x}_i)$ is described by (2.16). I_b is the uniform intensity of the background light. I_S is the intensity of the point

source, whose image is centered at $(x_0,0)$ or $(-x_0,0)$ on the photosensitive surface under hypothesis H_1 as shown by Figure 3.

The optimum statistic for binary detection of the point sources can be derived from the likelihood ratio in a way similar to (2.18), and we write

$$g_R = \sum_{i=0}^{N} n_i \ln H_R(\underset{\sim}{x}_i) , \tag{4.3}$$

where the function $H_R(\underset{\sim}{x}_i)$ defined in (2.17) becomes

$$\begin{aligned} H_R(\underset{\sim}{x}_i) &= I_1(\underset{\sim}{x}_i) / I_0(\underset{\sim}{x}_i) \\ &= 1 + \frac{I_S[\gamma_1(\underset{\sim}{x}_i) - \gamma_0(\underset{\sim}{x}_i)]}{I_b[1 + \frac{I_S}{I_b}\gamma_0(\underset{\sim}{x}_i)]} \\ &= 1 + D^2[u_1(\underset{\sim}{x}_i) - u_0(\underset{\sim}{x}_i)][1 + D^2 u_0(\underset{\sim}{x}_i)]^{-1} , \end{aligned} \tag{4.4}$$

and $u_k(x_i) = A_o \gamma_k(x_i)$, $k = 0, 1$, $D^2 = I_S/I_b A_o$. Here A_o is an arbitrarily defined finite area, as discussed in Chapter II.

Since the weighting function lies between 0 and 1, $0 < \gamma_k(\underset{\sim}{x}) < 1$ for $k = 0$ or 1. We will have $0 < H_R(\underset{\sim}{x}_i) < 1$ for some areas where $\gamma_0(\underset{\sim}{x}) > \gamma_1(\underset{\sim}{x})$. This implies that the statistic g_R is no longer a sum of non-negative random variables. As TW >> 1, the m.g.f. of the optimum statistic g_R according to (2.19) from Chapter II becomes

$$h_{Rk}(s) = \exp\left\{\alpha T I_b \int_A d^2\underline{x}[1+D^2 u_k(\underline{x})][(H_R(\underline{x}))^{-s}-1]\right\}, \quad k=0,1 \quad , \quad (4.5)$$

where A is the area of the receptor, T is the observation interval, and α is the coefficient defined in Chapter II. Since the average number difference $\Delta N = \sum_{i=1}^{N} (\bar{n}_{i1} - \bar{n}_{i0})$ vanishes in this case, the statistic g_R from (4.3) is the logarithm of the likelihood ratio defined by (2.11). It is easy to show $h_{R1}(s) = h_{R0}(s-1)$. Also when Bayes strategy is used, the decision level g_{R0} is zero when the prior probability is $\xi = \frac{1}{2}$ as we can see from (2.13).

In order to use the numerical method of steepest descent, the complex phase, defined by (A7) in Appendix A when (4.5) is used, can be written as

$$\phi_{Rk}(s) = g_{R0}^{-1}\alpha T I_b \int_A d^2\underline{x}[1+D^2 u_k(\underline{x})][(H_R(\underline{x}))^{-s}-1]+s, \quad k=0,1 \quad . \quad (4.6)$$

The saddle-point will be determined by solving the equation $\phi'_{Rk}(s)=0$ or

$$g_{R0} = \alpha T I_b \int_A d^2\underline{x}[1+D^2 u_k(\underline{x})](H_R(\underline{x}))^{-s} \ln H_R(\underline{x}), \quad \text{for } k=0,1 \quad . \quad (4.7)$$

The nth derivative of the complex phase for both H_1 and H_0 as $n \geq 2$ can be written as

$$\phi_{Rk}^{n}(s) = (-1)^n \alpha T I_b \int_A d^2\underline{x}[1+D^2 u_k(\underline{x})](H_R(\underline{x}))^{k-s} \ln^n H_R(\underline{x}) \quad , \quad (4.8)$$

for k=0,1

and $\phi_{R0}^{n}(s_0) = \phi_{R1}^{n}(s_1)$ for $n \geq 1$ where s_k is the saddle-point under H_k for k = 0,1 and satisfies (4.7) and (2.51). Because the function $H_R(\underline{x})$ has the term $\gamma_0(\underline{x})$ in the denominator as given in (4.4), the evaluation of (4.6), (4.7) or (4.8) will involve a double integration. The iteration procedure to search for the saddle point as discussed in Chapter II will be tedious numerically although it can be carried out by the digital computer. In the meantime, the nth cumulant under hypothesis H_k for k = 0 or 1 is

$$G_{Rk}^{n} = (-1)^n \frac{d^n}{ds^n} \ln h_{Rk}(s)\Big|_{s=0}$$

$$= (-1)^n \alpha T I_b \int_A d^2\underline{x}[1 + D^2 u_k(\underline{x})] \ln^n H_R(\underline{x}), \text{ for } k=0,1 \quad (4.9)$$

If all the nth cumulants for n > 2 are negligible in comparison with the second cumulant, the distribution of the statistic g_R can be approximated by a Gaussian function. The mean and variance of the statistic can be calculated from (4.9) at n = 1 and n = 2. We have not carried out any numerical example for this ideal detector. However, we will investigate the performance of the ideal detector with a Gaussian image in the next paragraph for the decision whether a single source is located at $\underline{x}$ or at $-\underline{x}$.

Ideal detector for binary detection in optical communication

In order to transmit the information about the bit "1" or the bit "0", an optical system can be used by focusing a radiant source either on the upper half plane or the lower half plane of a photosensitive surface. The observer will choose between the hypotheses: (H_1) the bit "1" and (H_0) the bit "0" on the basis of the set of photoelectrons ejected from a large number of small areas of the photosensitive surface. The intensity of the image of the light source at point ($\underline{x}_i$) of the surface under hypothesis H_k for k = 0 or 1 in the presence of the uniform background light can be described by

$$I_k(\underline{x}_i) = I_b + I_S \gamma_k(\underline{x}_i) \tag{4.10}$$

with $\gamma_k(\underline{x}_i) = \gamma(x_{1i}, x_{2i} + (-1)^k x_0)$, for k = 0 or 1.

where $\gamma(x_{1i}, x_{2i})$ is the weighting function and $(0,x_0)$ or $(0,-x_0)$ is the center location of the image on the upper half or the lower half of the photosensitive surface, and I_b is the uniform intensity of the background light.

The optimum statistic g_R from the likelihood ratio can be expressed according to (4.3) with $H_R(\underline{x})$ as the ratio of $I_1(\underline{x})$ and $I_0(\underline{x})$ defined by (4.10). g_R will be compared with the decision level g_{R0}, and hypothesis H_1 will be chosen if $g_R > g_{R0}$. Otherwise hypothesis H_0 will be chosen. The m.g.f. of the statistic g_R and its cumulants will be involved with double integration as discussed in the previous

paragraph. However, when the background light is negligible or absent so that $I_b = 0$, the distribution of the statistic can be derived directly from the inverse Fourier transform of the characteristic function when Gaussian images are postulated, and the performance of the ideal detector can be analyzed as follows.

The function $H_R(\underline{x})$ described in (4.4) at $I_b = 0$ becomes

$$H_R(\underline{x}_i) = I_1(\underline{x}_i)/I_0(\underline{x}_i)$$

$$= \gamma_1(\underline{x}_i)/\gamma_0(\underline{x}_i) , \tag{4.11}$$

where for the Gaussian images we have

$$\gamma_k(\underline{x}_i) = \frac{1}{2\pi\sigma^2} \exp\{-\frac{1}{2\sigma^2}[x_{1i}^2+(x_{2i} + (-1)^k x_0)^2]\}, \tag{4.12}$$

for $k = 0$ or 1 ,

and the function $H_R(\underline{x}_i)$ from (4.11) becomes

$$H_R(x_i) = \exp(2x_0 x_{2i}/\sigma^2), \; x_0 > 0 \; . \tag{4.13}$$

Thus the statistic g_R will be the sum of the numbers of photoelectrons ejected from each small area dA_i, $i = 1, 2...$ or N, weighted by the coordinate x_{2i} of the center location (x_{1i}, x_{2i}) of that area. As we pass the limit $dA_i \to 0$, the m.g.f. of the optimum statistic can be

written as

$$h_{Rk}(s) = \exp\left[\alpha T I_S \int_{-\infty}^{\infty}\int_{-\infty}^{\infty} dx_1 dx_2\ \gamma_k(\underline{x})\left[(H_R(\underline{x}))^{-s}-1\right]\right]$$

$$= \exp\left[N_s\left(\exp\left\{2\left(\frac{x_0}{\sigma}\right)^2\left[(-1)^k+s\right]s\right\}-1\right)\right], \qquad (4.14)$$

for k=0,1

with $N_s = \alpha T I_S$ as the total number of photoelectrons emitted from the photosensitive surface during the observation interval (0,T) because of the light from the source.

If we expand the right-hand side of (4.14) into a series of $\exp[2(\frac{x_0}{\sigma})^2\ ((-1)^k + s)\ s]$ we have

$$h_{Rk}(s) = \exp(-N_s)\sum_{n=0}^{\infty}\frac{N_s^{\,n}}{n!}\exp\left[-M_{nk}s + \frac{\sigma_n^{\,2}s^2}{2}\right], \qquad (4.15)$$

for k=0,1

where
$$M_{nk} = -2n\left(\frac{x_0}{\sigma}\right)^2(-1)^k \qquad \text{for } n=0,1,2\ldots$$

$$\sigma_n^{\,2} = 4n\left(\frac{x_0}{\sigma}\right)^2 \qquad k=0,1 \qquad . \qquad (4.16)$$

The m.g.f. $h_{Rk}(s)$ from (4.15) is a convergent power series where the nth term of the series is the m.g.f. of the Gaussian random variable with mean M_{nk} and variance $\sigma_n^{\,2}$ given by (4.16) and is weighted by a

factor $\exp(-N_s)\ N_s^{\,n}/n!$. The p.d.f. of the statistic g_R can be obtained by taking the inverse Fourier transform of its characteristic function and can be written as

$$P_k(g_R) = \exp(-N_s)\left\{\delta(g_R)+\sum_{n=1}^{\infty}\frac{N_s^{\,n}}{n!\sqrt{2\pi}\,\sigma_n}\exp\left[-\frac{1}{2\sigma_n^{\,2}}(g_R - M_{nk})^2\right]\right\}, \quad \text{for } k=0,1 \tag{4.17}$$

where $\delta(g_R)$ is the Dirac delta function[3].

The p.d.f. of the statistic g_R has the delta function at the origin. The probability that there is no photoelectron ejected at all is $\exp(-N_s)$.

The distribution of the statistic under hypothesis H_k for k=0 or 1 is

$$\begin{aligned} F_k(g_{R0}) &= P_r[g_R \le g_{R0}] = 1 - \int_{g_{R0}}^{\infty} P_k(g_R)\ dg_R \\ &= 1 - \exp(-N_s)\sum_{n=1}^{\infty}\frac{N_s^{\,n}}{n!}\ \text{erfc}\left(\frac{g_{R0} - M_{nk}}{\sigma_n}\right), \quad \text{for } g_{R0} \ge 0 \\ &= 1 - \exp(-N_s)\left[1 + \sum_{n=1}^{\infty}\frac{N_s^{\,n}}{n!}\ \text{erfc}\left(\frac{g_{R0} - M_{nk}}{\sigma_n}\right)\right], \end{aligned}$$

$$\text{for } g_{R0}<0 \tag{4.19}$$

with $\sigma_n^{\,2}$ and M_{nk} given by (4.16) and the function erfc(x) defined by (2.44) in Chapter II.

The nth cumulant of the statistic can be also derived as follows ,

$$G_{Rk}^{\,n} = (-1)^n \frac{d^n}{ds^n} \ln h_{Rk}(s)\big|_{s=0}$$

$$= (-1)^n N_s \left(\frac{2x_0}{\sigma^2}\right)^n \int_{-\infty}^{\infty} \frac{1}{\sqrt{2\pi}\,\sigma} \exp\left[-\frac{1}{2\sigma^2}(x_2+(-1)^k x_0)^2\right] x_2^n dx_2$$

$$= (-1)^n N_s \left(\frac{2x_0}{\sigma^2}\right)^n \mu_{nk}, \quad \text{for } k=0,1 , \tag{4.20}$$

where $$\mu_{nk} = \int_{-\infty}^{\infty} \frac{1}{\sqrt{2\pi}\,\sigma} \exp\left[-\frac{1}{2\sigma^2}(x_2 + (-1)^k x_0)^2\right] x_2^{\,n}\, dx_2$$

$$= \sigma^n E\left[X - (-1)^k \frac{x_0}{\sigma}\right]^n$$

$$= \sigma^n \sum_{r=0}^{n} \binom{n}{r} (-1)^{kr} \left(\frac{x_0}{\sigma}\right)^r E[X^{n-r}]$$

is the nth central moment[4] of a zero mean Gaussian random variable X with unit variance and

$$E[X^n] = 1\cdot 2\cdot 3 \ldots (n-1) \text{ for n even}$$
$$= 0 \qquad \text{for n odd,} \qquad \binom{n}{r} = \frac{n!}{r!(n-r)!} .$$

The average error probability according to (2.6) is equal to the Bayes cost when the relative costs $C_{10} - C_{00}$ and $C_{01} - C_{11}$ are equal and $C_{01} = C_{10} = 1$, $C_{00} = C_{11} = 0$. The decision level g_{R0} will be set at zero when $\xi = \frac{1}{2}$, and the minimum error probability of the ideal

detector can be calculated from

$$P_e = \frac{1}{2} Q_0 + \frac{1}{2}(1 - Q_d)$$

$$= \frac{1}{2} \exp(-N_s) \left[1 + 2 \sum_{n=1}^{\infty} \frac{N_s^n}{n!} \operatorname{erfc}(\sqrt{n} \frac{x_0}{\sigma})\right] \qquad (4.21)$$

for n=1,2,...

At N_s = 0.1, 0.5, 1, 2, and 5, the error probabilities of the ideal detector have been calculated and plotted as a function of the ratio $(\frac{2x_0}{\sigma})$ by the solid curves in Fig. 19 where $2x_0$ is the distance separating the images, which are centered at $(0,x_0)$ and $(0, -x_0)$ of the surface. σ is the width of the Gaussian image described in (4.12). The error probability P_e will be reduced as the distance $2x_0$ between the two images increases. However, P_e will be limited by a value of $\frac{1}{2} \exp(-N_s)$ as the ratio $2x_0/\sigma$ approaches to infinity. Therefore, the larger the value of N_s, the better the performance of the detector will be.

Figure 19 Average error probability P_e in binary bits detection vs. distance of separation ($2 x_0/\sigma$) between images for ideal detector, counting comparator, or simple detectors in the absence of background light; $N_s = 0.1, 1, 2, 5$.

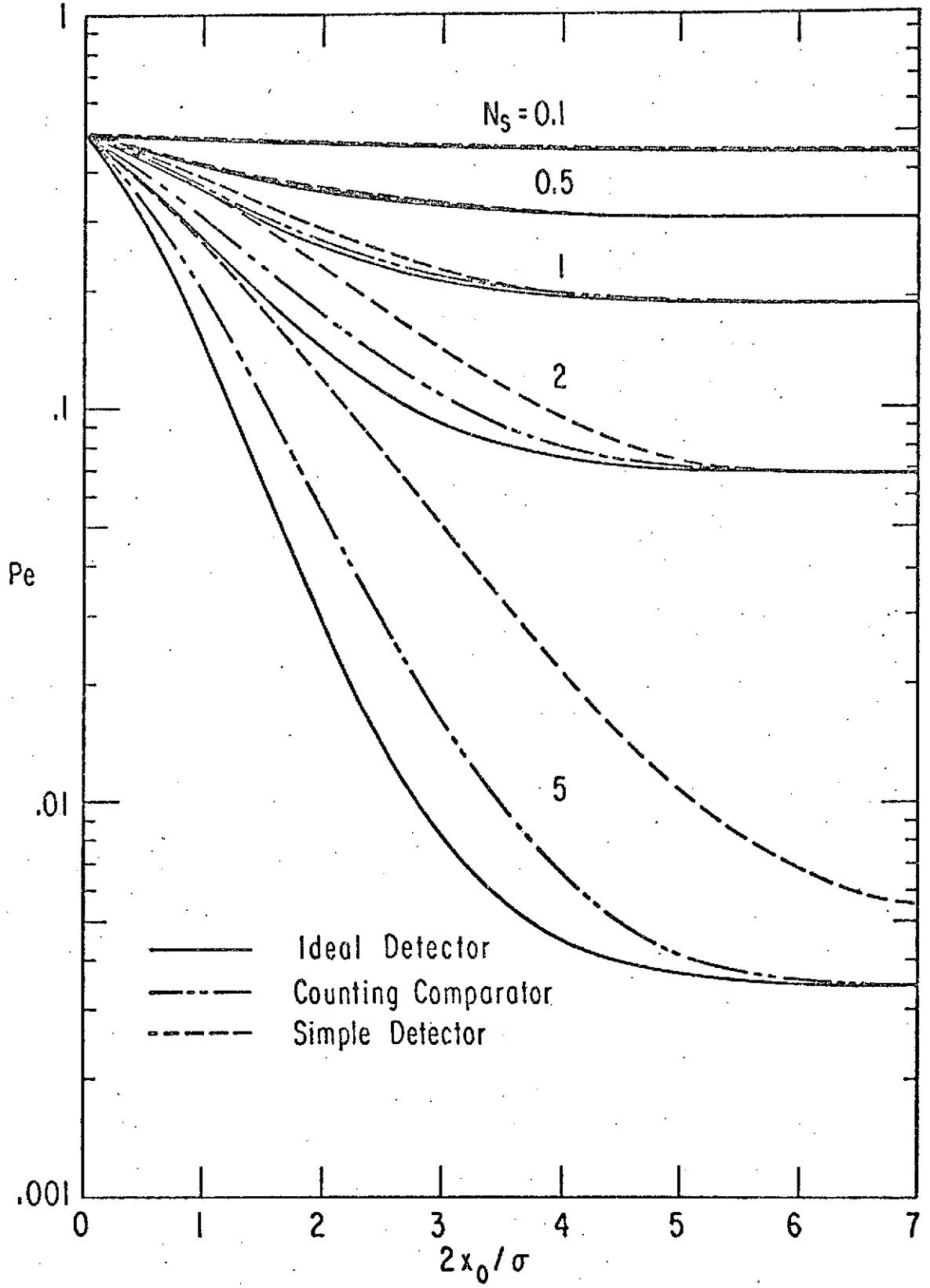
1
.1
.01
.001
Pe
$N_S = 0.1$
0.5
1
2
5
Ideal Detector
Counting Comparator
Simple Detector
0
1
2
3
4
5
6
7
$2x_0/\sigma$

Simple detector for detection of binary-bits

When background light also passes through the aperture and corrupts the object light, a simple way is to measure the total number of photoelectrons ejected from a finite area A' of the upper half photosensitive surface centered at $(0,x_0)$. The simple detector described in Chapter II thus can be used here to detect the binary bits. As $TW >> 1$, the number of photoelectrons ejected from the area A' has a Poisson distribution. The conditional probability under hypothesis H_k for $k = 0$ or 1 is given by (2.3) where the means can be determined from

$$\bar{n}_{T1} = \alpha T \iint_{A'} [I_b + I_S \gamma(x_1, x_2 - x_0)] \, dx_1 \, dx_2 ,$$

$$\bar{n}_{T0} = \alpha T \iint_{A'} [I_b + I_S \gamma(x_1, x_2 + x_0)] \, dx_1 \, dx_2 . \qquad (4.22)$$

For a Gaussian image, with $\gamma_k(\underline{x})$ given in (4.12) and $A' = \pi R_0^2 \sigma^2$ is the circular area of the upper half surface where $x_1^2 + (x_2 - x_0)^2 \leq R_0^2 \sigma^2$. We have

$$\bar{n}_{T1} = \alpha T \iint_{A'} \{I_b + I_S \frac{1}{2\pi\sigma^2} \exp[-\frac{1}{2\sigma^2}(x_1^2 + (x_2 - x_0)^2)]\} dx_1 \, dx_2$$

$$= \alpha\pi R_0^2 \sigma^2 T I_b + \alpha T \frac{I_S}{2\pi} \int_0^{2\pi} \int_0^{R_0} \exp(-\frac{R^2}{2}) \, R dR d\theta$$

$$= N_0 [\frac{1}{2} R_0^2 + D^2 (1 - \exp(-R_0^2/2))] ,$$

$$\bar{n}_{T0} = \alpha T \iint_{A'} [I_b + I_S \frac{1}{2n\sigma^2} \exp[-\frac{1}{2\sigma^2}(x_1^2+(x_2+x_0)^2)]]dx_1\ dx_2$$

$$= \alpha\pi R_0^2\sigma^2 T I_b + \alpha T \frac{I_S}{2\pi}\int_0^{2\pi}\int_0^{R_0} \exp[-\frac{R^2}{2} - \frac{2Rx_0}{\sigma}\cos\theta - \frac{2x_0^2}{\sigma^2}]$$

$$\cdot RdRd\theta$$

$$= N_0[\frac{1}{2}R_0 + D^2(1 - Q(\frac{2x_0}{\sigma}, R_0))] \quad , \tag{4.23}$$

where $Q(a,b)$ is the "Q function"[5] for constants a and b, and

$$N_0 = 2\pi\sigma^2\alpha T\ I_b$$

$$D^2 = N_0/\alpha T I_S = N_0/N_s \ .$$

N_0 is the average number of photoelectrons ejected from an area $2\pi\sigma^2$ during the interval (0,T), D^2 is the signal-to-noise ratio as defined in (2.57) and (2.58).

If A' is a square area, that is,we only consider the area $A' = 4R_0^2\sigma^2$ for $|x_2 - x_0| \le R_0\sigma$, $|x_1| \le R_0\sigma$ in the upper half plane, the means can be calculated as

$$\bar{n}_{T1} = \alpha T \int_{-R_0\sigma}^{R_0\sigma} dx_1 \int_{x_0-R_0\sigma}^{x_0+R_0\sigma} dx_2$$

$$\cdot \{I_b + I_S \frac{1}{2\pi\sigma^2} \exp\{-\frac{1}{2\sigma^2}[x_1^2 + (x_2 - x_0)^2]\}\}$$

$$= 4R_0^2\sigma^2\alpha T I_b + \alpha T \frac{I_S}{2\pi}\left[\int_{-R_0}^{R_0} \exp(-\frac{R^2}{2})dR\right]^2$$

$$= N_0[\frac{2R_0^2}{\pi} + D^2(1 - 2\,\mathrm{erfc}(R_0))^2] \quad ,$$

$$\bar{n}_{T0} = \alpha T \int_{-R_0\sigma}^{R_0\sigma} dx_1 \int_{x_0-R_0\sigma}^{x_0+R_0\sigma} dx_2 \{I_b + I_S \frac{1}{2\pi\sigma^2}$$

$$\cdot \exp[-\frac{1}{2\sigma^2}(x_1^2 + (x_2+x_0)^2]\}$$

$$= N_0\{\frac{2R_0^2}{\pi} + D^2(1 - 2\,\mathrm{erfc}(R_0))[\mathrm{erfc}(\frac{2x_0}{\sigma} - R_0)$$

$$- \mathrm{erfc}(\frac{2x_0}{\sigma} + R_0)]\} \quad . \tag{4.24}$$

The observer will compare the number of photoelectrons n ejected from the area A' with a decision level g_{R0} such that H_1 will be chosen if $n > g_{R0}$ and H_0 otherwise. The decision level can be determined according to (2.33) and

$$g_{R0} = (\ln \Lambda_{s0} + \bar{n}_{T1} - \bar{n}_{T0})[\ln(\bar{n}_{T1}/\bar{n}_{T0})]^{-1}, \tag{4.25}$$

where Λ_{s0} is the decision level on the likelihood ratio and can be calculated according to (2.2) when the cost functions are given. For the Neyman Pearson strategy, randomization must be used, and g_{R0} is then an integer, which can be determined from (2.74), where Q_0 is preassigned. The reliability and the average error probability can be calculated by using (2.73) and (2.6). As the background light also passes through the aperture, there is a certain optimum size of the observation area

at which for a fixed value of the false-alarm probability, the detection probability is maximum, as we have discussed in Chapter II.

The result and discussion would be the same if the observation area A' were taken from the lower half of the photosensitive surface and centered at $(0,-x_0)$. We only have to change the weighting function by

$$\gamma_k(\underline{x}) = \gamma(x_1, x_2 - (-1)^k x_0), \text{ for } k=0,1 , \tag{4.26}$$

where the mean numbers $\bar{n}_{T0}$ and $\bar{n}_{T1}$ observed from the lower half plane will be the same as given by (4.22), (4.23) or (4.24).

In order to compare with the ideal detector just discussed, we shall investigate the performance of the simple detector in the absence of background light. The observation area A' will be now taken as the whole upper (or lower) half plane. For a Gaussian image with $\gamma_k(\underline{x})$ given by (4.12) the mean numbers can be written as

$$\begin{aligned}
\bar{n}_{T1} &= N_s \int_{-\infty}^{\infty} dx_1 \int_0^{\infty} dx_2 \frac{1}{2\pi\sigma^2} \exp[-\frac{1}{2\sigma^2}(x_1^2+(x_2 - x_0)^2)] \\
&= N_s[1 - \text{erfc}(\frac{x_0}{\sigma})] , \\
\bar{n}_{T0} &= N_s \int_{-\infty}^{\infty} dx_1 \int_0^{\infty} dx_2 \frac{1}{2\pi\sigma^2} \exp[-\frac{1}{2\sigma^2}(x_1^2+(x_2+x_0)^2)] \\
&= N_s \text{ erfc}(\frac{x_0}{\sigma}) .
\end{aligned} \tag{4.27}$$

When the relative costs are equal and $\xi = \frac{1}{2}$, the decision level is $g_{R0} = (\bar{n}_{T1} - \bar{n}_{T0})[\ln(\bar{n}_{T1}/\bar{n}_{T0})]^{-1}$ for the Bayes strategy. The error probability P_e is calculated according to (2.77) and plotted as a function of the ratio $(2x_0/\sigma)$ by the dashed curves in Fig. 19 at N_s = 0.1, 0.5, 1, 2, and 5. As the ratio $(\frac{2x_0}{\sigma})$ approaches infinity, where $\bar{n}_{T1} \to N_s$ and $\bar{n}_{T0} \to 0$, the error probability P_e will be also limited by $\frac{1}{2}\exp(-N_s)$, which is half of the probability for n=0 with the average number N_s.

The error probability P_e of the simple detector in the absence of the background light can be further reduced if the optimum observation area is considered. That is, instead of taking the whole upper half plane, the observation area will be moved up from the center line by a distance x_d such that the error probability according to (2.77) is minimum. In other words, for the Gaussian image we can take the proper integral range of x_2 from (4.27) as (x_d,∞) instead of $(0,\infty)$ as $x_d > 0$ so that the probability P_e can be further minimized. For N_s = 5, the typical values of x_d at different values of ratio (x_0/σ) are listed in table 2. The minimized P_e is plotted as a function of $(2x_0/\sigma)$ in Fig. 20 where the error probabilities of the ideal detector and the simple detector at x_d=0 are also plotted.

When the background light also passes through the aperture, the observation area A' for Gaussian image discussed in (4.23) or (4.24) can be used. With the square area $A' = 4\sigma^2$ at R_0=1, the means are calculated from (4.24), and the error probabilities of the simple detector are plotted as a function of N_s for N_0 = 0, 0.1, 0.5, and

1 at $x_0/\sigma = 2$ in Fig. 21 by the dashed curves. In Fig. 22, the error probabilities are also plotted as a function of N_s at $x_0/\sigma = 1$ and $x_0/\sigma = 2$ for the square area $A' = 4\sigma^2$ by the dashed curves. When the mean number $\bar{n}_{T0}$ is fixed at 0.5, 1 or 2, the error probability of the simple detector is then plotted as a function of the number difference $\Delta N = \bar{n}_{T1} - \bar{n}_{T0}$ in Fig. 23 by the dashed curves.

Figure 20 Average error probability P_e in binary bits detection vs. distance ($2 x_0/\sigma$) for ideal detection and simple detector with fixed area or optimum area in the absence of the background light, $N_s = 5$.

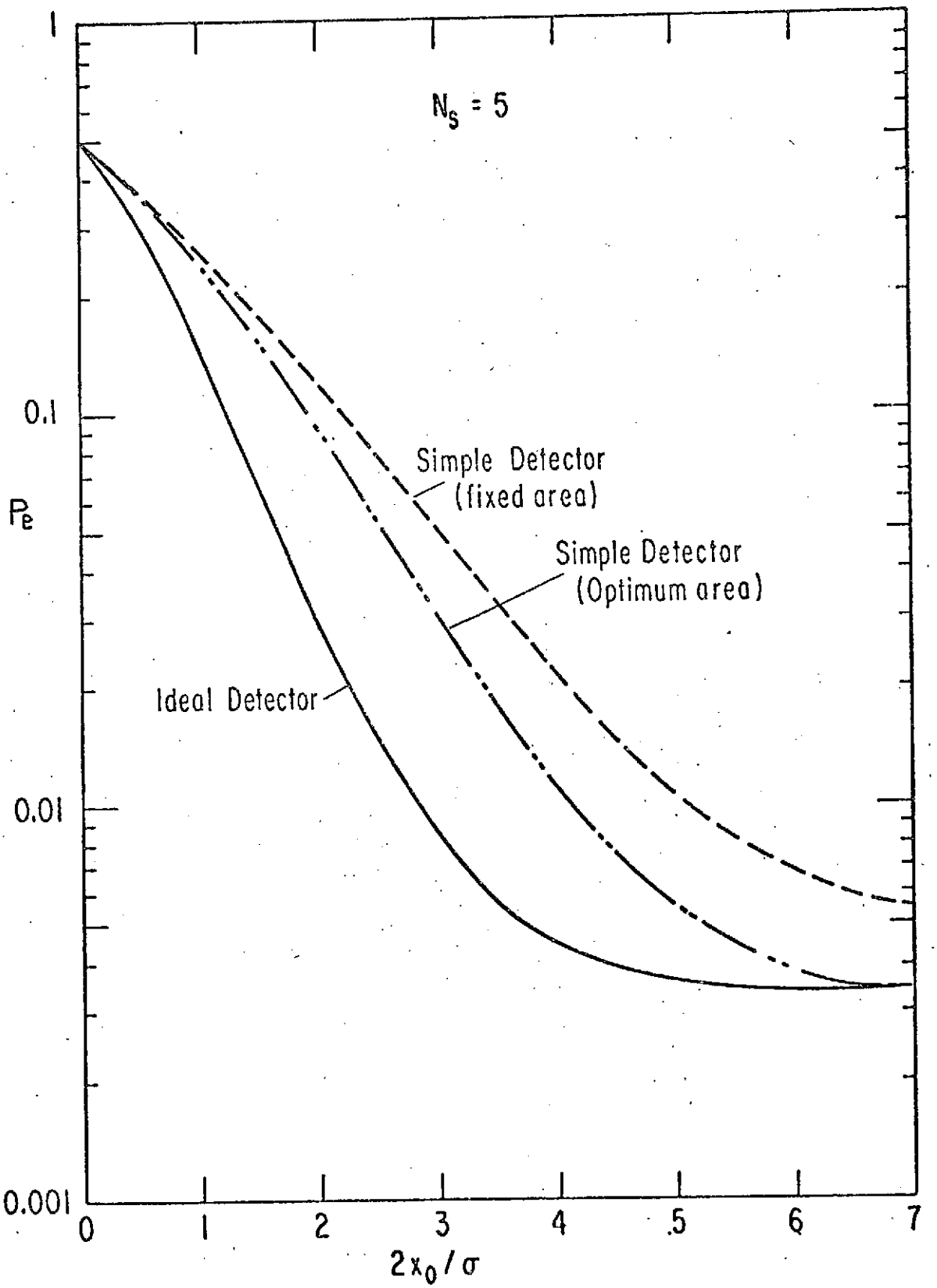
1
0.1
0.01
0.001
P_e
$N_s = 5$
Simple Detector
(fixed area)
Simple Detector
(Optimum area)
Ideal Detector
0
1
2
3
4
5
6
7
$2x_0/\sigma$

Figure 21 Average error probability P_e in binary detection vs. average number N_s for simple detector, counting comparator with square observation area $A' = 4\sigma^2$ at $R_0 = 1$ and $x_0/\sigma = 2$, $N_0 = 0, 0.1, 0.5, 1.$

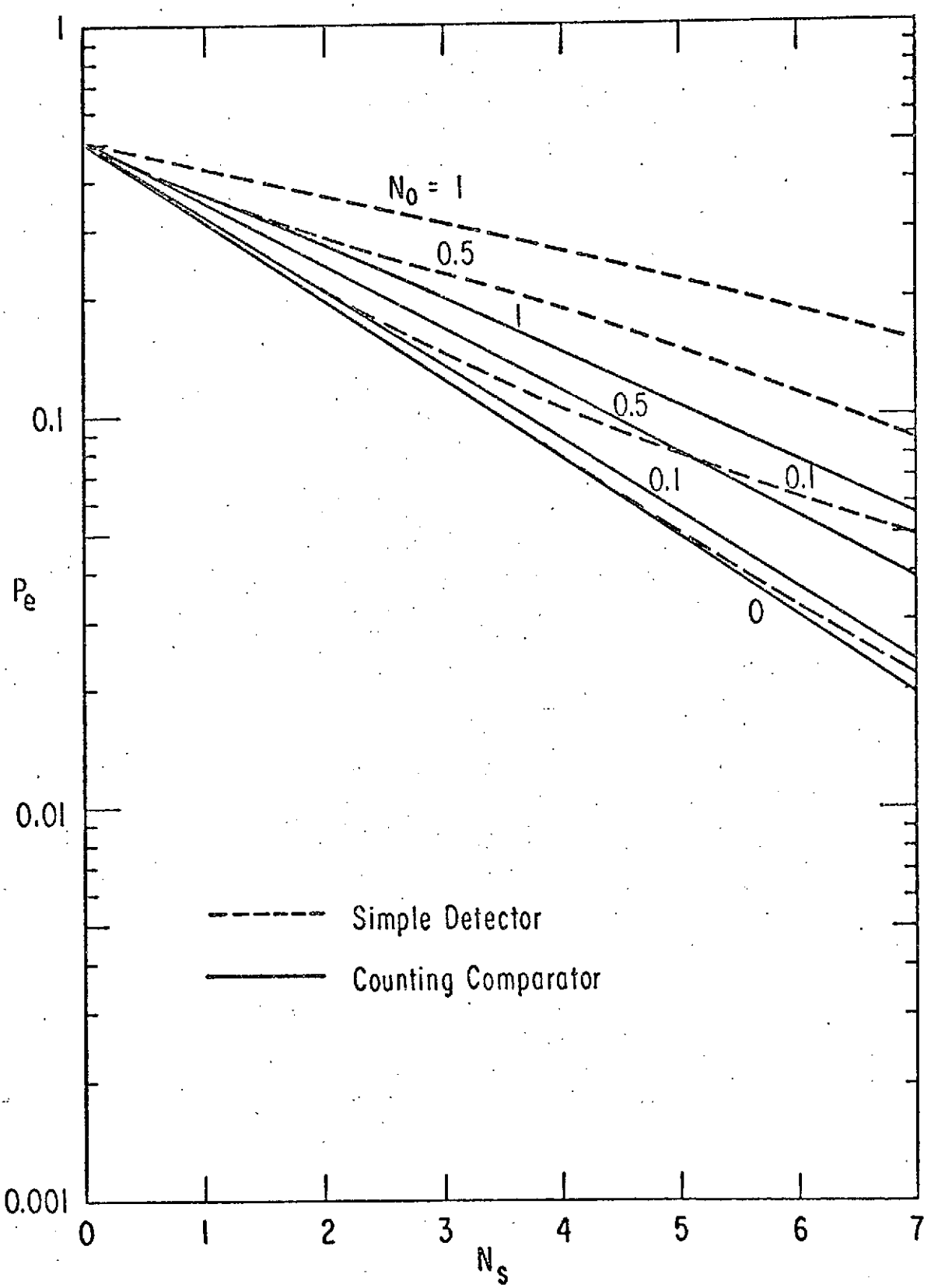
1
0.1
0.01
0.001
P_e
0
1
2
3
4
5
6
7
N_s
$N_0 = 1$
0.5
0.5
0.1
0.1
0
Simple Detector
Counting Comparator

Figure 22 Average error probability P_e in binary detection vs. average number N_s for simple detector and counting comparator with square observation area $A' = 4\sigma^2$ at $R_0 = 1$ and $N_0 = 0.1$; $x_0/\sigma = 1, 2$.

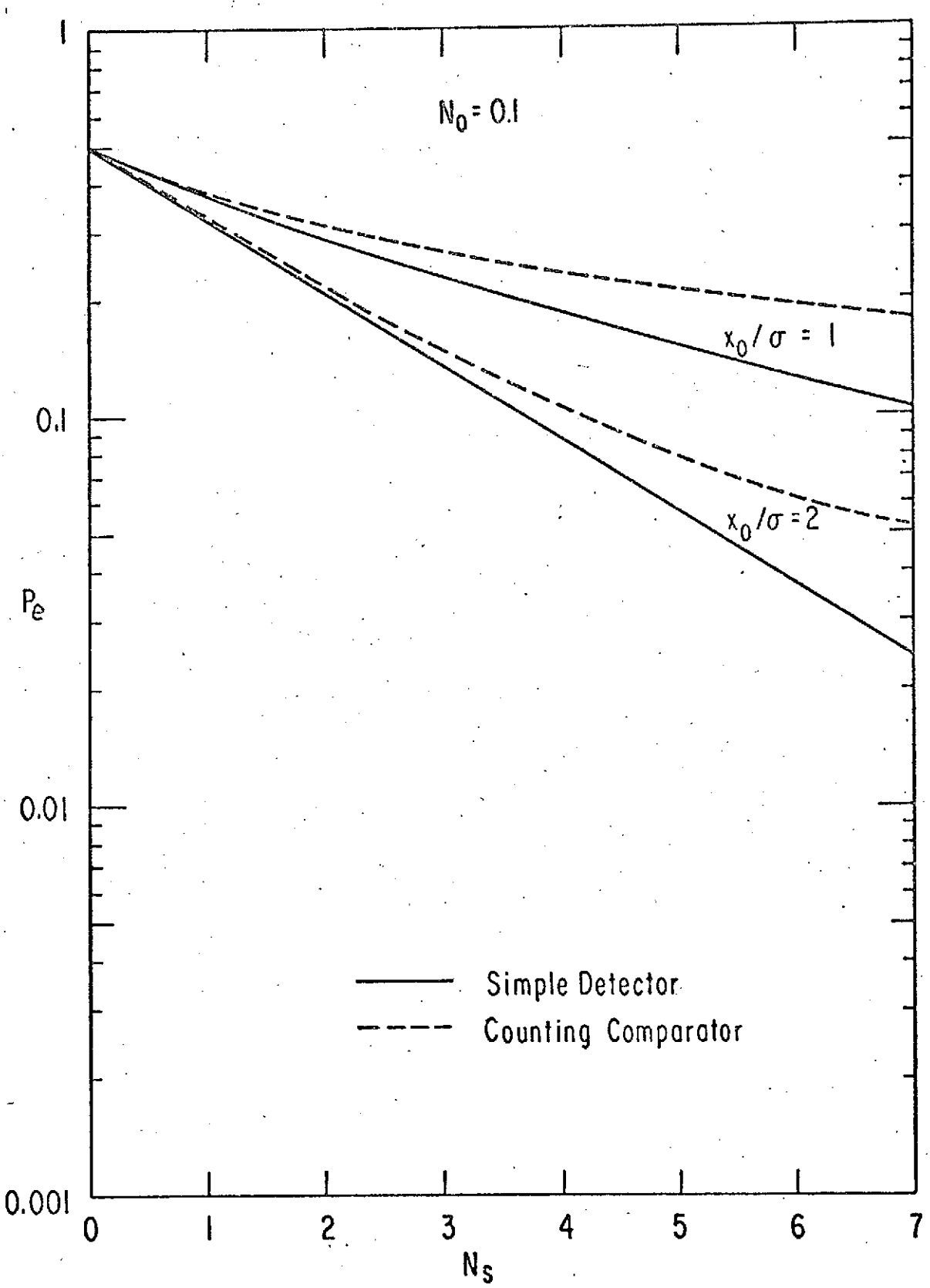
1
0.1
0.01
0.001
P_e
$N_0 = 0.1$
$x_0/\sigma = 1$
$x_0/\sigma = 2$
Simple Detector
Counting Comparator
0
1
2
3
4
5
6
7
N_S

Figure 23 Average error probability P_e in binary detection vs. average number difference ΔN for simple detector and counting comparator where $\Delta N = \bar{n}_{T1} - \bar{n}_{T0}$ with $\bar{n}_{Tk}$ as the mean number of photo-electrons observed from a finite area of one-half of the surface under hypothesis H_k for k=0, 1; $\bar{n}_{T0}$ = 0.5, 1, 2.

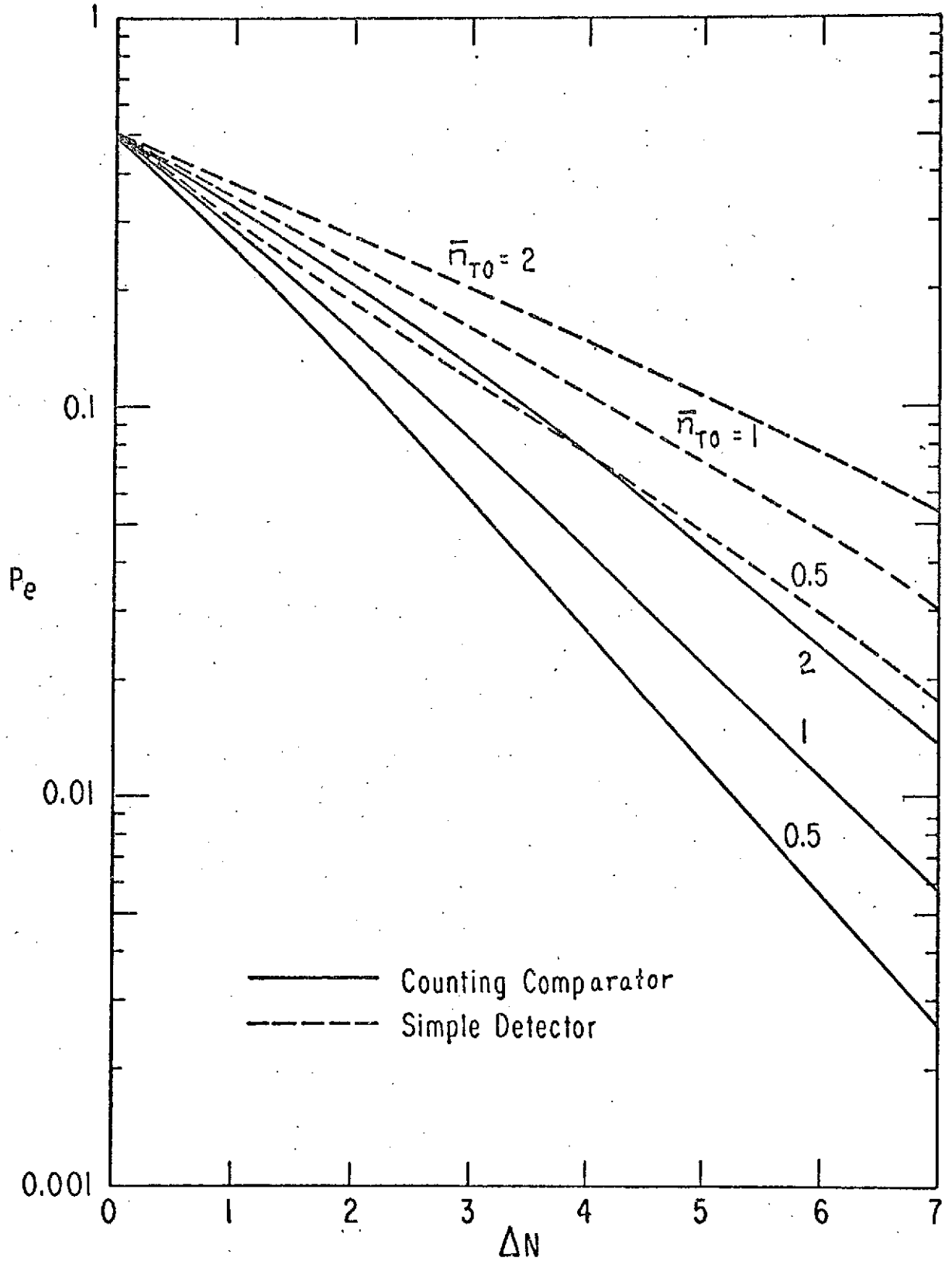
1
0.1
0.01
0.001
P_e
$\bar{n}_{TO} = 2$
$\bar{n}_{TO} = 1$
0.5
2
1
0.5
Counting Comparator
Simple Detector
0
1
2
3
4
5
6
7
ΔN

Counting comparator for detection of binary bits

Another simple receiver for detecting the radiant source located at either $(0,x_0)$ or $(0,-x_0)$, similar to the receiver discussed by Peters and Arguello[2], measures the total number n_u of photoelectrons emitted from the area A' centered at $(0,x_0)$ in the upper half photosensitive surface and compares it with the total number n_L of photoelectrons emitted from the area A'' centered at $(0,-x_0)$ of the lower half plane ($A'=A''$). The observer will choose H_1 if $n_u > n_L$ and H_0 if $n_u < n_L$. When $n_u = n_L$ hypothesis H_1 will be chosen with a probability f. The false-alarm probability and the detection probability according to (2.9) and (2.10) can be written as

$$Q_0 = Pr[n_u > n_L|H_0]+f\ Pr[n_u = n_L|H_0]$$

$$= \sum_{n=0}^{\infty}\sum_{m=1}^{\infty} P_0(n+m)\ P_1(n)+f \sum_{n=0}^{\infty} P_0(n)\ P_1(n)\ ,$$

$$Q_d = Pr[n_u > n_L|H_1] + f\ Pr[n_u = n_L|H_1]$$

$$= \sum_{n=0}^{\infty}\sum_{m=1}^{\infty} P_1(n+m)\ P_0(n)+f \sum_{n=0}^{\infty} P_1(n)\ P_0(n)\ ,$$

where $P_k(n) = \bar{n}_{Tk}^{\,n}\ e^{-\bar{n}_{Tk}}/n!$, for k=0,1 , (4.28)

with means $\bar{n}_{T1}$ and $\bar{n}_{T0}$ given in (4.22), (4.23), or (4.24). (4.28) can be expressed in simpler form. Since

$$\sum_{n=0}^{\infty} \sum_{m=1}^{\infty} P_0(n+m)\, P_1(n)$$

$$= \sum_{n=0}^{\infty} \sum_{m=1}^{\infty} \bar{n}_{T0}^{\,n+m}\, e^{-\bar{n}_{T0}}\, \bar{n}_{T1}^{\,n}\, e^{-\bar{n}_{T1}} \Big/ n!\,(m+n)!$$

$$= e^{-(\bar{n}_{T1} + \bar{n}_{T0})} \sum_{m=1}^{\infty} \left(\frac{\bar{n}_{T0}}{\bar{n}_{T1}}\right)^{\frac{m}{2}} I_m(ab)$$

$$= 1 - Q(a,b) \quad , \tag{4.29}$$

where $I_m(x) = \sum_{n=0}^{\infty} (x/2)^{m+2n} \Big/ n!\,(n+m)!$

is the modified Bessel function[6] for m=0,1,2... and

$$Q(a,b) = 1 - e^{-\frac{1}{2}(a^2 + b^2)} \sum_{m=1}^{\infty} \left(\frac{b}{a}\right)^m I_m(ab)$$

is the "Q function"[5] with

$$a = \sqrt{2\bar{n}_{T1}} \quad , \quad b = \sqrt{2\bar{n}_{T0}} \quad . \tag{4.30}$$

Also we can write

$$\sum_{n=0}^{\infty} P_1(n)\, P_0(n) = \sum_{n=0}^{\infty} (\bar{n}_{T0}\, \bar{n}_{T1})^n\, e^{-(\bar{n}_{T0} + \bar{n}_{T1})} \Big/ (n!)^2$$

$$= e^{-\frac{1}{2}(a^2 + b^2)}\, I_0(ab) \quad . \tag{4.31}$$

Therefore, for equal prior probabilities or $\xi = \frac{1}{2}$, the average error probability for making the decisions is

$$P_e = \frac{1}{2} Q_0 + \frac{1}{2}(1 - Q_d)$$

$$= \sum_{n=0}^{\infty} \sum_{m=1}^{\infty} P_0(n+m)\, P_1(n) + \frac{1}{2} \sum_{n=0}^{\infty} P_0(n)\, P_1(n)$$

$$= 1 - Q(a,b) + \frac{1}{2} \exp(-\tfrac{1}{2}(a^2 + b^2))\, I_0(ab) . \qquad (4.32)$$

The error probability P_e from (4.32) of the counting comparator has been evaluated in the absence of the background light for the Gaussian images with the mean numbers under H_1 and H_0 as given by (4.27). The error probabilities P_e of this receiver are plotted as a function of the ratio $(2x_0/\sigma)$ at N_s = 0.1, 0.5, 1, 2, and 5 in Fig. 19. The error probability decreases as the ratio $(2x_0/\sigma)$ increases. As $2x_0/\sigma$ approaches infinity, the error probability will be limited by $\frac{1}{2} \exp(-N_s)$.

When the background light also passes through the aperture, the error probabilities of this receiver are also calculated with a square observation area $A' = 4\sigma^2$ with $R_0 = 1$ and plotted as a function of N_s in Fig. 21 by the solid curves at N_0 = 0, 0.1, 0.5, and 1 for $x_0/\sigma = 2$. In Fig. 22, the error probabilities are plotted as a function of N_s when the same observation area $A' = 4\sigma^2$ is used and the average background number N_0 is fixed at 0.1 for x_0/σ = 1 and 2. In Fig. 23 the error probabilities are plotted as a function of the number

difference ΔN by the solid curves at fixed values of average number $\bar{n}_{T0}$, 0.5, 1, and 2. As the size of the square area A' is varied, the error probability P_e changes. The error probabilities of the counting comparator are plotted as a function of the length R_0 in Fig. 24 at different values of N_0, 0.1, 0.5, and 1.

Figure 24 Error probability P_e of the counting comparator vs. the length R_0 for the rectangular observation area; $N_s = 5$. The curves are indexed by the parameter N_0 defined in (2.57).

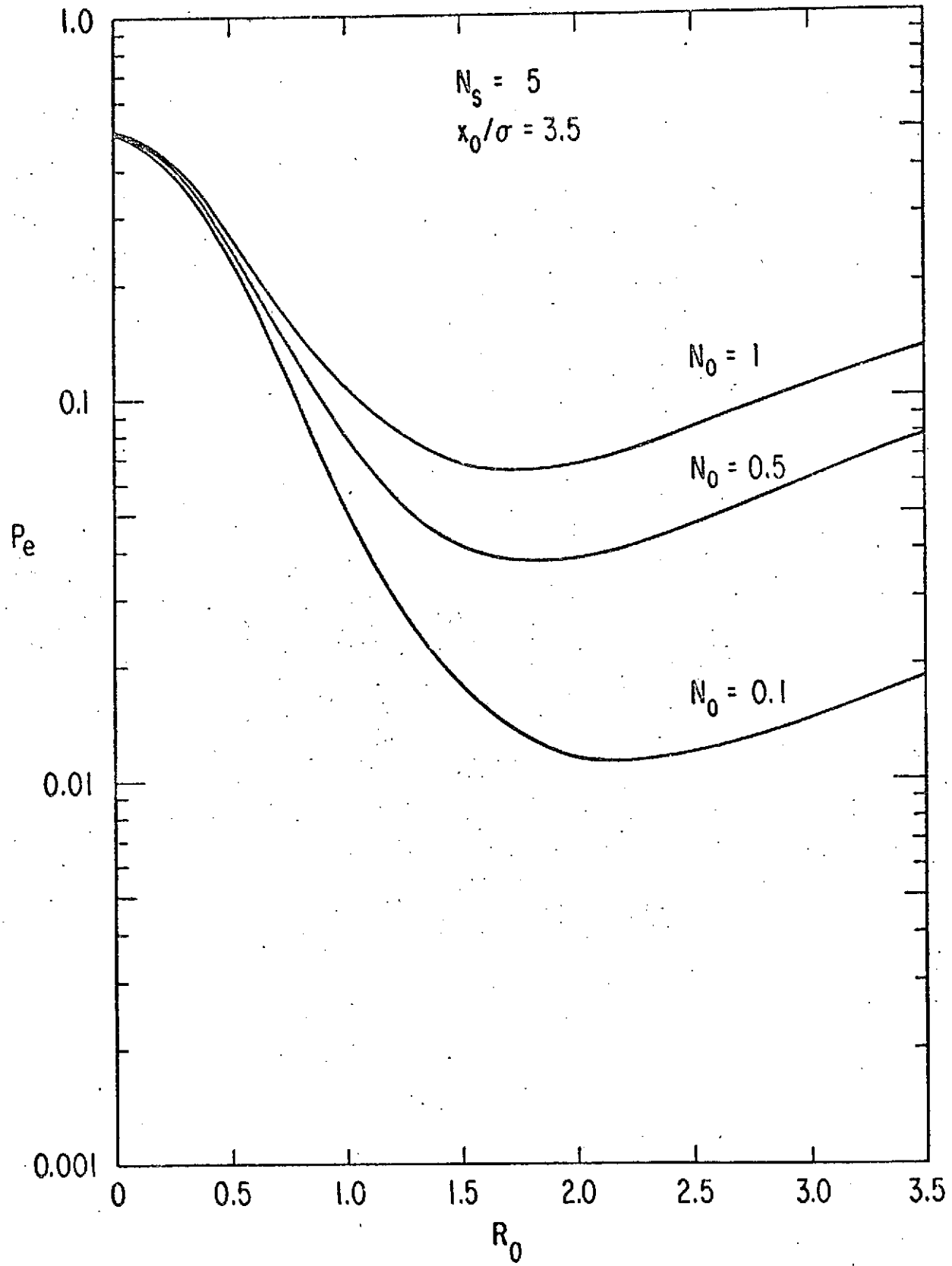
1.0
0.1
0.01
0.001
P_e
N_s = 5
x_0/σ = 3.5
N_0 = 1
N_0 = 0.5
N_0 = 0.1
0
0.5
1.0
1.5
2.0
2.5
3.0
3.5
R_0

Image location effects on the detectors in the absence of background light

The investigations of the detectors of binary bits that we have just discussed are based on the primary assumption that we know that the image is located at either $(0,x_0)$ or $(0,-x_0)$ exactly. We would like to investigate the performances of those detectors when the distance between the image is still $2x_0$, but the images are mislocated with a shift of $\pm\varepsilon$. That is the images are actually located at $(0,x_0')$ and $(0,-x_0'')$ under hypothesis H_1 and H_0 where $x_0' = x_0 + \varepsilon$, $x_0'' = x_0 - \varepsilon$ or $x_0' = x_0 - \varepsilon$, $x_0'' = x_0 + \varepsilon$ for $\varepsilon > 0$.

When the ideal detector is used, the expression of the function $H_R(\underset{\sim}{x}_i)$ from (4.13) can still be used, where the weighting function $\gamma_k(\underset{\sim}{x}_i)$ from (4.12) will be replaced with $x_0 = x_0'$ for $k = 1$ and $x_0 = x_0''$ for $k=0$. We can derive the m.g.f. of the optimum statistic g_R following (4.14), and the expression of the m.g.f. $h_{Rk}(s)$ from (4.15) can still be used with M_{nk} now replaced by

$$M_{nk} = -2n\frac{x_0x_0'}{\sigma^2}(-1)^k, \text{ for } k=1$$

$$= -2n\frac{x_0x_0''}{\sigma^2}(-1)^k, \text{ for } k=0,\ n=0,1,2... \qquad (4.33)$$

and σ_n^2 unchanged.

The false-alarm probability and detection probability with zero decision level can be expressed according to (4.19) as

$$Q_0 = P_r[g_R > 0|H_0]$$

$$= \exp(-N_s) \sum_{n=1}^{\infty} \frac{N_s^n}{n!} \operatorname{erfc}\left(\sqrt{n}\,\frac{x_0''}{\sigma}\right),$$

$$Q_d = P_r[g_R > 0|H_1]$$

$$= \exp(-N_s) \sum_{n=1}^{\infty} \frac{N_s^n}{n!} \left(1 - \operatorname{erfc}\left(\sqrt{n}\,\frac{x_0'}{\sigma}\right)\right) . \qquad (4.34)$$

The average error probability for equal prior probability or $\xi = \frac{1}{2}$ can be written as

$$P_e = \frac{1}{2} Q_0 + \frac{1}{2}(1 - Q_d)$$

$$= \frac{1}{2} \exp(-N_s)\left[1 + \sum_{n=1}^{\infty} \frac{N_s^n}{n!} \left(\operatorname{erfc}\left(\sqrt{n}\,\frac{x_0''}{\sigma}\right) + \operatorname{erfc}\left(\sqrt{n}\,\frac{x_0'}{\sigma}\right)\right)\right]. \qquad (4.35)$$

The error probability will be the same for either $x_0' = x_0 + \epsilon$ $x_0'' = x_0 - \epsilon$ or $x_0' = x_0 - \epsilon$, $x_0'' = x_0 + \epsilon$. That is, (4.35) is the average error probability of the ideal detector when the images are mislocated with a shift either ϵ or $-\epsilon$.

When the counting comparator is used, with the distance between the images fixed at $2x_0$, the mean numbers due to a shift ϵ or $-\epsilon$ of the actual image can be expressed as

$$\bar{n}_{T1\pm} = N_s\left[1 - \operatorname{erfc}\left(\frac{x_0 \pm \varepsilon}{\sigma}\right)\right],$$

$$\bar{n}_{T0\mp} = N_s \operatorname{erfc}\left(\frac{x_0 \pm \varepsilon}{\sigma}\right), \tag{4.36}$$

where $\bar{n}_{T1+}$, $\bar{n}_{T0-}$ are the means for a positive shift ε and $\bar{n}_{T1-}$, $\bar{n}_{T0+}$ are the means for a negative shift $-\varepsilon$. The false-alarm probability and the detection probability of the counting comparator when the images are misolcated at $(0,x_0)$ and $(0,-x_0)$ under hypothesis H_1 and H_0, while actually located at $(0,x_0+\varepsilon)$ and $(0,-x_0+\varepsilon)$ or $(0,x_0-\varepsilon)$ and $(0,-x_0-\varepsilon)$, can be written as

$$\begin{aligned} Q_{0\pm} &= \Pr[n_u > n_L | H_0] + f \Pr[n_u = n_L | H_0] \\ &= \sum_{n=0}^{\infty}\sum_{m=1}^{\infty} P_{1\mp}(n)\, P_{0\pm}(n+m) + f \sum_{n=0}^{\infty} P_{1\mp}(n)\, P_{0\pm}(n), \end{aligned}$$

$$\begin{aligned} Q_{d\pm} &= \Pr[n_u > n_L | H_1] + f \Pr[n_u = n_L | H_1] \\ &= 1 - \sum_{n=0}^{\infty}\sum_{m=0}^{\infty} P_{1\pm}(n)\, P_{0\mp}(n+m) + f \sum_{n=0}^{\infty} P_{1\pm}(n)\, P_{0\mp}(n), \end{aligned} \tag{4.37}$$

where $P_{k\pm}(n) = \bar{n}_{Tk\pm}^{\,n}\, e^{-\bar{n}_{Tk\pm}}/n!$, for $k=0,1$.

Q_{0+} and Q_{d+} are the false-alarm probability and the detection

probability for a positive shift ε while Q_{0-}, Q_{d-} are the probabilities for a negative shift $-\varepsilon$.

For equal prior probability $\xi = \frac{1}{2}$ and $f = \frac{1}{2}$, the average error probability will be the same for either a shift ε or $-\varepsilon$ and can be written as

$$
\begin{aligned}
P_{e\pm} &= \frac{1}{2} Q_{0\pm} + \frac{1}{2}(1 - Q_{d\pm}) \\
&= \frac{1}{2}\Big[\sum_{n=0}^{\infty} \sum_{m=1}^{\infty} P_{1\mp}(n)\, P_{0\pm}(n+m) + \frac{1}{2} \sum_{n=0}^{\infty} P_{1\mp}(n)\, P_{0\pm}(n) \\
&\quad + \sum_{n=0}^{\infty} \sum_{m=1}^{\infty} P_{1\pm}(n)\, P_{0\mp}(n+m) + \frac{1}{2} \sum_{n=0}^{\infty} P_{1\pm}(n)\, P_{0\mp}(n) \Big] \\
&= 1 - \frac{1}{2}\{Q(a_-, b_+) + Q(a_+, b_-) - \frac{1}{2}\Big[e^{-\frac{1}{2}(a_-^2 + b_+^2)} I_0(a_- b_+) \\
&\quad + e^{-\frac{1}{2}(a_+^2 + b_-^2)} I_0(a_+ b_-)\Big]\} \,,
\end{aligned}
\tag{4.38}
$$

where $a_{\pm} = \sqrt{2n_{T1\pm}}$, $b_{\pm} = \sqrt{2n_{T0\pm}}$ and $Q(a,b)$, $I_0(ab)$ are given in (4.29). P_{e+} is the error probability for a shift of ε and P_{e-} is the error probability for a shift of $-\varepsilon$. $P_{e+} = P_{e-}$ as we can see from (4.38).

The error probabilities of both the ideal detector and the counting comparator are calculated at different values of shift ε when (4.35) and (4.38) are used. In Fig. 25, the error probabilities of these two detectors are plotted as a function of the ratio $|\varepsilon|/x_0$ at $N_s = 2$, 5 and 8 with $x_0/\sigma = 1$. In Fig. 26 the error probabilities are plotted as a function of the ratio $|\varepsilon|/x_0$ at $x_0/\sigma = 1.5$, 2 and 4 with fixed value of N_s at 5.

Figure 25 Average error probability P_e in binary bits detection vs. the ratio $|\epsilon|/x_0$ due to the mislocation of the images for the ideal detector or the counting comparator at $x_0/\sigma = 1$; $N_s = 2$, 5, 8.

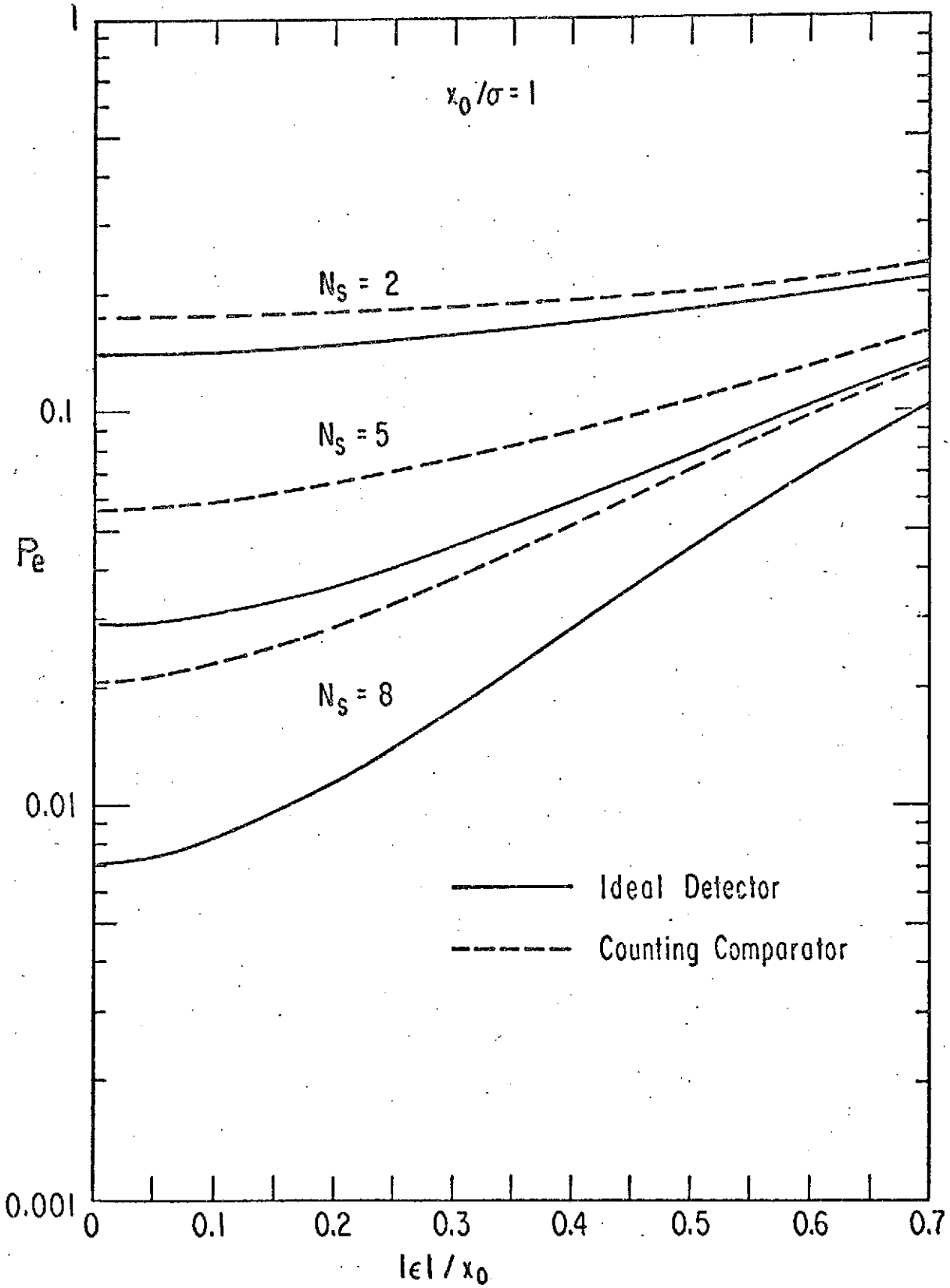
1
$x_0/\sigma = 1$
$N_S = 2$
0.1
$N_S = 5$
P_e
$N_S = 8$
0.01
Ideal Detector
Counting Comparator
0.001
0
0.1
0.2
0.3
0.4
0.5
0.6
0.7
$|\epsilon| / x_0$

Figure 26 Average error probability P_e in binary bits detection vs. the ratio $|\varepsilon|/x_0$ due to the mislocation of the images for the ideal detector and the counting comparator for fixed value $N_s = 5$; $x_0/\sigma = 1.5, 2, 4$.

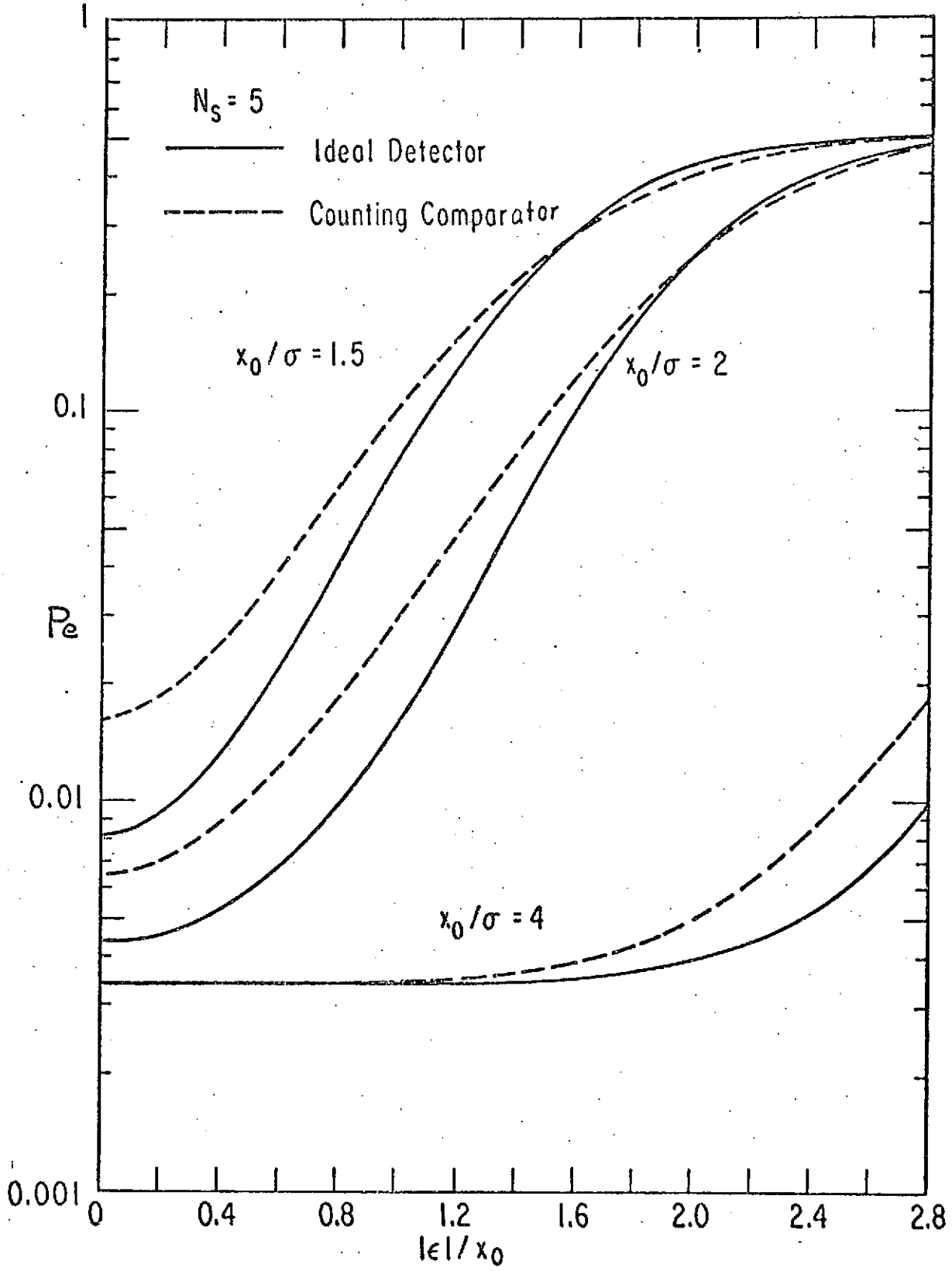
1
0.1
0.01
0.001
Pe
$N_S = 5$
Ideal Detector
Counting Comparator
$x_0/\sigma = 1.5$
$x_0/\sigma = 2$
$x_0/\sigma = 4$
0
0.4
0.8
1.2
1.6
2.0
2.4
2.8
$|\epsilon|/x_0$

Discussion

In the absence of uniform background light, registering the locations of the ejected photoelectrons for the detection of either one of the two Gaussian images, as we have discussed in this chapter, not only utilizes more of the information, but also effectively reduces the mean value of the optimum statistic under H_0 and thus improves the performance of the ideal detector. As for the simple detector, the gain by optimizing the observation area will be limited because varying the area will affect both the mean numbers $\bar{n}_{T0}$ and $\bar{n}_{T1}$ as defined in (4.27). Therefore, the performance of the ideal detector is better than that of the simple detector, as we can see from Fig. 19 and Fig. 20. When the counting comparator is used, the observed numbers of the photoelectrons ejected from both the upper half surface and the lower half surface will be used, while for the simple detector only the number of photoelectrons ejected from the upper half surface (or the lower half surface) will be utilized for making decision. In other words, the counting comparator utilizes more information than the simple detector, but less information than the ideal detector. Thus the performance is better than that of the simple detector, but not as good as that of the ideal detector as shown in Fig. 19.

When background light also passes through the aperture, the average error probability for making decisions will be increased. In the meantime, the observer must define a finite observation area when any one of the detectors will be used. For the simple detector or the counting comparator, the finite observation area can be chosen such

that for a fixed false-alarm probability, the detection probability of the detector will be as large as possible. The proper size of the square area for the counting comparator to be used at $0.1 \leq N_0 \leq 1$ is $R_0 = 2$ or $A' = 16\sigma^2$ as we can see from Fig. 24. For a finite square area $4\sigma^2$, the average error probabilities for both simple detector and counting comparator will increase as the background light increases or the ratio x_0/σ decreases as shown in Fig. 21, Fig. 22, and Fig. 23.

When Gaussian images are postulated, the performance of the detectors for detecting binary bits will also depend on the prior knowledge about the locations of the images. The average probability of making errors in each decision will be increased if the images for bit "1" and bit "0" are mislocated. The severity of mislocation will also depend on the distance $2x_0$ separating the images. For example, when the ratio $x_0/\sigma = 4$, the effect on either the ideal detector or the counting comparator due to mislocation will be insignificant until the ratio of shift $|\varepsilon|/x_0$ is greater than 1.2, as we can see from Fig. 26. Furthermore, the effect on the counting comparator of mislocation of the images will be little smaller than that on the ideal detector as shown in Fig. 25 or Fig. 26 and at $x_0/\sigma = 1.5$; for example, the average error probability of the counting comparator becomes smaller than that of the ideal detector when $|\varepsilon|/x_0$ is greater than 1.6, as shown in Figure 26,

Table 2 - Optimum Distance for Simple Detector

x_0/σ	0.1	0.5	0.75	1.0	1.25	1.5	2.0	3.0
x_d/σ	0.16	0.52	1.09	1.1	1.1	1.08	1.04	0.84

Footnotes

Chapter IV

1. Helstrom [27].
2. Peters and Arguello [28].
3. Papoulis [29], p. 155, eq. (5.77).
4. Papoulis [29], p. 146.
5. Helstrom [10], Appendix F.
6. I. S. Gradshteyn and I. M. Ryzhik [30], p. 961, eq.(8.445).

References

1. Mandel, L. and E. Wolf, Coherence properties of optical fields. Rev.Mod.Phys., Vol.37 No.2, pp. 231-287, April,1965.

2. Mandel, L., Fluctuations of photon beams: The distribution of the photo-electrons. Proc.Phys.Soc., Vol.74, pp. 233-243, September, 1959.

3. Helstrom, C. W., Distribution of photoelectric counts from partially polarized Gaussian light. Proc.Phys.Soc., Vol.83, pp. 777-782, 1964.

4. Siegert, A. J. F., Passage of stationary noise through linear and non-linear devices. IEEE Trans. on Inf. Theory, Vol IT-3, pp. 4-25, March, 1954.

5. Helstrom, C. W., Detection and resolution of optical signals. IEEE Tran. on Inf. Theory, Vol. IT-10, pp. 275-287, October, 1964.

6. Farrell, Edward J., Information content of photoelectric star images. J.Opt.Soc.Am., Vol.56, pp. 578-587, May, 1966.

7. Rice, S. O., Uniform asymptotic expansions for saddle point integrals: Application to a probability distribution occurring in noise theory. Bell Sys.Tech.J., Vol.47, pp. 1971-2013, November, 1968.

8. Daniels, H. G., Saddle point approximations in statistics. Ann. Math.Statistics, Vol.25, pp. 631-650, September, 1954.

9. Middleton, D. and R. Esposito, Simultaneous optimum detection and estimation of signals in noise. IEEE Tran. on Inf. Theory, pp. 434-444, May, 1968.

10. Helstrom, C. W., Statistical theory of signal detection. Second edition, Pergamon Press, Oxford, 1968.

11. Goodman, J. W., Introduction to Fourier optics. McGraw-Hill, Inc., New York, 1968.

12. Wolf, E., A microscopic theory of interference and diffraction of light from finite sources II: Fields with a spectral range of arbitrary width. Proc.Roy.Soc., A230, pp. 246-265, June, 1955.

13. Mandel, L., Intensity fluctuation of partially polarization light. Proc.Phys.Soc., Vol.81, pp. 1104-1114, June, 1963.

C3

14. Helstrom, C. W., Detection and resolution of incoherent objects seen through a turbulent medium. J.Opt.Soc.Am., Vol.59, pp. 331-341, March, 1969.

15. Mandel, L., Fluctuations of light beams. Progress in Optics, E. Wolf, ed., Vol.2, pp. 181-248, 1963.

16. Bar-David, I., Communication under the Poisson regime. IEEE Trans. on Inf. Theory, Vol.IT-15, pp. 31-37, January, 1969.

17. Helstrom, C. W., Detectability of coherent optical signals in a heterodyne receiver. J.Opt.Soc.Am.,Vol.57, pp. 353-361, March, 1967.

18. Helstrom, C. W., Detection and resolution of incoherent objects by a background-limited optical system. J.Opt.Soc.Am., Vol.59, pp. 164-175, February, 1969.

19. Papoulis, A., The Fourier integral and its applications. McGraw-Hill, Inc., New York, 1962.

20. Van Trees, Harry L., Detection, estimation, and modulation theory, Part I. J. Wiley and Sons, Inc., New York, 1968.

21. Helstrom, C. W., Quantum detection theory. Progress in Optics. E. Wolf, ed., Vol.10, pp. 291-369, 1972.

22. Helstrom, C. W. and L. L. Wang, Optimum detection of an optical image on a photoelectric surface. IEEE Trans. on Aerospace and Electronics Systems (in press).

23. Gnedenko, B. V. and A. N. Kolmogorov, Limit distributions for sums of independent random variables. Translated by K. L. Chang, revised edition. Addison Wesley Pub. Co., California, 1968.

24. Feller, William, An introduction to probability theory and its applications, Vol.II. Second edition, J. Wiley and Sons, Inc., New York, 1966.

25. Wang, L. L., Numerical calculation of cumulative probability from the moment-generating function. Proc.IEEE, Vol.60, pp. 1452-1453, November, 1972.

26. Middleton, D., Topics in communication theory, McGraw-Hill, Inc. New York, 1965.

27. Helstrom, C. W., The resolution of point sources of light as analyzed by quantum detection theory. IEEE Trans. on Inf. Theory, 1973 (in press).

28. Peters, W. N. and R. J. Arguello, Fading and polarization noise of a PCMIP system. IEEE J. of Qun.Elec., Vol.QE-3, No. 11, pp. 532-539, November, 1967.

29. Papoulis, A., Probability, random variables, and stochastic processes. McGraw-Hill, Inc. New York, 1965.

30. Gradshteyn, I. S. and I. M. Ryzhik, Table of integrals, series and products. 4th Edition, Translation edited by Alan Jeffrey, Academic Press, New York, 1965.

31. Cramér , Harold, Random variables and probability distributions. Third edition. Cambridge University Press., New York, 1970.

32. Parzen, Emanuel, Modern probability theory and its applications. Wiley, New York, 1960.

33. Erdélyi, A., Asymptotic expansions. Dover Publications, Inc., 1956.

34. Jeffreys, Harold, Asymptotic approximations. Oxford Univ. Press, London, 1962.

35. Ursell, F., Integrals with a large parameter, the continuation of uniform asymptotic expansions. Proc.Camb.Phil.Soc., Vol.61, pp. 113-128, January 1965.

36. Bleistein, N., Uniform asymptotic expansions of integrals with stationary point near algebraic singularity. Comm:Pure and App.Math, Vol.19, pp. 353-370, August, 1966.

37. Mazo, J. E. and J. Salz, Probability of error for quadratic detector. Bell Sys.Tech.J., Vol.44, pp 2165-2185, November, 1965.

38. Lukacs, E., Characteristic functions. Hafner Pub. Co., New York, 1960.

APPENDIX A

Asymptotic Expansion Approximation of the Tail Distribution by the Method of Steepest Descent

In detection theory, the evaluation of the cumulative distribution for a statistic is often important, and it is required to reach a certain accuracy. For example, when the Neyman-Pearson criterion is used, the decision level of the likelihood-ratio detector must be calculated from the preassigned false-alarm probability Q_0. As Q_0 is small, there may be a serious error in the decision level if the cumulative distribution cannot be accurately calculated. The statistic we will discuss in this Appendix is of the type of the sum of N independent random variables and can be written in general as

$$Z = \sum_{i=1}^{N} X_i \qquad i = 1, 2, \ldots N . \tag{A1}$$

When $\{X_i\}$ are identical random variables and N is large, the central limit theorem [1],[2] can be applied. If $\{X_i\}$ are independent but not identical, the distribution of Z may be dominated by one of the random variables and can be approximated by the Gaussian distribution when conditions such as Lyapunov's condition[3] are satisfied. On the other hand, the distribution of the statistic Z can be derived from the inverse Fourier transform of its characteristic function when the inverse integral can be approximated by the asymptotic expansion series through the steepest-descent method. For detailed treatment of the steepest-descent approximation we refer to the works of many

authors[4-7]. For applications of the steepest-descent method in statistics we refer to the works of the authors[8-10]. Here we will discuss the asymptotic expansion approximation of the integral with only one saddle point.

The characteristic function[11] of the random variable Z is defined by

$$h(\omega) = E[e^{i\omega Z}] = \int_{-\infty}^{\infty} e^{i\omega Z} \, dF(Z) \, , \tag{A2}$$

where $F(Z_0) = Pr[Z \leq Z_0]$ is the distribution of the random variable Z.

The probability that Z exceeds a value Z_0 can be written as

$$Q(Z_0) = Pr[Z > Z_0] = 1 - \int_{-\infty}^{\infty} U(Z_0 - Z) \, dF(Z) \, , \tag{A3}$$

where U(x) is the step function.

If we take the Fourier transform of $Q(Z_0)$ by discarding the portion of the integral which oscillates with infinite rapidity, we have

$$\begin{aligned} \mathcal{F}[Q(Z_0)] &= \int_{-\infty}^{\infty} e^{-i\omega Z_0} \, Q(Z_0) \, dZ \\ &= 2\pi\delta(\omega) - \frac{1}{i\omega} h(-\omega) \, , \end{aligned} \tag{A4}$$

where $\delta(\omega)$ is the Dirac delta function.

The probability $Q(Z_0)$ can then be expressed in terms of $h(-\omega)$ by taking the inverse Fourier transform of (A4). That is

$$Q(Z_0) = \mathcal{F}^{-1}\mathcal{F}[Q(Z_0)]$$

$$= 1 - \frac{1}{2\pi}\int_{-\infty}^{\infty} e^{-i\omega Z_0} \frac{h(-\omega)}{i\omega}\, d\omega \qquad \text{(A5)}$$

where $\mathcal{F}, \mathcal{F}^{-1}$ are the Fourier transform and inverse Fourier transform operators respectively.

When the integral on the right-hand side of (A5) cannot be evaluated exactly, the method of steepest-descent can be used to approximate the tail probability $Q(Z_0)$. The integral from (A5) can be extended to a contour integral as

$$Q(Z_0) = 1 - \frac{1}{2\pi i}\int_{c_1} \frac{1}{s} \exp[Z_0\, \phi(s)]\, ds. \qquad \text{(A6)}$$

The contour c_1 of the integration is a straight line running from $\alpha_o - i\infty$ to $\alpha_o + i\infty$ for $\alpha_o > 0$ in the complex plane s with real values of Z_0. Here

$$\phi(s) = s + Z_0^{-1} \ln h(s) \qquad \text{(A7)}$$

is the complex phase of the integral, and $h(s) = E[e^{-sZ}]$ is the m.g.f. of the random variable Z as defined by (A2) with $s = i\omega$. The integral in (A6) can be approximated by taking the integration path on the complex plane so that the imaginary part of $\phi(s)$ is constant (path of the steepest descent) along the path, which also passes through the real saddle point s_0 upon which the modulus of $e^{Z_0\phi(s)}$ decreases most rapidly. The saddle point s_0 can be determined from the equation

$\frac{d}{ds}\phi(s) = 0$ or

$$Z_0 = - h'(s_0)/h(s_0) \ . \qquad \text{(A8)}$$

Since the origin is also a singular point of the integral, the contributions from taking the integral path through the saddle point s_0 and around the singularity $s = 0$ cannot be treated separately when s_0 is small or near to the origin. Rice[9] presented a more general discussion for cases involving more than one saddle point. In our case the complex phase $\phi(s)$ has only one saddle point as discussed in Appendix B. If $\phi(s)$ is analytic in the neighborhood of the origin, $\phi(s)$ behaves much like a second-order polynomial in s. This suggests changing the variable of the integral from s to u in such a way that

$$\varphi(u) = u^2 - 2u_0\, u = \phi(s) \qquad \text{(A9)}$$

is the new complex phase[12] in the u plane with u_0 as the new saddle point corresponding to s_0 in the s-plane, and $\varphi(u_0) = \phi(s_0)$. The new saddle point u_0 can be determined from (A9) as

$$u_0 = \text{sign}(s_0)\ (-\phi(s_0))^{\frac{1}{2}}, \qquad \text{(A10)}$$

where the function sign(x) = 1 for $x > 0$, sign(x) = - 1 for $x < 0$, so that u_0 and s_0 have the same sign. $\phi(s_0)$ is the complex phase at $s = s_0$ and is assumed to be non-positive. Thus, integral on the right-hand side of (A6) can be expanded into a uniform asymptotic

series of powers Z_0^{-1} as

$$\int_{c_1} \frac{1}{s} \exp[Z_0\, \phi(s)]ds$$

$$= \int_{c_1'} \frac{1}{u} f(u)\, \exp[Z_0(u^2 - 2\, u_0\, u)]du$$

$$= k_0(Z_0) + k_1(Z_0) \sum_{n=1}^{\infty} A_n\, Z_0^{-n} \quad , \qquad \text{(A11)}$$

where

$$f(u) = uds/sdu \ ,$$

$$k_0(Z_0) = \int_{c_1'} u^{-1} \exp[Z_0(u^2 - 2\, u_0 u\ )]du \ ,$$

$$k_1(Z_0) = \int_{c_1'} \exp[Z_0(u^2 - 2\, u_0\, u)]du \ ,$$

with c_1' running from $\alpha' - i\infty$ to $\alpha' + i\infty$ for $\alpha' > 0$ in the complex u plane. A_n is the coefficient of the nth term in the expansion and can be determined from the Ursell method as discussed by Rice[13].

Thus, the probability from (A6) can be approximated by the uniform asymptotic expansion series as

$$Q(Z_0) = 1 - E(Z_0) - I(Z_0) \ , \qquad \text{(A12)}$$

where

$$E(Z_0) = \begin{cases} 1 - \operatorname{erfc}\left[(-2\, Z_0\, \phi(Z_0))^{\frac{1}{2}}\right], & \text{for } s_0 < 0 \\ \operatorname{erfc}\left[(-2\, Z_0\, \phi(Z_0))^{\frac{1}{2}}\right], & \text{for } s_0 > 0 \end{cases}$$

and

$$I(Z_0) = \frac{\exp[Z_0\, \phi(s_0)]}{[2\pi\, Z_0\, \phi^{(2)}(s_0)\,]^{\frac{1}{2}}} \sum_{k=0}^{\infty} \left\{ \left(\frac{-2}{Z_0\, \phi^{(2)}(s_0)} \right)^k s_0^{-1} \cdot \sum_{n=0}^{2k} (-s_0)^{-2k+n} \sum_{\ell=0}^{n} A_{\ell,n} \left(\frac{1}{2}\right)_{\ell+k} - \operatorname{sign}(s_0)\, \left(\frac{1}{2}\right)_k \left(\frac{-\phi^{(2)}(s_0)}{2\phi(s_0)} \right)^{\frac{1}{2}} (Z_0\, \phi(s_0))^{-k} \right\},$$

where

$$\operatorname{erfc} y = \frac{1}{\sqrt{2\pi}} \int_y^{\infty} \exp(-\beta^2/2)\, d\beta,$$

and

$$A_{\ell,n} = \begin{cases} 0, & \text{for } n < \ell \text{ or } \ell = 0,\ n \geq 1 \\ 1, & \text{for } n = \ell = 0 \end{cases}$$

$$A_{\ell+1,\, n+1} = \frac{-2}{n+1} \sum_{m=1}^{n-\ell+1} \frac{m\, \phi^{(m+n)}(s_0)}{(m+2)!\, \phi^{(2)}(s_0)}\, A_{\ell,n-m+1}$$

$$\left(\frac{1}{2}\right)_m = \frac{1}{2}\left(\frac{1}{2}+1\right)\left(\frac{1}{2}+2\right)\cdots\left(\frac{1}{2}+m-1\right), \quad \left(\frac{1}{2}\right)_0 = 1.$$

$A_{\ell,n}$ are the coefficients which can be calculated by the recurrence relation through the nth derivative $\phi^n(s_0)$ of the complex phase, where

$$\phi^{n}(s) = Z_0^{-1} \left(\frac{d}{ds}\right)^{n} \ln h(s), \quad \text{for } n \geq 2, \qquad \text{(A13)}$$

and is evaluated at the saddle point $s = s_0$. This scheme can be easily programmed for a digital computer. The tail distribution $Q(Z_0)$ is obtained by adding up the terms in the asymptotic expansion given by (A12) until they become insignificantly small or they stop decreasing and begin to increase.

When Z is a discrete random variable, the tail distribution can be written as

$$Q(Z_0) = \sum_{Z > Z_0}^{\infty} p(Z), \qquad \text{(A14)}$$

where p(Z) is the probability of the random variable Z and the m.g.f. can be written as

$$h_d(s) = E[e^{-sZ}] = \sum_{Z=0}^{\infty} p(Z)\, e^{-sZ}. \qquad \text{(A15)}$$

The calculation of the tail distribution is simpler and more accurate if one first approximates the probability p(Z) and then adds up the probabilities for all $Z > Z_0$ as given by (A14). For example, when Z takes only integral values, we can express the probability by the contour integral[14] and approximate it by the uniform asymptotic series as

$$p(Z) = \frac{1}{2\pi i} \int_{c_d} e^{Z\phi_d(s)} ds$$

$$\simeq \frac{\exp[Z\ \phi_d(s_0)\ ]}{[2\pi\ Z\ \phi_d^{(2)}(s\ )\ ]^{\frac{1}{2}}} \sum_{m=0}^{\infty}$$

$$\cdot \left(\frac{-2}{Z\ \phi_d^{(2)}(s_0)}\right)^m \sum_{\ell=0}^{2m} A_{\ell,2m} \left(\frac{1}{2}\right)_{\ell+m} , \quad \text{(A16)}$$

where c_d is the contour running from $\alpha'' - i\pi$ to $\alpha'' + i\pi$, $\alpha'' > 0$ and

$$\phi_d(s) = Z^{-1} \ln h_d(s) + s \quad . \quad \text{(A17)}$$

The saddle point s_0, the coefficients, $A_{\ell,2m}$ and the derivative of the complex phase $\phi_d(s)$ can be determined as before.

To illustrate the applications of the asymptotic-expansion approximation, three well-known distributions, Gaussian, gamma,and Poisson will be discussed as follows:

Gaussian distribution

The p.d.f. of Gaussian distribution is given by

$$p(Z) = \frac{1}{\sqrt{2\pi}\sigma} \exp[-\frac{1}{2\sigma^2} (Z - m)^2] , \quad \text{(A18)}$$

with m, σ as the mean and variance. The m.g.f. h(s) is given by

$$h(s) = \exp[-\ s\ m + \frac{\sigma^2 s^2}{2}\ ] \quad . \quad \text{(A19)}$$

The saddle point can be determined from $\frac{d}{ds}\phi(s) = 0$ or by (A8). We have

$$s_0 = (m - Z_0)/\sigma^2 \ . \tag{A20}$$

The complex phase and its nth derivatives evaluated at s_0 are

$$\phi(s_0) = Z_0^{-1} \ln h(s_0) + s_0 = Z_0^{-1}(m - Z_0)^2/2\sigma^2 \ ,$$

$$\phi''(s_0) = \sigma^2/Z_0 \ ,$$

$$\phi'(s_0) = \phi^n(s_0) = 0 \ , \quad \text{for } n \geq 2 \ . \tag{A21}$$

Thus, the coefficient $A_{\ell,n} = 0$ for all ℓ, $n \neq 0$ and $I(g_0)$ vanishes; also, the tail distribution becomes

$$\begin{aligned} Q(Z_0) = 1 - E(Z_0) &= \operatorname{erfc}\left[\left|\frac{m - Z_0}{\sigma}\right|\right], \quad s_0 < 0 \\ &= 1 - \operatorname{erfc}\left[\left|\frac{m - Z_0}{\sigma}\right|\right], \quad s_0 > 0 \end{aligned} \tag{A22}$$

as it should be for Gaussian distribution.

Gamma distribution

The p.d.f. of a gamma distribution is given by

$$p(Z) = \frac{\lambda}{\Gamma(\beta)} (\lambda Z)^{\beta-1} e^{-\lambda Z}, \quad \beta > 0, \ \lambda > 0, \ Z > 0$$

$$= 0 \qquad \text{otherwise} . \tag{A23}$$

The m.g.f.[15] is given by

$$h(s) = \left(1 + \frac{s}{\lambda}\right)^{-\beta} . \tag{A24}$$

The saddle point s_0 is determined from (A8) or

$$s_0 = Z_0^{-1} \beta - \lambda, \quad Z_0 > 0 . \tag{A25}$$

The complex phase and its nth derivative evaluated at s_0 are

$$\phi(s_0) = Z_0^{-1} [-\beta \ln(\beta/Z_0\lambda) + \beta - \lambda Z_0] ,$$

$$\phi^n(s_0) = (-1)^n (n-1)! (Z_0/\beta)^{n-1}, \quad \text{for} \quad n \geq 2 . \tag{A26}$$

The special case at $\lambda = 1$, $\beta = 1$ is the exponential distribution where

$$p(Z) = e^{-Z} , \quad Z > 0$$

$$= 0 \qquad \text{otherwise} . \tag{A27}$$

The complex phase and its derivatives of the exponential distribution evaluated at the saddle point from (A25) and (A26) are

$$s_0 = Z_0^{-1} - 1 ,$$

$$\phi(s_0) = Z_0^{-1} (1 + \ell n\, Z_0) - 1 ,$$

$$\phi^n(s_0) = (-1)^n Z_0^{n-1} (n - 1)! \quad \text{for } n \geq 2. \qquad (A28)$$

The numerical calculation of the tail distribution by using the asymptotic expansion series given in (A12) for the exponential distribution has been carried out and compared with the exact value. The percentage of relative error is listed in Table 3.

Poisson distribution

$$p(Z) = e^{-\lambda} \lambda^Z / Z! \quad , \quad Z = 0, 1, \ldots$$
$$= 0 \quad \text{otherwise} \quad . \qquad (A29)$$

The m.g.f. is

$$h_d(s) = \exp[\lambda(e^{-s} - 1)] \quad . \qquad (A30)$$

The saddle point s_0 is solved from (A8) or

$$s_0 = \ell n\, (\lambda/Z) \quad . \qquad (A31)$$

The complex phase and its nth derivatives evaluated at s_0 are

$$\phi(s_0) = 1 - \lambda Z^{-1} + \ell n(\lambda Z^{-1}) ,$$

$$\phi^n(s_0) = (-1)^n, \quad \text{for} \quad n \geq 2 . \tag{A32}$$

The tail distribution has been evaluated by first approximating the probability p(Z) with the asymptotic expansion series given in (A16) and then adding up the probabilities for all $Z > Z_0$. The relative error by comparing with the exact value is listed in Table 4.

Table 3 - Percentage Error of Exponential Distribution

z_0	0.05	0.3	0.6	0.7	2.5	10	20	40	60
Error %	0.0072	0.0194	0.3243	0.3310	-0.0174	-0.0866	-0.0866	0.2039	0.6614

Table 4 - Percentage Error of Poisson Distribution

z_0	6	10	14	18	22	26	30	35
Error %	-0.0061	-0.0062	-0.0087	-0.0049	-0.0043	-0.0058	-0.0045	-0.0028

Footnotes

1. Gnedenko and Kolmogorov [13].
2. Cramér [31], Chapter VI.
3. Parzen [32], Chapter 10, § 4.
4. Erdélyi [33], Chapter I, II.
5. Jeffreys [34], Chapter I, II.
6. Ursell [35].
7. Bleistein [36].
8. Daniels [8].
9. Rice [7].
10. Mazo and Salz [37].
11. Lukacs [38], Chapter I, eq (1.36).
12. Rice [7], Appendix B.
13. Rice [7], pp. 1984-1990.
14. Daniels [8], § 8.
15. Lukacs [38], Chapter I.

Appendix B

Iteration Procedure for Finding the Saddle Point in the Asymptotic Expansion Series

In this Appendix we will show that there is only one real saddle point of the contour integral given by (A6) in Appendix A for approximating the tail distribution of the optimum statistic g or the threshold statistic g_θ from (2.18) or (2.26). The formulas used for searching for the saddle point when the Neyman–Pearson criterion is applied will be given.

The cumulant-generating function for the ideal detector is given by (2.20) from Chapter II as

$$c_k(s) = \ln h_k(s) = \alpha T I_b \int_A H^k(\underset{\sim}{x})[(H(\underset{\sim}{x}))^{-s}-1]d^2\underset{\sim}{x}\,,$$

$$k = 0, 1\,. \tag{B1}$$

The m.g.f. $M(s, g_0)$ of the positive statistic g is defined by

$$\begin{aligned} M(s,g_0) &= E[e^{-s(g-g_0)}] \\ &= \int_0^\infty e^{-s(g-g_0)}\, dF_k(g) \\ &= \exp[g_0 s + c_k(s)] \\ &= \exp[g_0\, \phi_k(s)]\,, \quad k = 0, 1 \end{aligned} \tag{B2}$$

and can be expressed as a function of $\phi_k(s)$ as given in (2.48).

As we investigate the complex phase $\phi_k(s)$ for k = 0, 1 and its first and second derivatives from (2.53)

$$\phi_k'(s) = - g_0^{-1} \alpha T I_b \int_A [H(\underset{\sim}{x})]^{k-s} \ln H(\underset{\sim}{x}) \, d^2\underset{\sim}{x} + 1 ,$$

$$\phi_k''(s) = g_0^{-1} \alpha T I_b \int_A [H(\underset{\sim}{x})]^{k-s} \ln^2 H(\underset{\sim}{x}) \, d^2\underset{\sim}{x} ,$$

$$k = 0, 1 ,$$

we have $\phi_k'(-\infty) = -\infty$, $\phi_k'(\infty) = 1$ and $\phi_k''(s) > 0$ for all real values of s. Then $\phi_k'(s)$ is a non-decreasing function of real s. Furthermore, the cumulant-generating function $C_k(s)$ exists in $-\infty < s < \infty$. Therefore, according to the theorems 6.1 and 6.2 of Daniels[1], there is only one real root, which is simple, of $\phi_k'(s) = 0$ for $g_0 > 0$ and no more real roots otherwise. This is true also for the threshold statistic g_θ.

When the Neyman–Pearson strategy is used, the false-alarm probability Q_0 is preassigned. To search for the saddle point s_0 under H_0, we must arbitrarily pick the initial values s_{0N} and s_{0P} in such a way that the false-alarm probability calculated at s_{0N} or s_{0P} by using the asymptotic series from (A12) will be Q_{0N} or Q_{0P} and

$$Q_{0N} < Q_0 < Q_{0P} .$$

A trial value s_0^T of the saddle point then will be determined from the equation

$$s_0^T = s_{0N} + \frac{s_{0P} - s_{0N}}{Q_{0P} - Q_{0N}} (Q_0 - Q_{0N}) . \qquad (B3)$$

The trial value of the decision level g_0^T and probability Q_0^T can be calculated by substituting s_0^T into (2.62) and (2.55) for the ideal detector or (2.69) and (2.55) for the threshold detector. If $Q_0^T > Q_0$, the values of s_{0P} and Q_{0P} will be replaced by the values s_0^T and Q_0^T. If $Q_0^T < Q_0$, the values of s_{0N} and Q_{0N} will be replaced instead. Thus, a new trial value s_0^T will be obtained according to (B3), and the procedure will be repeated until the calculated values Q_0^T approaches the preassigned value Q_0 within a tolerable error. The decision level g_0 is obtained from the final trial value g_0^T. For the ideal detector, the saddle point s_1 under H_1 can be determined from (2.51). For the threshold detector, the saddle point s_1 under H_1 must be searched for again by iteration. That is, after the decision level $g_{\theta 0}$ is obtained, we must arbitrarily pick the initial values s_{1N} and s_{1P} in such a way that the decision levels calculated from (2.69) are g_N and g_P and $g_N < g_{\theta 0} < g_P$. The trial value of s_1^T will be determined from

$$s_1^T = s_{1N} + \frac{s_{1P} - s_{1N}}{g_P - g_N} (g_{\theta 0} - g_N) . \qquad (B4)$$

By substituting the calculated value s_1^T into (2.69), the trial value $g_{\theta 0}^T$ is determined. If $g_{\theta 0}^T > g_{\theta 0}, g_P$ and s_{1P} will be replaced by $g_{\theta 0}^T$

and s_1^T, otherwise g_N and s_{1N} will be replaced instead. A new trial value s_1^T will be determined again from (B4). Repeat the procedure until the calculated value $g_{\theta O}^T$ approaches the decision level $g_{\theta O}$ within a tolerable error. The final trial value s_1^T will be used to calculate the detection probability Q_d for the threshold detector by using (2.55).

For calculating the integral, Simpson's rule has been used for the numerical integrations. The number of points used in the integration procedure depends on the relative error the system requires. In our calculations we use about 50 points at most times. More points can be used when higher accuracy is required. Furthermore, when the saddle point s_k (k = 0, or 1) is near zero, double precision may be required to calculate the saddle point s_k so that the term $I_k(g_0)$ in (2.55) can be evaluated accurately.

The typical behavior of the saddle point s_0 of the ideal detector for a Gaussian image is given in Fig. 27 where the values of s_0 are plotted as a function of signal-to-noise ratio D^2 at $N_0 = 0.5$ and 5, with preassigned false-alarm probabilities $Q_0 = 10^{-3}$ and 10^{-5}.

Figure 27 Saddle point s_0 vs. the signal-to-noise ratio D^2 for a Gaussian image; $N_0 = 0.5, 5$, $Q_0 = 10^{-3}, 10^{-5}$.

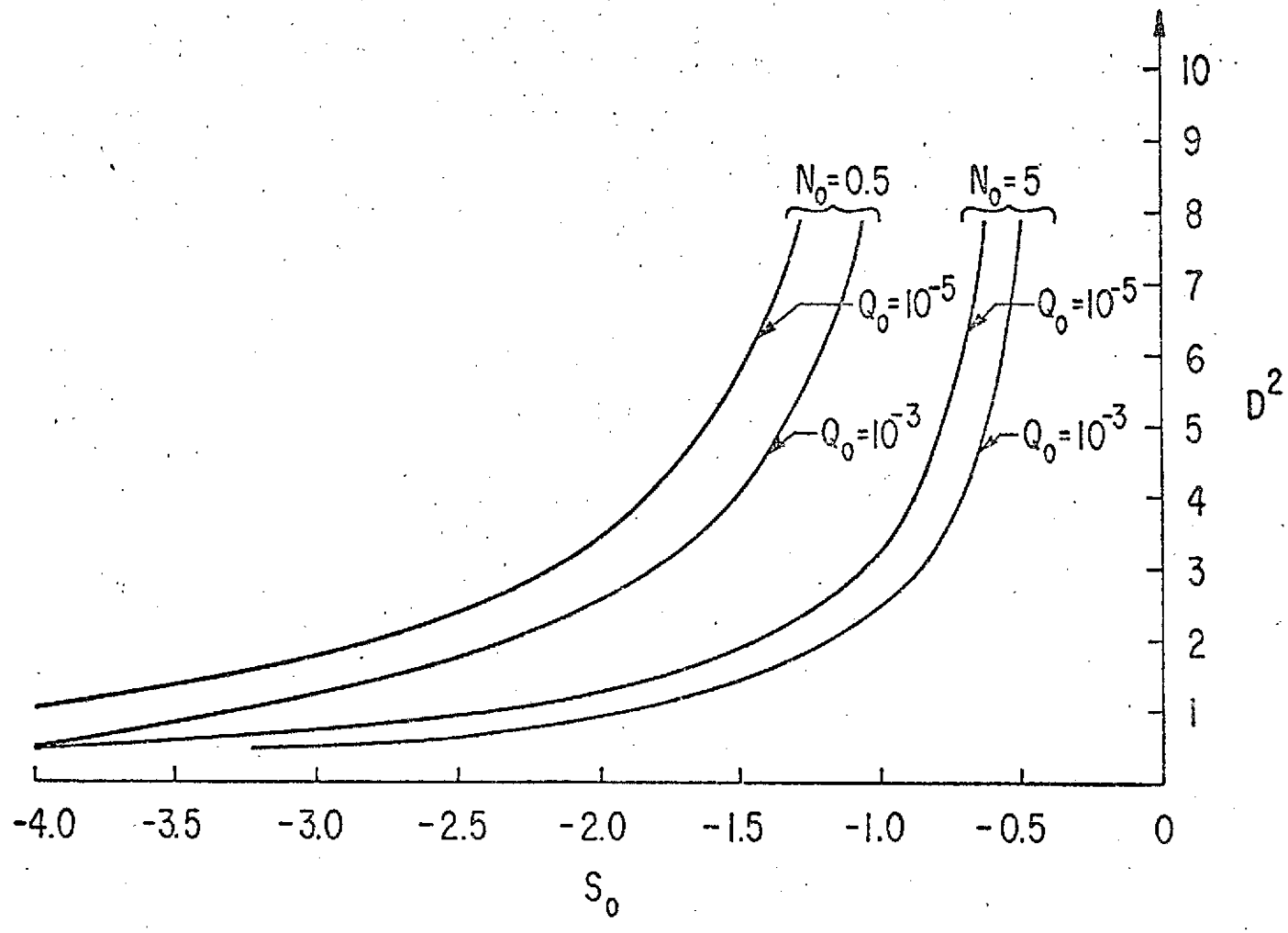
$N_0 = 0.5$
$N_0 = 5$
$Q_0 = 10^{-5}$
$Q_0 = 10^{-5}$
$Q_0 = 10^{-3}$
$Q_0 = 10^{-3}$
10
9
8
7
6
5
4
3
2
1
D^2
-4.0
-3.5
-3.0
-2.5
-2.0
-1.5
-1.0
-0.5
0
S_0

Footnotes

1. Daniels[8], §6.